Demonstrating the Role of Histidine as a Cytosolic Buffer of Ni(II) Ions in Escherichia coli

MARTELL, SAMANTHA,JANE

Demonstrating the Role of Histidine as a Cytosolic Buffer of Ni(II) Ions in *Escherichia coli*

Samantha Jane Martell

Thesis submitted for the degree of Master of Science

Department of Biosciences

Durham University

2022

College of St Hild and St Bede

Durham University

Contents

List of Figures

List of Tables

List of Abbreviations

aa	amino acid
Amp	ampicillin
bp	base pair
Da	Daltons
ddH_2O	double-distilled water
dNTP	deoxynucleotide triphosphate
EDTA	ethylenediaminetetraacetic acid
Hol	histidinol
ICP-MS	Inductively coupled plasma mass spectrometry
Kan	kanamycin
kb	kilobases
LB	lysogeny broth
MU	Miller units
nt(s)	nucleotide(s)
O/N	overnight
OD_X	optical density at a given wavelength of light, x
ONPG	o-nitrophenyl-β-D-galactoside
P_{gene}	refers to the promoter region of the specified gene
PCR	polymerase chain reaction
rpm	revolutions per minute
TAE	tris-acetate-EDTA,
Tris	tris (hydroxymethyl) aminomethane
TSS	transformation and storage solution
WT	wild-type

Statement of Copyright

Abstract

Transition metals are cofactors in many essential proteins. The correct function of these proteins hinges on metalation by their cognate metal ion, regardless of its ranking in the Irving-Williams series of metal-complex affinities. In the bacterial cytosol, evidence suggests that buffer molecules compete with proteins for metal ions, which will partition according to their relative affinities for various possible binding sites. Controlling metal availability in this manner prevents mismetallation by more competitive metals. This thesis seeks to test the buffer model using a genetic approach to alter cytosolic buffer molecule levels. A key test of the hypothesis will be changes in the cellular metalation of a metal-responsive transcription factor (RcnR), as proteins responsible for regulating metal homeostasis have affinities finely poised to sense the level of buffered metal, altering gene expression to match metal supply with demand.

L-histidine (His) is a candidate buffer of Ni(II) in *E. coli*. His levels were altered by mutating *hisG*, which encodes the feedback-inhibited first enzyme in the His biosynthetic pathway. A small library of mutant strains with altered levels of cytosolic His was generated. These strains were tested for growth sensitivity to Ni(II), and changes in Ni(II) and Co(II) responsive gene regulation by the RcnR sensor. Strains that produce more His, as assessed by qualitative bioassay for His excretion, were more resistant to the effects of Ni(II) on cell growth and showed a diminished transcriptional response to Ni(II). Strains that produced less His showed increased sensitivity to Ni(II) in a growth assay. In contrast, increased cytosolic His levels did not affect the Co(II)-responsiveness of RcnR compared to the parent strain. Thus, this work shows that His is a cytosolic buffer of Ni(II) in *E. coli* but is not a universal metal buffer.

Acknowledgements

First and foremost, I would like to thank my supervisor, Peter Chivers for his support and guidance through a fairly unique and challenging academic year. I have learned and grown under your direction and mentorship, and (hopefully) emerged a better scientist. Thank you for encouraging me to build on my soft skills (maybe one day I will actually do a presentation in front of people) and thank you for your help in writing this thesis.

Thank you to the denizens of CG204: Jack Bolton, Matthew Boutflower, Sophie Clough, Samantha Firth, Andrew Foster, Will Michaels, Louisa Stewart, Josh Wadsworth, and Tessa Young. Special thanks go to Sam for her advice on using Q5 polymerase and Andrew for his help with job applications. I would also like to thank my second supervisor, Karrera Djoko, for her insight and knowledge, and for being a generally lovely and approachable person.

Thank you to the staff the College of St. Hild and St. Bede: Simon, Laura, Joanne, Nicola, Jane, Phil, Keith, and the rest of the porters, for your support and encouragement throughout the year.

Thank you to my friends from Cheshire: Mel, Anna, and Grace.

And finally, thank you to my family: Mum, Dad, Jack, and both sets of Grandparents. I could not have done it without you.

Chapter 1: Introduction

1.1 Bacterial Metal Homeostasis

Metal ions are essential nutrients in cells, where they are used as cofactors for protein structure and function. Processes crucial to life, including respiration, photosynthesis, and nitrogen fixation, are all dependent on transition metal ion cofactors. In catalytic centres, they can increase the acidity, electrophilicity and/or nucleophilicity of the reacting species, promote heterolysis, and facilitate redox reactions (Andreini et al., 2008; Waldron et al., 2009; Hood and Skaar, 2012). Outside of catalysis, metals are incorporated into storage proteins and transcription factors (Hood and Skaar, 2012).

Integral to the functioning of these processes is the acquisition of the correct metal by a protein. Whilst proteins can provide some level of selection themselves (for example, donor ligands can impart bias in favour of the correct metal, or the binding pocket may exclude metals with the wrong charge), proteins are ultimately flexible and impart little steric selection, especially when nascent (Frausto da Silva and Williams, 2001; Waldron et al., 2009; Robinson and Glasfeld, 2020). In this scenario, the favourability of formation of a protein-metal complex is determined by the ligand field stabilisation energies of the metals themselves, as described in the Irving-Williams series of transition metals (Equation 1.1) (Irving and Williams, 1953; Dudev and Lim, 2008; Waldron et al., 2009). Cu(II) and Zn(II) form the most stable complexes, followed by Ni(II), Co(II), Fe(II), Mn(II), and Mg(II). To avoid the mismetallation of proteins, the cell must populate binding sites with the correct metal, irrespective of how strongly or weakly it binds. It is currently understood that this is achieved by controlling the availability of metal in the cytosol (Waldron et al., 2009; Foster et al., 2014; Foster et al., 2017; Osman et al., 2019).

$$\mathrm{Mg(II) < Mn(II) < Fe(II) < Co(II) < Ni(II) < Cu(II)\ (Cu(I)) > Zn(II)} \qquad 1.1$$

Recent studies suggest that metal ions in the cytosol are buffered by small molecules, such that many metals are buffered to less than one hydrated ion per cell (Foster et al., 2017; Osman et al., 2019). A competition will exist between the metal-buffer complexes and those proteins that require metal for function; metal ions likely

directly exchange between the buffer molecules and proteins, partitioning according to their relative affinities (Equation 1.2, where B is the buffer, M is a metal ion and P is a metal-utilising protein) (Osman et al., 2019). The composition of the cytosol ensures the availability of transition metals is maintained in an order that is the inverse of the Irving-Williams series (Foster et al., 2017; Osman et al., 2019). In summary, evidence suggests that there is a negligible quantity of hydrated free metal ion in the cell; instead, available metal ions associate with buffer molecules to form a kinetically accessible pool of metal ions. The competition for metal between buffer molecules and proteins effectively means metals ranked higher in the Irving-Williams series are maintained at lower intracellular availabilities, preventing the mismetallation of proteins by more competitive metals (Foster et al., 2017; Osman et al., 2019).

$$B{\bullet}M + P \rightleftharpoons B + P{\bullet}M \qquad 1.2$$

Thus, when considering the metal content of a bacterial cell, two parameters must be defined (Outten and O'Halloran, 2001; Waldron and Robinson, 2009):

(1) The total metal content, including metal already incorporated into proteins and other molecules. There is an expectation that these metals are not kinetically labile until the proteins or other molecules are degraded.
(2) The labile pool, or the quantity of metal that is kinetically accessible.

Both will vary with the species and situational needs of the bacterium. For example, Ni(II) is required for some aspects of anaerobic metabolism in *E. coli* (Wu et al., 1994; Li and Zamble, 2009). As part of the cellular response to a lack of oxygen, the expression of the Ni(II) import system NikABCDE is upregulated to acquire more Ni(II) from the extracellular environment. As another example, manganese is required for photosynthetic growth in cyanobacteria and is transported across the outer membrane in a light-dependent manner (Keren et al., 2002).

Metal homeostasis in bacteria can more generally be defined as meeting the total metal requirements of the cell whilst maintaining buffered metal levels. Metals cannot be synthesised or degraded, so homeostasis in bacteria generally relies on adjusting levels of import and export. Extracellular metal concentrations are often much lower than intracellular and metal ions are concentrated against a gradient on

import (Outten and O'Halloran, 2001). As a result, most metal import systems are high-affinity, selective, and require either the direct hydrolysis of ATP (primary transport) or proton motive force (PMF; secondary transport) (Ma, Jacobsen and Giedroc, 2009; Li and Zamble, 2009; Sydor and Zamble, 2013). Transporters requiring the hydrolysis of ATP are involved in the import of cobalt (CbiMNQO; Rodionov et al., 2006), iron (IrtAB; Rodriguez and Smith, 2006), nickel (NikABCDE; Navarro, Wu and Mandrand-Berthelot, 1993) and zinc (ZnuABC; Patzer and Hantke, 1998). In Gram-negative bacteria, porins facilitate the passive, non-specific movement of metals across the outer membrane (Delcour, 2003). Additionally, TonB, in cooperation with ExbB and ExbD, supplies energy to dedicated transporters for the active transport of metals across the outer membrane (Noinaj et al., 2010; Zeer-Wanklyn and Zamble, 2017).

Like metal import, high-affinity and specific metal export is an energy-dependent process. Three main families of metal efflux systems have been described (Nies, 2003; Guilhen, Taha and Veyrier, 2013): the resistance-nodulation-cell division-type transporters, P-type ATPases, and cation diffusion facilitator transporters. Other families encoding transition metal export systems include the chromate ion transporter (CHR) family, NreB-like proteins, CntR-like proteins, and RcnA-like proteins (Nies, 2003; Rodrigue, Effantin and Mandrand-Berthelot, 2005).

These systems are of critical importance as both metal overload and starvation are toxic to the cell. Although some intracellular targets have been identified, the exact cellular processes affected by metal toxicity are not fully characterised. The most likely mechanism by which metal toxicity takes place is the mismetallation of key proteins. In the scenario of metal excess, more reactive metals will displace less reactive metals, resulting in altered activity. For example, [4Fe-4S] clusters can be mismetallated by copper, cobalt, silver, mercury, cadmium, and zinc in *E. coli* (Ranquet et al., 2007; Macomber and Imlay, 2009; Xu and Imlay, 2012). Copper will inhibit glutamate biosynthesis via glutamine oxoglutarate aminotransferase; this interference is primarily associated with the loss of [4Fe-4S] biosynthesis (Djoko et al., 2017). An excess of metal can also cause indirect toxicity via oxidative stress (Valko, Morris and Cronin, 2005; Chen et al., 2010; Sydor and Zamble, 2013; Djoko et al., 2015).

The expression of import and export systems is regulated transcription factors which respond to the availability of metal in the labile pool (Guerra and Giedroc, 2012; Chandrangsu, Rensing and Helmann, 2017), described in the following section.

1.2 Metal-Sensing Regulatory Transcription Factors

In response to changes in metal availability, bacteria will transcribe specific genes or regulons, the expression of which is typically regulated by a metal-responsive regulatory transcription factor – a sensor (Guerra and Giedroc, 2012; Chandrangsu, Rensing and Helmann, 2017). These sensors are multimeric DNA-binding proteins that directly bind their cognate metal at a separate, exchangeable site, allosterically activating or inhibiting DNA-binding properties (Waldron and Robinson, 2009). Importantly, the sensors detect and respond to changes in the labile pool (Osman et al., 2019). They form a key component of metal homeostasis and allow bacteria to selectively import and export metals according to the metal availability in the labile pool.

Integral to this process is the ability of the sensor to selectively bind and respond to its cognate metal, whilst being unaffected by competing ions. If the sensors themselves are mismetallated, the proper regulation of homeostatic mechanisms is threatened. Sensors must be able to discern between metals if they are to effectively meet the metal demands of the cell. Like all metalloproteins, sensors are flexible and the process by which they differentiate between metals is a sum of multiple effects (Waldron and Robinson, 2009; Chandrangsu, Rensing and Helmann, 2017; Foster et al., 2017; Scott, 2018; Osman et al., 2019):

(1) Affinity: sensors interact with the labile pool, and their affinities are poised to detect deviations from the optimum metal availability.
(2) Allostery: binding of the cognate metal induces a conformational change within the sensor necessary to alter DNA binding. Mismetallation does not always trigger an allosteric transition.
(3) Abundance: the intracellular level of the sensor itself can also affect selectivity. Some sensors are autoregulatory.

1.3 Metal Buffering in Bacteria

Buffer molecules, proteins requiring metal to function, and sensors will all compete for metal ions in the cytosol. The metal ions will ultimately partition according to their relative affinities. Whilst the total metal content of a cell is relatively easy to measure, the size of the labile pool is harder to define (Osman et al., 2019). As the affinities of sensors are poised to detect changes in the labile pool, the availability of a metal in the buffer can be inferred from the transcriptional response of its cognate sensor (Osman et al., 2019). The buffered set point is considered to be the quantity of metal that causes 50 % of the maximal response (Osman et al., 2019). However, describing these availabilities as concentrations results in values that are not physiologically relevant; for some metals, they translate to less than one hydrated metal ion per cell (Osman et al., 2019; Young et al., 2021). Instead, the availabilities of these buffered metals are expressed as free energies (ΔG; calculated as described in Equations 1.3 and 1.4, where M is a metal ion, S is its cognate sensor, R is the molar gas constant, and T is temperature in Kelvin) (Osman et al., 2019).

$$M + S \overset{K_A}{\rightleftharpoons} M{\bullet}S \tag{1.3}$$

$$\Delta G = -RT\ln(K_A) \tag{1.4}$$

Whilst the specific molecules involved in bacterial metal buffering are largely unidentified, they probably consist of small molecules and specific buffering proteins (Chandrangsu, Rensing and Helmann, 2017). Several small molecules have been identified as potential buffers thus far. Bacillithiol has been identified as a buffer of Zn(II) in *Bacillus subtilis* (Ma et al., 2014). Glutathione has been identified as a potential buffer of chromate, Zn(II), Cd(II) and Cu(II) in *Escherichia coli* (Helbig et al., 2008; Macomber and Imlay, 2009) and a buffer of Cu(I) in *Streptococcus pyogenes* (Stewart et al., 2020). Histidine has been identified as a potential buffer of Zn(II) in *Acinetobacter baumannii* (Nairn et al., 2016) and of Ni(II) in cyanobacteria (*in vitro*) (Foster et al., 2017).

This project seeks to characterise the components of the bacterial cytosol responsible for controlling the size of the labile pool. More specifically, this project seeks to understand what role, if any, L-histidine (hereby referred to as His) plays in

the cytosolic buffering of Ni(II) in *E. coli*. A genetic approach was used to adjust levels of His biosynthesis in *E. coli* and potentially influence the size of the labile pool.

1.4 Ni(II) Homeostasis in *Escherichia coli*

Nine Ni(II)-containing enzymes have been identified, of which *E. coli* uses one (Mulrooney and Hausinger, 2003; Li and Zamble, 2009; Boer, Mulrooney and Hausinger, 2014; Maier and Benoit, 2019). Overall, the Ni(II) requirements of *E. coli* and the systems involved in homeostasis are well defined and limited in number (Chivers, 2017; Higgins, 2019). *E. coli* is a facultative anaerobe (Nataro and Kaper, 1998) and under anaerobic conditions expresses four different [NiFe]-hydrogenases, each of which is associated with a different metabolic pathway (Böck et al., 2006; Forzi and Sawers, 2007; Higgins, 2019). Hydrogenase enzymes catalyse the reversible reaction between two protons and two electrons to generate molecular hydrogen (Fontecilla-Camps et al., 2009); [NiFe]-hydrogenases are generally hydrogen-consuming enzymes (Pinske and Sawers, 2016). Hydrogen production provides a means for *E. coli* to rid itself of excess reducing equivalents during anaerobic and fermentative growth (Pinske and Sawers, 2016; Gevorgyan, Trchounian and Trchounian, 2018).

To adapt to oxygen limitation, cells will change their gene expression patterns using global regulators such as FNR (*f*umarate-*n*it rate *r*egulator) (Wu et al., 1989). Among other genes, FNR positively controls the transcription of NikABCDE (Wu et al., 1989; Myers et al., 2013), encoding the high-affinity Ni(II)-uptake system *nikABCDE*. NikABCDE is an ATP-binding cassette (ABC) type transporter (Navarro, Wu and Mandrand-Berthelot, 1993). Once Ni(II) enters the cytoplasm, it immediately associates with unknown buffer molecules. The insertion of Ni(II) into [NiFe]-hydrogenases is assisted by metallochaperone proteins, a class of protein required for the insertion of specific metals into specific proteins during their biosynthesis (Waldron and Robinson, 2009; Capdevila, Edmonds and Giedroc, 2017). These metallochaperones include HypA, HypB and SlyD (Hube, Blokesch and Böck, 2002; Reissmann et al., 2003; Zhang et al., 2005; Leach and Zamble, 2007; Chung and Zamble, 2011).

Even when not required as an essential nutrient, the intracellular availability of Ni(II) is tightly controlled owing to its relatively high position in the Irving-Williams series (Equation 1.1) (Irving and Williams, 1953; Li and Zamble, 2009). In *E. coli*, cytosolic Ni(II) levels are monitored by two structurally and functionally distinct sensors: NikR and RcnR (Figure 1.3). NikR is a Ni(II)-dependent co-repressor and metalated NikR represses transcription of *nikABCDE* (Chivers and Sauer, 1999; Chivers and Sauer, 2000). RcnR is a Co(II)/Ni(II)-dependent de-repressor and unmetalated RcnR will repress the transcription of the *rcnAB*, which encodes a Ni(II)/Co(II) export system (Iwig, Rowe and Chivers, 2006). A general summary of Ni(II) homeostasis in *E. coli* is shown in Figure 1.1. Figure 1.2 provides an overview of the thermodynamically coupled allosteric states of a sensor protein (S).

The distinct roles of NikR and RcnR are reflected by their metal- and DNA-binding affinities (given in Figure 1.2). The Ni(II)-dependent regulation of P_{rcnA} and P_{nik} is sequential, and expression of P_{rcnA} is not induced until P_{nik} expression is maximally repressed, in defined minimal and rich media (Iwig, Rowe and Chivers, 2006). Indeed, the Ni(II) affinity of RcnR is 16-fold weaker than that of NikR, and simulations suggest NikR DNA occupancy is almost 100 % before RcnR begins to respond to metal (Scott, 2018). Differences in K_{-3} and K_{-4} (Figure 1.2) reflect the roles of NikR as a Ni(II)-dependent co-repressor, and RcnR as a Ni(II)-dependent de-repressor of import and export, respectively. The transcription factors controlling the expression of the Ni(II) importer NikABCDE and exporter RcnA, NikR and RcnR respectively, are further described in Sections 1.4.1 and 1.4.2.

One site of Ni(II) toxicity has been identified in *E. coli*; fructose-1,6-bisphopshate aldolase (FbaA), a Zn(II) metalloenzyme (Macomber, Elsey and Hausinger, 2011). Growth on different carbon sources suggests that Ni(II) blocks glycolysis between the entrance of fructose carbon and glycerol carbon, consistent with Ni(II) binding to and mismetallating FbaA.

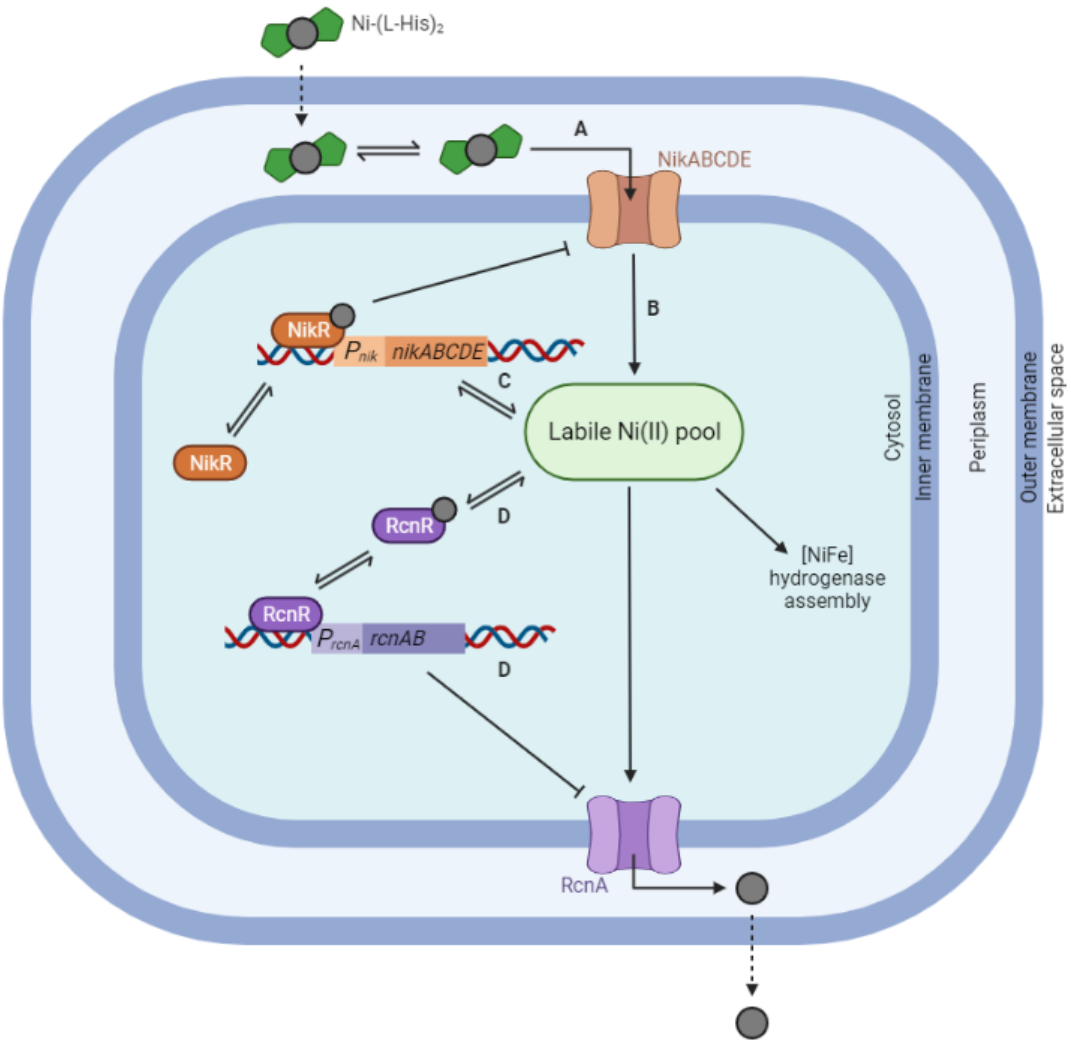

Figure 1.1: Ni(II) homeostasis in *E. coli*

Under anaerobic conditions, Ni(II) is required to supply [NiFe] hydrogenases (Wu and Mandrand-Berthelot, 1986; Wu et al., 1989; Navarro, Wu and Mandrand‐Berthelot, 1993). (**A**) A Ni-(L-His)$_2$ complex is transported across the inner membrane to the cytosol via NikABCDE (Chivers et al., 2012), the expression of which is up regulated by FNR (Navarro, Wu and Mandrand‐Berthelot, 1993); (**B**) In the cytosol, Ni(II) immediately associates with buffer molecules and is incorporated into the labile pool (Foster et al., 2017; Osman et al., 2019); (**C**) Once enough Ni(II) has been acquired by the cell, NikR will be metalated and repress the expression of the NikABCDE import system (Chivers and Sauer, 1999); (**D**) If the cell is experiencing an excess of Ni(II), RcnR is metalated and the expression of the RcnA export system is de-repressed (Iwig, Rowe and Chivers, 2006; Iwig et al., 2008). Figure adapted from Scott, 2018 and Brawley and Lindahl, 2021. Figure generated using Biorender.com.

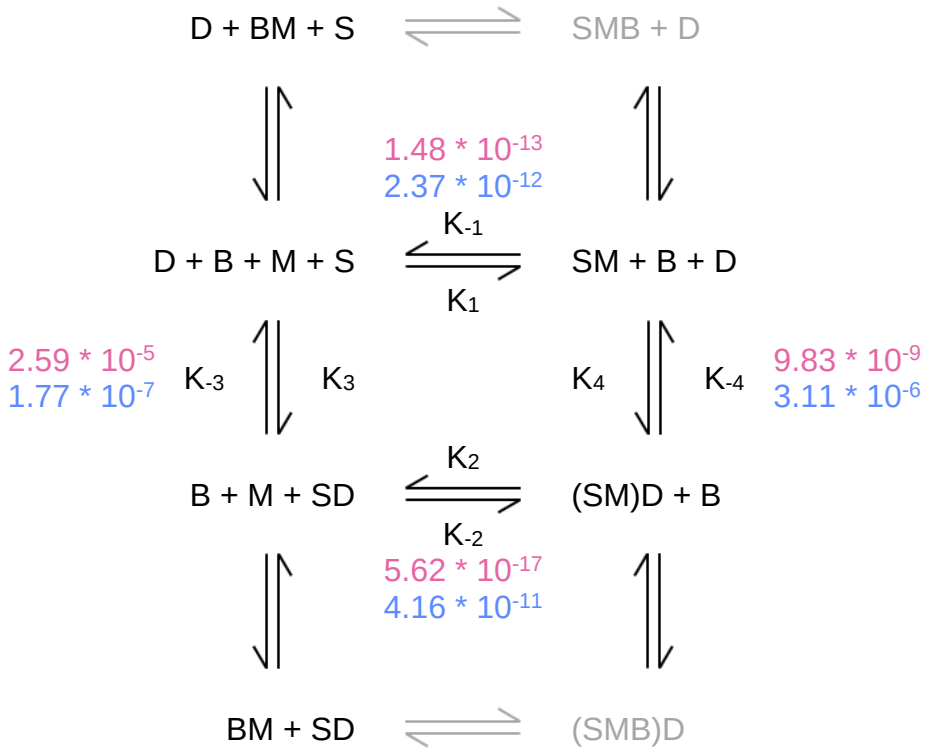

Figure 1.2: Schematic representing the partitioning of metal ions between sensors and buffer molecules

Where D is DNA promoter region, B is the buffer molecule, M is the metal ion, and S is the sensor. Stepwise affinity values (molar) for Ni(II) and DNA binding of NikR and RcnR in *Salmonella* are given in pale magenta and blue, respectively (Scott, 2018). Figure adapted from Scott, 2018 and Osman et al., 2019.

1.4.1 NikR – a Regulator of Ni(II) Import

NikR has increased DNA-binding affinity in the presence of Ni(II), resulting in decreased transcription of *nikABCDE* (De Pina et al., 1999; Chivers and Sauer, 1999; Rowe, Starnes and Chivers, 2005). *nikABCDE* encodes the aforementioned NikABCDE Ni(II) import system. NikR is a modular, tetrameric protein (Schreiter et al., 2006). The primary Ni(II) binding sites (four per tetramer) are located at the interface between C-terminal monomers (Chivers and Sauer, 1999; Chivers and Sauer, 2002; Schreiter et al., 2003). Ni(II) does not control the oligomeric state of NikR (Carrington et al., 2003) but metal binding at the high affinity binding site is required for interaction with DNA (Figure 1.3). Other divalent transition metals are capable of binding NikR *in vitro* and in an absence of buffer, with affinities consistent with the Irving-Williams series, and are capable of activating the sensor for DNA binding, albeit with reduced affinity (Bloom and Zamble, 2004; Leitch et al., 2007).

1.4.2 RcnR – a Regulator of Ni(II) Export

RcnA is a Ni(II) efflux protein (Rodrigue, Effantin and Mandrand-Berthelot, 2005). The expression of *rcnA* is controlled by RcnR, a small regulatory protein and the founding member of the RcnR/ CsoR class of metalloregulators (Iwig, Rowe and Chivers, 2006). RcnR has reduced DNA-binding affinity in the presence of its cognate metals, Ni(II) and Co(II) (Liu et al., 2007; Ma, Jacobsen and Giedroc, 2009), resulting in increased transcription of *rcnA*. Proteins in the RcnR/ CsoR family are tetrameric; the metal binding sites are located between monomers and there are four per tetramer. No structural data for *E. coli* RcnR itself, although a crystal structure is available for InrS, a Ni(II)-responsive member of the RcnR/ CsoR family (Figure 1.4) (Foster et al., 2017). Overall, little is known about allosteric network and conformational changes within RcnR on metal binding. RcnR forms a six-coordinate complex with Ni(II) or Co(II). The coordination involves the only cysteine in the protein, C35 (Iwig et al., 2008). There is also evidence to suggest that H3, H64 and H60 are involved in Ni(II) and Co(II) sensing, but are not essential for Ni(II) coordination (Iwig et al., 2008; Higgins, Chivers and Maroney, 2012; Higgins et al., 2013).

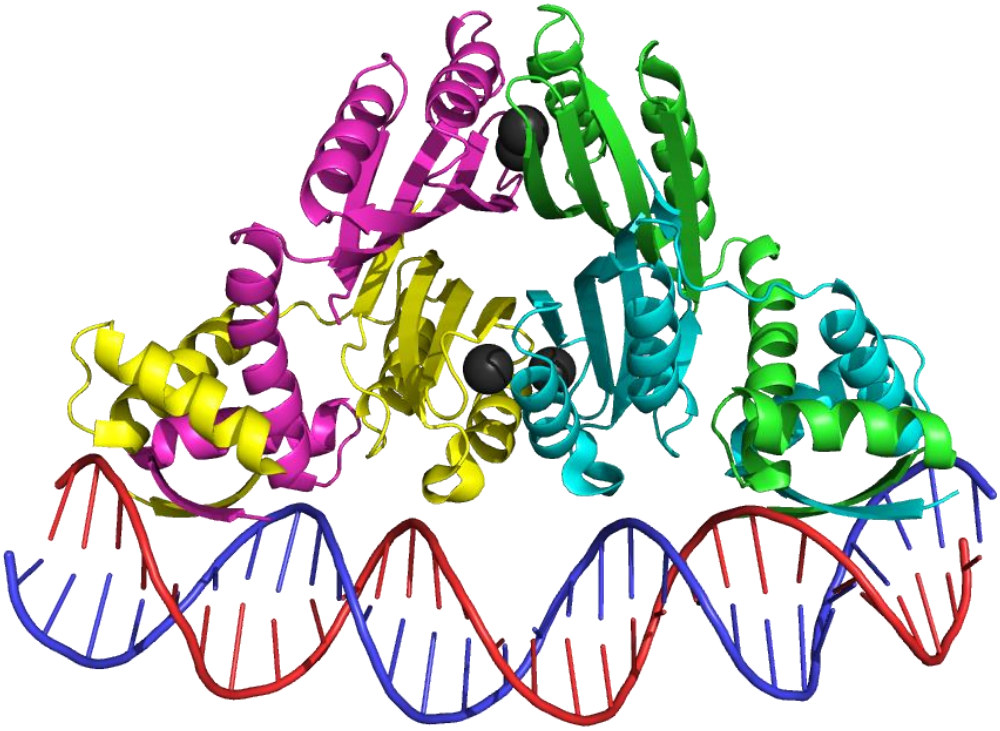

Figure 1.3: NikR is a Ni(II)-dependent co-repressor
Cartoon diagram of metalated *E. coli* NikR tetramer bound to DNA (Schreiter et al., 2006). Each monomer is coloured separately. Ni(II) ions are coloured in grey. Figure generated using PyMOL (Schrödinger and DeLano, 2020).

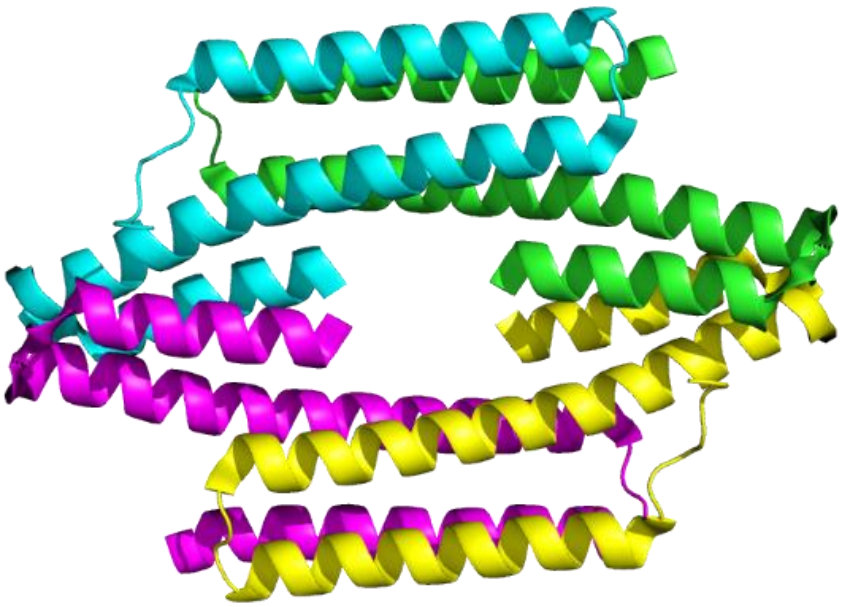

Figure 1.4: Some members of the RcnR/CsoR family of sensors are Ni(II)/Co(II)-dependent de-repressors

Cartoon diagram of InrS from Synechocystis PCC6803 coloured by monomer (Foster et al., 2017). Produced using PyMOL (Schrödinger and DeLano, 2020).

1.5 Identification of a Candidate Ni(II) Buffer in *E. coli*

The Ni(II)-protein requirements and homeostatic machinery in *E. coli* are well understood. However, the components of the cytosolic buffer have not yet been identified. A likely candidate for at least one component of the buffer is His.

NikA, the Ni(II)-binding component of the NikABCDE-transport system, imports a Ni-(L-His)$_2$ complex (Chivers et al., 2012). The effect of His on *nikABCDE* expression under anaerobic conditions was studied using a P_{nik}-*lacZ* reporter. In the presence of 400 μM His, the basal level of P_{nik}-*lacZ* expression was lowered 2.5-fold, correlating with an increased intracellular Ni(II) content. The $NiCl_2$ concentration required to reduce cell growth more than 10% was also shifted. This implies that the transition to complete repression of P_{nik} is a stress response that can be avoided by buffering of Ni(II) ions in a stable complex.

Ni(II) can stably bind His as a Ni-(L-His)$_2$ complex (Figure 1.5). His was previously identified as an *in vitro* competitor for Ni(II) against InrS, an RcnR homolog found in cyanobacteria (Foster et al., 2017). His is present in the cyanobacterial cytosol at concentrations of 45 μM. A ten-fold increase in His did not outcompete InrS for Ni(II), but a 100-fold increase largely outcompeted the sensor. Exclusion of glutathione and ATP, two other metabolites known to form stable Ni(II) complexes (Kaczmarek, Szczepanik and Jezowska-Bojczuk, 2005), did not affect competition of InrS for Ni(II). Hence, the affinity of InrS for Ni(II) is tuned for competition with cytosolic levels of His.

There is further preliminary *in vivo* evidence to suggest His biosynthesis is relevant to Ni(II) stress tolerance. High-throughput phenomic profiling of *E. coli* produced a dataset in which the fitness of single-gene knockouts were assessed on solid media under various stress conditions (Nichols et al., 2011). The tolerance of knockouts in the His biosynthetic pathway for metal stress and the *his* biosynthesis operon are shown in Figure 1.6. The negative relative fitness score indicates that strains unable to synthesise His, even in rich media, are sensitive to metal ions. The pathway also produces 5-aminoimidazole-4-carboxamide ribonucleotide (AICAR), which is required for purine biosynthesis. However, the similar effect of deletions in all biosynthetic genes rules out an effect on purine biosynthesis.

A

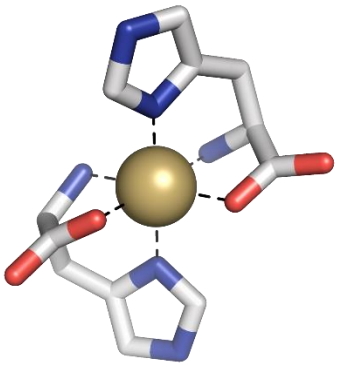

B

$$\text{His} + \text{Ni(II)} \underset{K_D = 0.0155}{\rightleftharpoons} \text{Ni•His} + \text{His} \underset{K_D = 0.2140}{\rightleftharpoons} \text{Ni•His}_2$$

Figure 1.5: Ni(II)•(L-His)$_2$ complex
(**A**) Structure from Fraser and Harding, 1967. Produced using PyMOL (Schrödinger and DeLano, 2020); (**B**) Stepwise formation of the Ni(II)•(L-His)$_2$ complex. Values from Zhang, Akilesh and Wilcox, 2000.

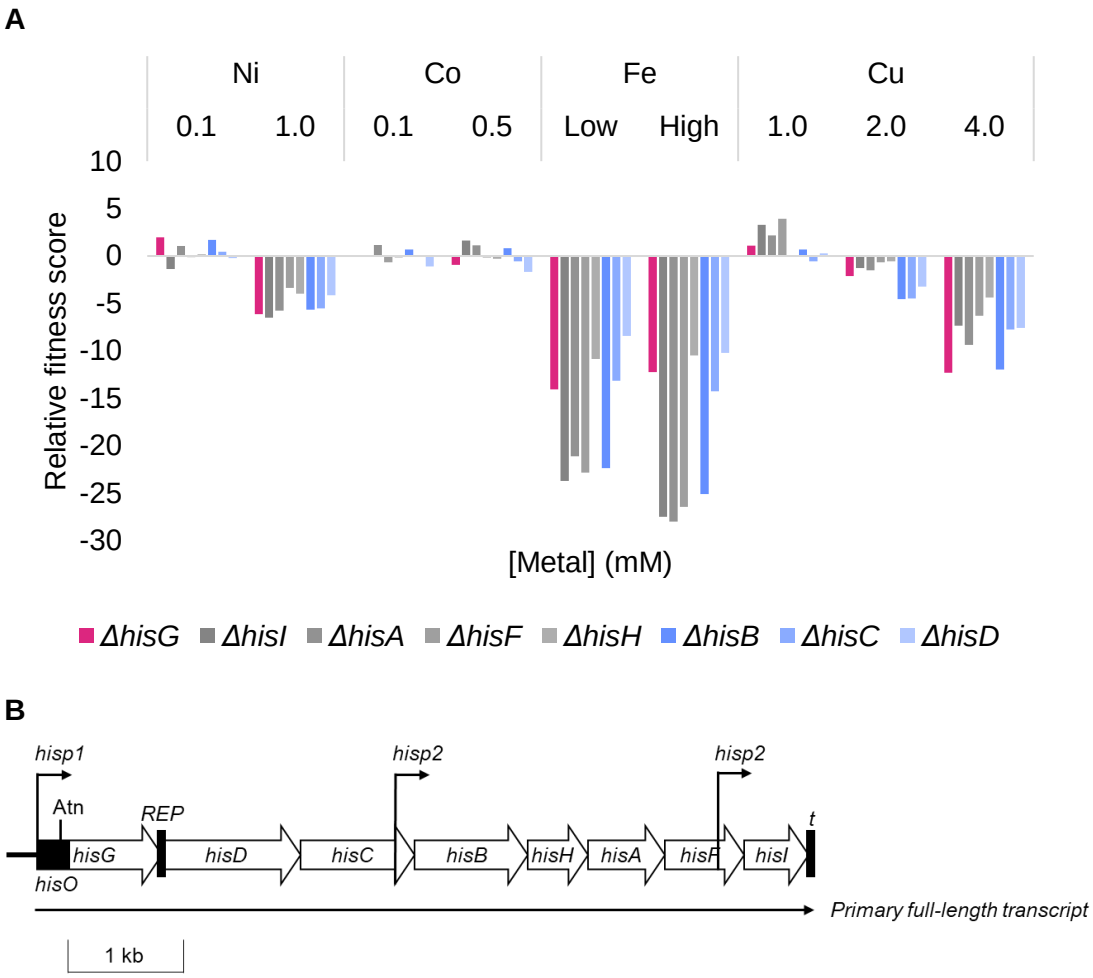

Figure 1.6: Single-gene deletion mutants deficient in the His biosynthetic pathway are less tolerant of metal stress compared to wild-type E. coli

(**A**) Data adapted from Nichols et al., 2011. Metal concentrations are given as presented in the dataset; Fe "Low" and Fe "High" were not defined. Enzymes presented in order of appearance in the biosynthetic pathway (Figure 1.7). *ΔhisG* shown in magenta. Enzymes in the pathway after the production of AICAR are shown in blue; (**B**) The *his* biosynthetic operon in *E. coli. hisp1* is the primary promoter; *hisp2* and *hisp3* are internal promoters; Atn is the *his* attenuator sequence; *t* is the terminator. Adapted from Ramos-Montañez and Winkler, 2009.

This project aims to determine the role of His in Ni(II) buffering. This will be achieved by perturbing the His biosynthetic pathway in *E. coli* to produce a number of strains with differing intracellular His levels.

1.6 Histidine Biosynthesis in *Escherichia coli*

The His biosynthetic pathway is functionally conserved in all organisms able to synthesise His, including bacteria, archaea, lower eukaryotes and plants (Kulis-Horn, Persicke and Kalinowski, 2015). The *his* operon encodes the eight enzymes required for His biosynthesis (Figure 1.6B) (Winkler and Ramos-Montañez, 2009; Kulis-Horn, Persicke and Kalinowski, 2014). Careful management of the pathway is imperative in ensuring cell fitness as the synthesis of one His molecule requires energy equivalent to approximately 41 molecules of ATP (Brenner and Ames, 1971; Winkler and Ramos-Montañez, 2009). The rate of His biosynthesis is controlled in two main ways: by regulating expression of the *his* operon (Section 1.6.1), and by controlling the flow of intermediates through the pathway (Section 1.6.2) (Winkler and Ramos-Montañez, 2009).

1.6.1 Regulation of *his* Operon Expression

The transcription of the *his* operon is thought to be regulated via two mechanisms (Winkler and Ramos-Montañez, 2009):

(1) Initiation of transcription at the primary promoter, *hisp1*, is upregulated in the presence of ppGpp (Stephens, Artz and Ames, 1975; Winkler, Zawodny and Hartman, 1979; Riggs et al., 1986; Shand et al., 1989).

(2) An attenuation mechanism that responds to intracellular concentration of His-tRNA^{His} (Lewis and Ames, 1972). The concentration of tRNA^{His} is determined by cellular His levels, histidyl-tRNA synthetase activity and chromosomal DNA supercoiling levels (Lewis and Ames, 1972; Winkler and Ramos-Montañez, 2009).

When grown in rich medium, the amount of His biosynthetic enzymes decreases fourfold (Brenner and Ames, 1971; Winkler, Roth and Hartman, 1978). This change appears to be in response to ppGpp levels rather than His-tRNA^{His}. Overall, *his*

operon expression appears to be largely unaffected by the presence of His in the growth medium (Stephens, Artz and Ames, 1975; Winkler, Zawodny and Hartman, 1979; Riggs et al., 1986; Shand et al., 1989); even when 77 to 88 % of $tRNA^{His}$ molecules are charged with His, there is still readthrough transcription beyond the attenuator region (Johnston et al., 1980; Johnston and Roth, 1981).

1.6.2 Regulation of HisG

Regulation of HisG, the first enzyme in His biosynthesis (Figure 1.7), is crucial in controlling the flow of carbon towards His biosynthesis (Winkler and Ramos-Montañez, 2009). HisG catalyses the Mg^{2+}-dependent condensation of ATP and phosphoribosylpyrophosphate (PRPP) to form N'-5'phosphoribosyl-ATP (PR-ATP). HisG enzymes can be divided into two subcategories: "long" and "short" form. This project focuses on the long form HisG found in *E. coli* (and *Salmonella enterica* serovar Typhimurium (hereby referred to as *Salmonella*) and *Campylobacter jejuni*, amongst others).

There are four main ways in which HisG is regulated (Brenner and Ames, 1971; Winkler and Ramos-Montañez, 2009; Zhang et al., 2012):

(1) Non-competitive feedback inhibition by His.
(2) Competitive inhibition by ADP and AMP.
(3) Competitive product inhibition by PR-ATP.
(4) Inhibition by the alarmone ppGpp (in the presence of partially inhibiting concentrations of His).

In wild-type *E. coli* and *Salmonella* growing in minimal medium, the rate of His biosynthesis appears to be controlled mainly by regulation of HisG; His-secreting mutants with a feedback-deregulated HisG can be selected for by growth in the presence of the His analogue and HisG inhibitor 2-thiazole alanine (Sheppardz, 1964).

HisG is a homohexamer, with each monomer consisting of three domains (Figure 1.8). Domain I binds ATP, adjacent to the PRPP binding site between Domains I and II. Domain III is located at the C-terminus and contains the site of His binding. The His binds at the interface between two adjacent subunits in the

assembled enzyme. His binding triggers significant conformation change, leading to steric hindrance at the active site (Figure 1.8A-D) (Pacholarz et al., 2017; Mittelstädt et al., 2018). There are several key residues at the site of allosteric inhibition (Figure 1.8E), namely M230, H232 and T252, all of which make direct contacts to the His ligand (Lohkamp et al., 2004).

1.6.3 Engineering HisG to perturb Histidine Production

A number of residues key to controlling the activity of HisG have been identified (Lohkamp et al., 2004). Recent studies aim to engineer strains with maximal His production for industrial purposes (Zhang et al., 2012; Kulis-Horn, Persicke and Kalinowski, 2014; Kulis-Horn, Persicke and Kalinowski, 2015; Wu et al., 2020). Mutations resulting in suspected decreased intracellular His levels have been described but remain poorly characterised (Ng, Ingraham and Marr, 1962; O'Donovan and Ingraham, 1965; O'Donovan, Kearney and Ingraham, 1965; Fink, Kłopotowski and Ames, 1967; Hartman et al., 1971). Some of these mutants were His auxotrophs and were widely used in the Ames test (Mortelmans and Zeiger, 2000).

Overall, the regulation of HisG is well characterised in prokaryotes, making it an ideal target for mutagenesis to alter cytosolic His levels. Although most strain engineering studies use *C. jejuni* or *Salmonella*, these two species carry similar HisGs to *E. coli* (66.2 % and 95.7 % sequence identity, respectively) (Huang and Miller, 1991; The UniProt Consortium et al., 2021).

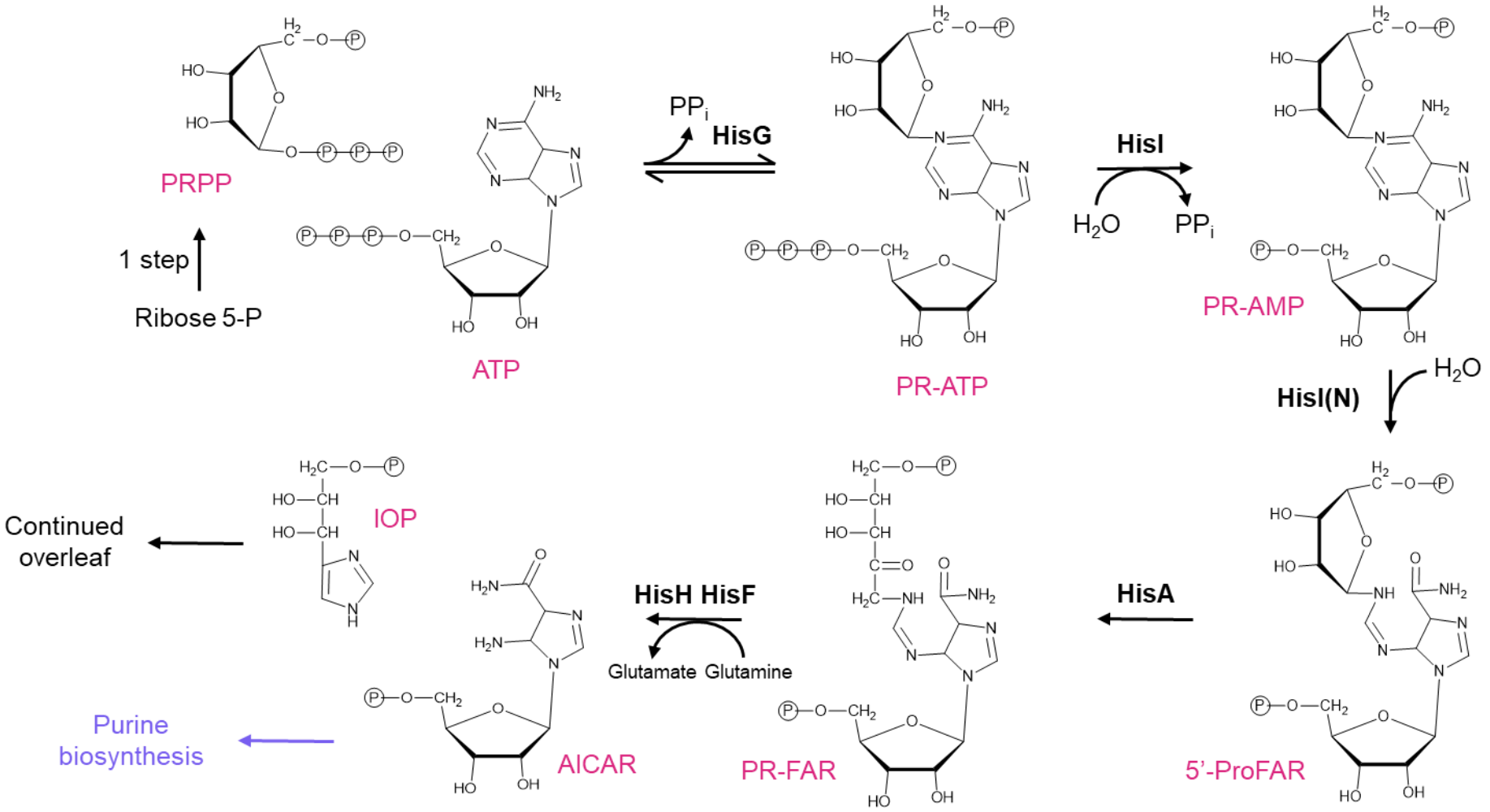
PRPP
1 step
Ribose 5-P
ATP
PPi
HisG
PR-ATP
HisI
H2O
PPi
PR-AMP
HisI(N)
H2O
5'-ProFAR
HisA
HisH HisF
Glutamate Glutamine
PR-FAR
AICAR
IOP
Continued overleaf
Purine biosynthesis

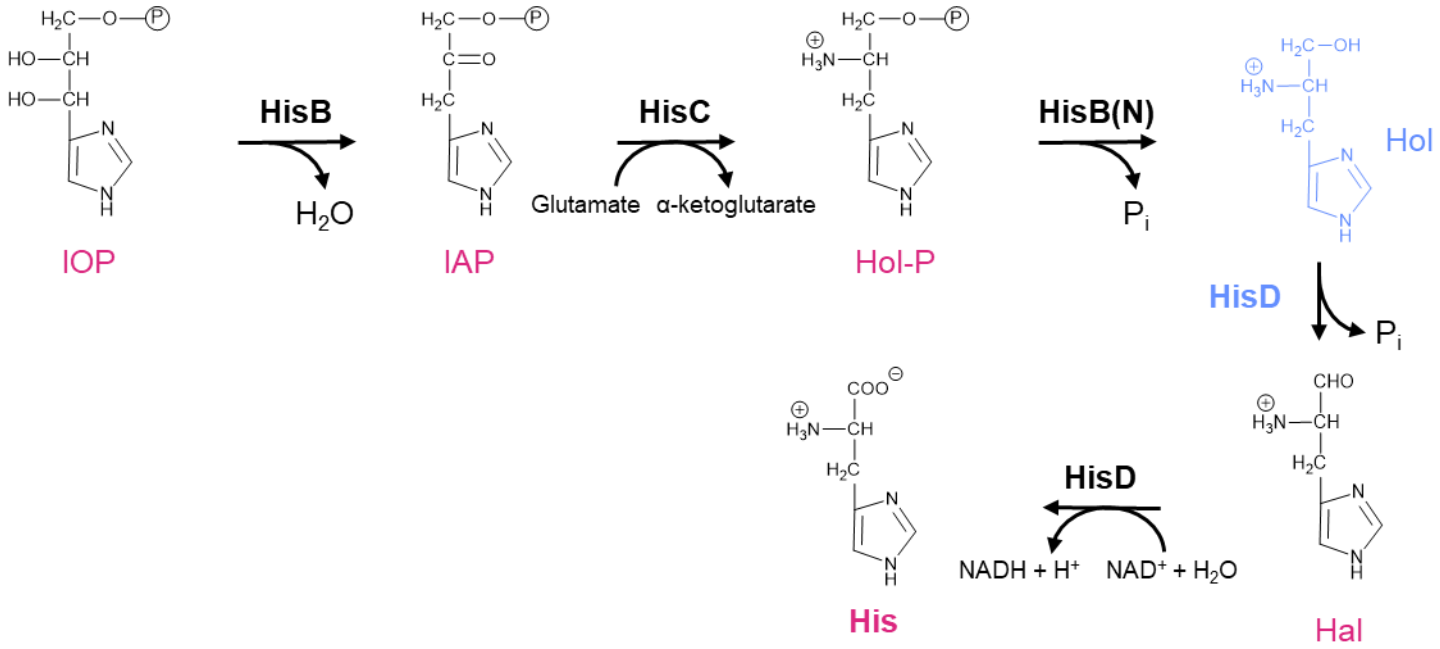

Figure 1.7: The His biosynthetic pathway

PRPP, phosphoribosylpyrophosphate; PPi, pyrophosphate; PR-ATP, N'-5'phosphoribosyl-ATP; PR-AMP, N'-5'phosphoribosyl-AMP; 5'-ProFAR, pro-phosphoribosyl formimino-5-aminoimidazole-4-carboxamide ribonucleotide; PRFAR, phosphoribosyl formimino-5-aminoimidazole-4-carboxamide ribonucleotide; IGP, imidazoleglycerol phosphate; AICAR, 5-aminoimidazole-4-carboxamide ribonucleotide; IAP, imidazole-acetol phosphate; Hol-P, L-histidinol phosphate; Hol, L-histidinol; Hal, L-histidinal. Enzyme activities, HisG, ATP-phosphoribosyl transferase; HisI(C), PR-ATP pyrophosphohydrase; HisI(N), PR-AMP cyclohydrolase; HisA, 5'-ProFAR isomerase; HisH, IGP synthase subunit (glutaminase); HisF, IGP synthase subunit (cyclo-ligase); HisB(C), IGP dehydratase; HisC, Hol-P aminotransferase; HisB(N), Hol-P phosphatase; HisD, Hol dehydrogenase (Winkler and Ramos-Montañez, 2009; Kulis-Horn, Persicke and Kalinowski, 2014). HisD and Hol have been highlighted due to their later relevance to the project.

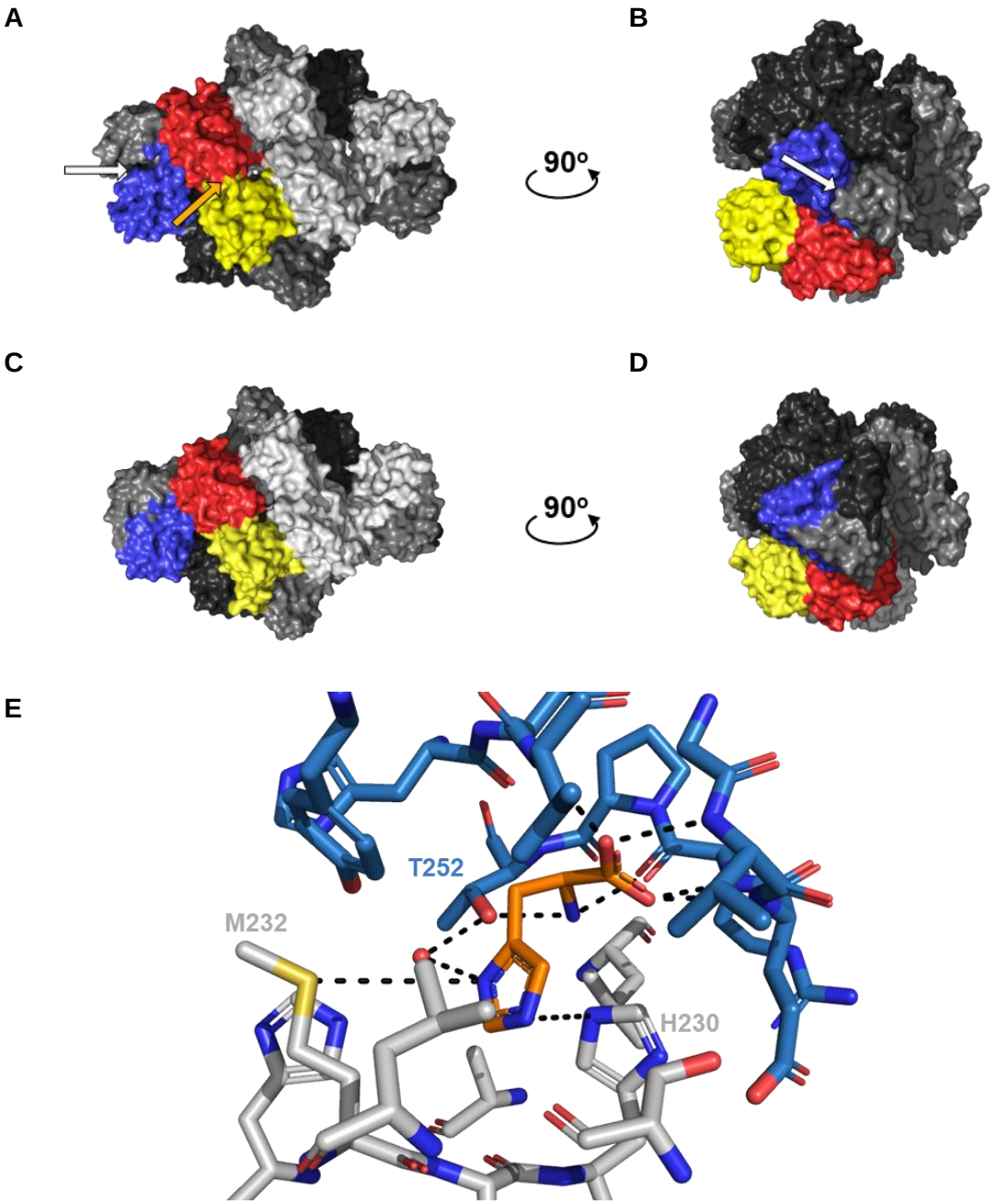

Figure 1.8: The *Campylobacter jejuni* HisG enzyme, $HisG_{Cj}$
(**A**) Active $HisG_{Cj}$ with substrate ATP bound at the catalytic side ; (**B**) Active $HisG_{Cj}$ rotated 90° from (**A**) such that the His binding site is at the forefront; (**C**) Inhibited HisG with competitive inhibitor AMP and allosteric inhibitor His bound; (**D**) Active $HisG_{Cj}$ rotated 90° from (**C**) such that the His binding site is at the forefront; (**E**) Stick representation of the allosteric His binding site, located at the interface between two monomers coloured grey and blue. $HisG_{Cj}$ is a homohexameric enzyme (Mittelstädt et al., 2016); in this figure, one monomer has been coloured according to domain, where Domain I is red, Domain II is yellow, and Domain III is blue (Lohkamp et al., 2004). The other five monomers are varying shades of grey. As labelled in (**A**), orange arrow indicates the catalytic site; white arrow indicates the His binding site for the coloured monomer. $HisG_{Cj}$ has 66.2 % sequence identity with $HisG_{Ec}$ (calculated using Expasy SIM; Huang and Miller, 1991). Figures generated using PyMOL (Schrödinger and DeLano, 2020).

1.7 Aims of the Project

The correct metalation of proteins is vital to life. As proteins are flexible, most are unable to specifically select for their cognate metal (Waldron et al., 2009). Hence, a protein's affinity for a metal is largely determined by the position of said metal within the Irving-Williams series, irrespective of actual cognate metal (Irving and Williams, 1953; Waldron et al., 2009). The cell avoids the mismetallation of proteins by controlling the availability of metal in the cytosol, forming a labile pool of metal in which ions are associated with buffer molecules and there is negligible free metal present (Foster et al., 2017; Osman et al., 2019). The buffer molecules compete with proteins requiring their cognate metal for function, and effectively allow the cell to maintain metal availabilities to the inverse of the Irving-Williams series (Foster et al., 2017; Osman et al., 2019). The sensors responsible for regulating the expression of the systems that enforce homeostasis also interact with this labile pool of metal, and have affinities poised to detect and respond to any changes (Foster et al., 2017; Osman et al., 2019). Whilst the transcriptional responses of sensors have been used to define the availability of metal in the labile pool, the affinity of a sensor for its cognate metal does not determine the size of the labile pool. Instead, the affinity of a sensor is tuned to the buffered availability of metal in the cell and the affinity of a sensor is poised to compete with the polydisperse buffer (Foster et al., 2017). For example, a mutant Ni(II) sensor with lowered affinity for Ni(II) is unable to compete for the metal in the cytosol (Foster et al., 2017). It follows that the interactions between sensors and buffer molecules could further be studied if the amount of buffer molecule present was altered.

This project seeks to test the hypothesis that His may be a component of the cytosolic buffer of Ni(II) in *E. coli*. Using a genetic approach, a point mutation will be introduced within HisG's site of allosteric inhibition. This should produce an enzyme with altered affinity for the allosteric inhibitor His. A library of recombinants with varying intracellular His levels will be produced. These recombinants will then be used to study effect of His on the Ni(II)-dependent transcriptional response of RcnR.

Chapter 2: Materials and Methods

2.1 Media, Reagents and Solutions

Media and solutions used in this project are summarised in Table 2.1 and Table 2.2. All media and solutions were made up in ultra-pure Milli-Q water (18.2 MΩ•cm). Where appropriate, media and solutions were sterilised via autoclaving 121 ℃ for 15 min or via filtration using a 0.22 μm filter.

Table 2.1: Media used in this project

Medium	Ingredients[a]
LB[b]	2.5 g tryptone 1.25 g yeast extract 1.25 g NaCl ddH_2O to 250 mL
1X M63 media[b,c]	50 mL 5X M63 salts[d] 2 mL 50% (w/v) glucose solution 250 μL 1 M $MgSO_4$ 6.25 μL 10 mM $FeSO_4$ 50 μL 100 μM $ZnCl_2$ H_2O to 250 mL

a, given in the quantities typically made in.
b, added 4.25 g agar to generate solid media, final concentration 1.7 % (w/v).
c, hereafter referred to as M63 media.
d, described in Table 2.2.

Table 2.2: Solutions used in this project

Solution	Ingredients[a]
5X M63 salts[b,c]	2.5 g $(NH_4)_2SO_4$ 17 g KH_2PO_4 KOH to pH 7.00 (approx. 5 g) ddH_2O to 250 mL
LacZ assay buffer[d]	16.1 g $Na_2HPO_4 \cdot 7H_2O$ 5.5 g $NaH_2PO4 \cdot H_2O$ 0.375 g KCl 0.125 g $MgSO_4$ ddH_2O to 500 mL
Phosphate-buffered saline[b]	4 g NaCl 0.1 g KCl 0.72 g Na_2HPO_4 (anhydrous) 0.12 g KH_2PO_4 (anhydrous) ddH_2O to 500 mL
0.1 M $NiSO_4$ stock	Lab stock
0.5 M $CoCl_2$ stock	1.19 g $CoCl_2 \cdot 6H_2O$ ddH_2O to 50 mL
SDS separating gel solution[e]	1.625 mL 40 % (v/v) acrylamide (13 % (v/v) final concentration) 1.25 mL Tris-SDS pH 8.8 ddH_2O to 5 mL
SDS stacking gel solution[f]	0.65 mL 40% acrylamide 0.65 mL 4X Tris-SDS pH 8.8b ddH_2O to 5 mL
ICP-MS sample preparation washing buffer	1.19 g HEPES 45.54 g sorbitol ddH_2O to 500 mL

a, given in the quantities typically made in.
b, Ausubel et al, 2002.
c, stirred with Chelex-100 resin (equivalent to 2 mL volume) for 1 hour prior to filtration with 0.22 µm filter.
d, Miller, 1972.
e, add 5 µL TEMED and 50 µL 10% (v/v) ammonium persulfate and mix before pouring.
f, add 5 µL TEMED and 25 µL 10% (v/v) ammonium persulfate and mix before pouring.

Table 2.3: Supplements used in this project

Solution	Ingredients[a]
50 % (w/v) glucose solution	50 g D-glucose 50 mL ddH_2O
10 % (w/v) arabinose solution	Lab stock
Kanamycin	Melford
Ampicillin	Sigma
5X amino acid stock (excl. His)	35.6 mg alanine 452.9 mg arginine 26.4 mg asparagine 26.6 mg aspartate 6.1 mg cysteine 44.1 mg glutamate 43.9 mg glutamine 30.0 mg glycine 26.2 mg isoleucine 52.5 mg leucine 29.2 mg lysine 14.9 mg methionine 33.0 mg phenylalanine 23.0 mg proline 525.5 mg serine 23.8 mg threonine 10.2 mg tryptophan 18.1 mg tyrosine 35.1 mg valine ddH_2O to 100 mL
10 mM adenine stock	67.57 mg adenine ddH_2O to 50 mL
0.2 M histidine stock	Lab stock
0.2 M histidinol stock	Lab stock

a, given in the quantities typically made in.

2.2 Bacterial Strains

E. coli strains used in this project are listed in Table 2.4.

Table 2.4: Strains of *E. coli* used in this project

Strain	Genotype	Source
BW25113 (parent strain)	*lacI*^{q} *rrnB*$_{T14}$ Δ*lacZ*$_{WJ16}$ *hsdR514* Δ*araBA*Δ$_{AH33}$ Δ*rhaBA*Δ$_{LD78}$	Lab stock
BW25113 Δ*hisG*[a]	BW25113 *hisG::kan*^{r}	Dr. David Weinkove (Durham University Department of Biosciences)
BW25113/pKD46[b]	BW25113 *hisG::kan*^{r}; pKD46 *amp*^{r}	Prepared by Dr. Peter Chivers
BW25113 P_{rcnA}-*lacZ*[c]	BW25113 *hisG*$_{WT}$/*hisG*$_{T252}$ P_{rcnA}-*lacZ*	Prepared by Dr. Peter Chivers

a, hereafter referred to as *ΔhisG*.
b, Datsenko and Wanner, 2000.
c, denotes strains carrying a modified *hisG* gene and a P_{rcnA}-*lacZ* reporter construct.

2.3 Molecular Biology Manipulations

This project employed three different PCR processes for the following purposes:

(1) a two-step process was used to generate a DNA fragment carrying a randomised codon (*hisG*$_{T252}$).

(2) colony PCR.

(3) generation of DNA for sequencing.

Oligonucleotide primers used are listed in Table 2.5. The master mix compositions are listed in Table 2.6. The PCR protocols are listed in Table 2.7.

Table 2.5: Oligonucleotide primers used in this project

Code	Description	Sequence (5'-3')
1[a]	*hisG* upstream 5'	CATTCAGATCTTCCAGTGGTGC
2	*hisG* downstream 3'	GCTTTCAGAGGCGGAAATCGC
3	Internal 3' T252	CCAGCGGCAGAATVNNTGGGCGTTCGGC[b]
4	Internal 5' T252	TGCCGAACGCCCANNBATTCTGCCGCTG[b]
k1	Kan forward 3'	CAGTCATAGCCGAATAGCCT[c]
k2	Kan backward 5'	CGGTGCCCTGAATGAACTGC[c]
Seq	Sequencing	CAGCTGGCGTTGTTGCTCCGC

a, Positions of Primers 1, 2, 3 and 4 relative to or within the *hisG* gene are shown in Appendix 1.

b, Codons carrying randomised bases are underlined. B = C, G, or T; N = A, C, G, or T; V = A, C, G.

c, Datsenko and Wanner, 2000. Positions of k1 and k2 within *kan*^{r} are given in Appendix 1.

Table 2.6: Master mix compositions for PCR protocols

Component	Volume (µL) (1) *hisG*$_{T252}$ generation (Step 1 and Step 2)	(2) Colony PCR	(3) *hisG* fragments for sequencing
5X PCR buffer[a]	10	5	10
Template DNA	*Varies*	-	1[b]
5' primer (100 pM/ µL)	0.5	0.25	0.5
3' primer (100 pM/ µL)	0.5	0.25	0.5
10X 4dNTP mix	0.5	0.25	0.5
Taq DNA polymerase[c]	0.5	0.25	-
Pfu DNA polymerase[c]	0.1	-	-
Q5 DNA polymerase[d]	-	-	0.4
	50	25	50

a, 5X Taq DNA polymerase buffer contains 7.5 mM $MgCl_2$ for a final concentration of 1.5 mM. 5X Q5 DNA polymerase buffer contains 10 mM $MgCl_2$ for a final concentration of 2 mM.
b, See Section 2.3.1.
c, Promega.
d, New England Biolabs.

Table 2.7: PCR protocols

Step	Purpose	(1) *hisG*$_{T252}$ generation		(2) Colony PCR	(3) *hisG* fragments for sequencing
		Step 1	Step 2		
1	Initial denaturation	95 ℃, 2 min	95 ℃, 2 min	95 ℃, 5 min	95 ℃, 5 min
2	Denaturation	95 ℃, 30 s	95 ℃, 30 s	95 ℃, 30 s	95 ℃, 10 s
3	Annealing	60 ℃, 30 s	64 ℃, 30 s	60 ℃, 30 s	60 ℃, 30 s
4	Extension	72 ℃, 90 s	72 ℃, 90 s	72 ℃, 60 s	72 ℃, 30 s
		Repeat steps 2-4 × 28	Repeat steps 2-4 × 10 Repeat steps 2-4 × 18 (Step 3 at 59 ℃)	Repeat steps 2-4 × 28	Repeat steps 2-4 × 28
5	Final extension	72 ℃, 5 min	72 ℃, 5 min	72 ℃, 5 min	72 ℃, 5 min
6	Hold	4 ℃	4 ℃	4 ℃	4 ℃

2.3.1 Template DNA preparation using Q5 DNA polymerase

E. coli recombinant strains were grown overnight at 37 °C on LB agar to isolate single colonies. Four to five colonies of a recombinant were re-suspended in 500 µL PBS buffer, then a 200 µL aliquot of the re-suspended cells was boiled (10 min) then centrifuged to remove cell debris (5 min, 13,300 rpm, 4 °C). 5 µL of resulting supernatant was diluted 20-fold in PBS and used as a DNA template.

2.4 Analysis, Purification, and Quantification of DNA Fragments

2.4.1 Analysis of DNA Fragment Amplification by Agarose Gel Electrophoresis

PCR fragments were analysed in 1 % (w/v) agarose gel (made with EtBr 1 µL / 100 mL gel) and 1X TAE buffer (Ausubel, 1996). Gels were run at 100 V for 40-50 min. A 100 bp and/or 1 kb DNA Ladder (ThermoFisher) were used as molecular weight markers. If loading dye was not present in the PCR buffer, then Promega Blue/Orange 6X dye was added to a 1X final concentration. Agarose gels were imaged using a BioRad Gel Doc XR+ Gel Documentation system (Department of Biosciences, Durham University) and the Image Lab Image Capture and Analysis software. Samples volumes of 5 µL were loaded to assess the success of a PCR reaction, and 50 µL volumes were loaded when fragment purification was necessary (Table 2.7).

2.4.2 DNA Purification Methods

Three methods were used for the purification of DNA, based on downstream use and purity of the sample. When necessary to purify the fragment of interest form a mixture, samples were purified from an agarose gel. Bands were excised then purified using a Sigma GenElute™ Gel Extraction Kit following the manufacturer's instructions. Purified DNA was stored at -20 °C.

PCR fragments from colony PCR using for DNA sequencing intended were purified using NEB Monarch PCR & DNA clean-up kit after analysis by agarose gel electrophoresis. Kits were used according to the manufacturer's instructions except that DNA was eluted in 10 µL ddH_2O and stored at -20 °C.

DNA concentrations of PCR products were measured using a Nanodrop Spectrophotometer (Thermo Scientific), using the relationship OD_{260} of 1 = 50 ng / μL dsDNA.

When required to increase DNA concentration prior to subsequent steps, samples were precipitated by ethanol purification either after gel purification or directly from the PCR reaction mixture. For precipitation, 0.1 volume of 3 M sodium acetate (pH 5.5) and 0.7 volume 100 % (v/v) isopropanol were added to the sample and mixed thoroughly. Samples were then centrifuged (30 min at 13,300 rpm, 4 ℃) and the supernatant discarded. The sample was then washed with 70 % (v/v) ethanol (original sample volume) and centrifuged (15 min at 13,300 rpm, 4 ℃), after which the supernatant was then removed and the sample air dried. DNA was resuspended in 10 μL ddH_2O stored at -20 ℃.

2.4.3 DNA Sequencing

DNA was sequenced by DBS Genomics, Durham University. The upstream primer Seq (Table 2.5) was used.

2.5 Transformation of a Δ*hisG* knockout

HisG-recombinants were selectable because of the restoration of growth on solid minimal medium lacking His. *ΔhisG E. coli* containing pKD46 was streaked on LB ampicillin solid medium and incubated at 30 ℃ for 14-16 h. A single colony was picked and inoculated in 5 mL LB containing 0.1 % (w/v) arabinose and 100 μg / mL ampicillin and grown at 30 ℃ until $OD_{600} \approx 0.4$. Cells were chilled on ice for 15 min then pelleted (5 min at 10000 rpm, 4 ℃), the supernatant discarded. The pellet was resuspended in ice-cold ddH_2O (2.5 mL) and centrifuged as above, and the supernatant removed. This wash was repeated twice. The cells were resuspended in ice-cold ddH_2O (50 μL), 1 μL low-salt DNA was added and the sample was electroporated using a Cell-Porator (BioRad) using the manufacturer's pre-set programme for 1.5 mm spacing electroporation cuvettes. Immediately after electroporation, 1 mL of LB was added to the cells and then resulting sample was transferred to a 1.5 mL microfuge tube and incubated at 37 ℃ (190 rpm 1 h) before plating on M63 minimal media and incubating for 18 hours at 37 ℃.

2.6 Growth Curves

Growth curve measurements were performed using a SPECTROstar Nano plate reader (BMG Labtech). Starter liquid cultures were prepared by inoculating 1 mL medium with 1 colony from a fresh LB plate re-streaked from freezer stock. For replicate experiments, separate starter cultures from different individual colonies were set up. Starter cultures were incubated in a benchtop shaker for 18 - 24 h (37 °C, 150 rpm) unless stated otherwise. Prior to use, the OD_{600} of a 1:3 dilution (with ddH_2O) of the O/N culture was measured using a MultiskanGO spectrophotometer (ThermoScientific) to determine the dilution required for the growth curve culture.

A Greiner 24-well plate was used with 600 µL liquid medium per well (path length 0.309 cm, per manufacturers pre-set correction). Any additions to the media (e.g. Ni(II), His or Hol) were prepared from the stocks listed in Table 2.2 and Table 2.3, such that the addition of 5 µL solution resulted in the required final concentration in a 600 µL well. Wells were inoculated with liquid cultures grown overnight to a specified starting OD_{600} value (0.02 when using M63 media; 0.001 when using LB media).

Growth assays were performed for 24 hours. Temperature was maintained at 37°C with 200 rpm double orbital shaking and OD_{600} measurements were taken every 345 seconds (5 min 45 s, the maximum time allowed between measurements for this instrument).

OD_{600} measurements were corrected for background and pathlength as described in Equation 2.1 (where t = time and ℓ = path length). When experiments were performed in biological triplicate, the doubling time of each replicate was calculated using the GrowthCurver R package (see Appendix 2) (Sprouffske and Wagner, 2016). These values were used to calculate the mean and standard deviation of the doubling time for a given recombinant and Ni(II) concentration. Lag times were manually calculated for each replicate. Similar to doubling time, the value from each replicate was used to calculate the mean and standard deviation for a given recombinant and Ni(II) concentration.

$$\mathrm{OD}_{600_{\mathrm{corrected}}} = \frac{\mathrm{OD}_{600_t} - \mathrm{OD}_{600_{t=0}}}{\ell} \qquad 2.1$$

2.7 LacZ Expression Assays

Ni-dependent gene expression of recombinants generated in Section 2.5 was assayed via a single-copy P_{rcnA}-*lacZ* reporter introduced into each strain by P1 phage transduction. Due to time constraints, these transduction were performed by Dr. Peter Chivers.

Liquid growth assays were set-up as described in Section 2.6 using M63 media and a range of Ni(II) concentrations. Two protocols were used for the addition of Ni(II) stock. To study the acute response to Ni(II) stress, cells were grown to $OD_{600} \approx 0.35$ before Ni(II) stock was added. The cells were then grown for a further hour before measuring LacZ activity. To study the chronic response to Ni(II) stress, cells were grown in media containing Ni(II) from inoculation with O/N cultures and LacZ activity was measured at $OD_{600} \approx 0.35$. To measure LacZ activity, 200 μL liquid culture was removed and mixed with 300 μL LacZ buffer, two drops of chloroform, and one drop of 0.1 % (v/v) SDS. Samples were vortexed for 5 s to permeabilize the cell wall then incubated at 28 °C for 10 minutes before adding 100 μL ONPG (4 mg / mL). Reactions were quenched (250 μL 0.1 M Na_2CO_3) when a yellow colour was visible. The quench time varied depending upon the amount of Ni(II) in the sample. Quenched samples were centrifuged (15 min at 13,300 rpm, 4 °C) to remove cell debris and OD_{420} measurements were recorded using the Multiskan GO spectrophotometer.

Miller Units (or LacZ activity) were be calculated using Equation 2.2 (t = incubation time (min); V = volume of cell culture per 1 mL reaction; Miller, 1972).

$$MU = \frac{1000 * OD_{420}}{t * V * OD_{600}} \qquad 2.2$$

When performed in biological triplicate, the relative LacZ activity of each measurement was calculated by dividing each measurement by the highest LacZ activity of WT2. These values were then used to calculate the mean and standard deviation of the relative LacZ activity.

2.8 SDS-PAGE

All buffers used for SDS-PAGE were as described in Ausubel et al, 1996.

Overnight liquid cultures were prepared as described in Section 2.6 using M63 media and used to inoculate 1 mL cultures at OD_{600} = 0.05. Cultures were grown until OD_{600} ≈ 0.6, at which point 100 µL was removed. Cells were pelleted (5 min at 13,300 rpm, 4 °C) and the supernatant removed. Pellets were resuspended in 50 µL 1X SDS sample buffer. Samples were lysed (95 °C, 10 min) and cell debris was removed by centrifugation (5 min at 13,300 rpm, 4 °C). Samples were run on 13 % (v/v) polyacrylamide separating gels with 1X SDS running buffer at 200 V for ~ 45 min. After electrophoresis, gels were stained with InstantBlue™ (Expedeon) for a minimum of 1 hour. PageRuler™ protein molecular weight ladder was used to estimate protein size. Gels were imaged using the BioRad Gel Doc XR+ system.

Gels were further analysed using ImageJ (Schneider, Rasband and Eliceiri, 2012). The Gel Doc capture was converted to 16-bit greyscale image and inverted. Lanes were selected using the "Rectangle Selection Tool"; the "Analyze > Plot Profile" function was then used to summarise the Grey Values as a function of distance for each lane. These traces were used to identify bands that differed between wells.

2.9 His Secretion Bioassay

A plate assay was developed to test for His secretion by HisG T252 variants, based on well-established approaches (Sheppardz, 1964). Here, an *E. coli ΔhisG* starter culture was prepared as described in Section 2.6 using M63 media supplemented with 1 mM His or Hol. This culture was diluted back to an initial OD_{600} of 0.05 in 1 mL of supplemented M63 media and grown until OD_{600} ≈ 0.3 (3 – 5 h, 37 °C, 190 rpm). The remaining culture was centrifuged (5 min, 13,300 rpm, 4°C) and the supernatant removed. The cell pellet was resuspended in M63 media and the centrifuged again. This step was repeated twice to remove residual His or Hol from the growth medium. After the second wash and centrifugation, the pellet was stored on ice before resuspension in 1 mL M63 media followed by immediate mixing with 4 mL molten M63 agar (1 % (w/v) agar; ~ 40 °C). This mixture was immediately poured onto a previously prepared M63 plate (1 % (w/v) agar; ~ 0.5 cm depth) to create a top agar layer containing *ΔhisG*. Plates were allowed to air dry for 20-30 minutes. 3 µL liquid cultures were spotted onto plates, allowed to air dry for 20-30 minutes, and incubated for 18 hrs at 37 °C. Agar

plates were imaged using a BioRad Gel Doc XR+ Gel Documentation system and the Image Lab Image Capture and Analysis software or using a phone camera.

2.10 Calibration of Cell Culture Optical Density Measurements

Two spectrophotometers (SPECTROstar Nano plate reader, BMG Labtech and Multiskan GO spectrophotometer, Thermo Scientific) were used in this project to monitor bacterial liquid culture density. Two approaches were used to calibrate OD_{600} readings between instruments and with colony forming units to identify potential changes in cell-size or morphology in recombinants.

For calibrating readings between instruments liquid growth cultures were set up as described in Section 2.6. At specific OD_{600} values on the plate reader, 200 µL aliquots of liquid culture were removed and their OD_{600} values then measured using the UV spectrophotometer. The two values were plotted to identify deviations from 1:1 correlation for the parent strain and selected T252 variants.

To calibrate OD_{600} with CFU/mL, liquid growth cultures were set up as described in Section 2.6. Cells were grown to the desired OD_{600}, and 10 µL aliquots were removed, added to 990 µL sterile ddH_2O (1:100 dilution) and vortexed to thoroughly mix the cells. Then, 1 µL of each dilution was added to 999 µL ddH_2O (1:1000 dilution) and vortexed as above. Finally, 100 µL of these final dilutions (overall 1:100000) were spread on an LB agar plates and grown for 18 h at 37 °C. Colonies were counted using OpenCFU software (Geissmann, 2013) with some manual adjustments, and the data plotted to determine the correlation between OD_{600} and CFU mL^{-1} for each variant.

2.11 ICP-MS Analysis of Ni(II) Content

Metal content of $NiSO_4$ stocks and liquid growth cultures were measured using inductively coupled plasma mass spectrometry (ICP-MS). Liquid growth assays were performed in biological triplicate as described in Section 2.6 using M63 media. Ni(II) stock was added at the beginning of the growth assay. Liquid cultures (5 mL) were grown until OD_{600} ~ 0.35. Cultures were then transferred to an ice-bath for 10 min to stop cell growth. Cells were pelleted (10 min at 4000 rpm, 4 °C) and the supernatant removed. The pellet was resuspended in ice-cold isotonic HEPES/Sorbitol buffer

containing 500 μM EDTA and the sample centrifuged as above. The pellets were resuspended and pelleted a further two times, omitting the EDTA from the buffer. After the last centrifugation, the pellets were resuspended in 400 μL 65 % (v/v) HNO_3 and incubated for 48 h at 20 °C to allow digestion of organic matter.

The digested samples were centrifuged to remove any debris (15 min at 13.3 k rpm, 4 ℃). 300 μL of the sample was then added to 2.4 mL 2.5 % (v/v) HNO_3 and 300 μL 100 ppb Ag internal standard solution and mixed by vortexing.

Different $NiSO_4$ stocks were diluted to generate concentrations between 30 – 100 ppb in 2.4 mL (2.5 % (v/v) HNO_3), after which internal standard solution (300 μL 100 ppb Ag300) and matrix match (300 μL 65 % (v/v) HNO_3) were added. A standard curve (from 0 to 100 ppb) was prepared by diluting pre-prepared multi-metal stocks (Mn, Fe, Co, Ni, Cu and Zn) into 2.5 % (v/v) HNO_3 (total volume 2.4 mL), then adding internal standard and matrix match as above.

Samples were stored at room temperature and analysis of $^{60}Ni(II)$ content was carried out within days by the Durham University ICP-MS facility (Dr. Andrew Foster).

2.12 Dynafit Modelling

The DNA occupancy of RcnR and NikR as a function of Ni(II) content was analysed using Dynafit (Kuzmič, 1996). Dynafit uses a nonlinear least squares regression to generate fits for experimental data (Kuzmič, 1996). The interactions between DNA promoter, sensor and metal are defined in Figure 1.2. His was simulated to interact with Ni(II) in a 2:1 ratio as described in Figure 1.5 The cytosolic His concentrations of *E. coli* grown on various carbon sources (Table 2.8) were used to guide concentrations of buffer molecules (Bennett et al., 2009).

The script used in this project are given in Appendix 3. This Dynafit script can be used to model the DNA occupancy of the Ni(II) and Co(II)-responsive sensor RcnR as a function of Ni(II) concentration in the presence buffer molecule(s) (Kuzmič, 1996; Scott, 2018; Bowers, 2020). For presentation in this report, DNA occupancy was normalised as described in Equation 2.3.

$$\text{Normalised Fractional DNA occupancy} = \frac{\text{Fractional DNA occupancy}}{\text{Maximum Fractional DNA occupancy}} \quad 2.3$$

Ni(II) concentrations were converted to number of Ni(II) atoms per cell as described in Equation 2.4, where the concentration is given in μM, N_A is Avogadro's number ($6.02 * 10^{23}$ mol^{-1}), and V is the volume of an *E. coli* cell ($1 * 10^{-15}$ L).

$$\text{Atoms per cell} = \text{concentration} * 10^{-6} * N_A * V \quad 2.4$$

Table 2.8: Concentrations of His and Asp in aerobic, exponentially growing *E. coli*

Carbon source	His (μM)
Glucose	45.8 – 99.7
Glycerol	97.8 – 313
Acetate	43.9 – 217

Values from Bennett et al., 2009.

Chapter 3: Results

The experiments presented herein test the hypothesis that L-Histidine (His) buffers Ni(II) ions in a bacterial cytosol. By mutating the *hisG* gene to perturb the inhibition of HisG by His, a library of recombinant *E. coli* strains with modified cytosolic His levels was produced. These recombinants were then compared against a wild-type recombinant, and each other, in various assays to test for changes in Ni(II) buffering that would correlate with His levels.

This project was planned to accommodate reduced lab access due to social distancing restrictions for the first 6 months. Unfortunately, normal lab access was not possible until after 9 months, which limited attempts to carry out experiments to measure intracellular His levels, in particular. A detail summary of effects on this project are summarised in the attached Covid-19 Academic Impact Statement. Planned and suggestions for future work are also included in the Discussion of this report.

3.1 A Histidine Biosynthesis Mutant is Sensitive to Ni(II) Stress in Rich Medium

Previous work (Nichols et al., 2011) studying single-gene knockouts in *E. coli* suggested that knockout mutants in genes of the His biosynthetic pathway are sensitive to metal stress when grown on solid media (Figure 1.6). To verify this result, a Keio *hisG* knockout, Δ*hisG*, was obtained (Baba et al., 2006) (Table 2.4). The presence of a kan^r insertion was confirmed by examining the size of the *hisG* gene (Figure 3.1).

A

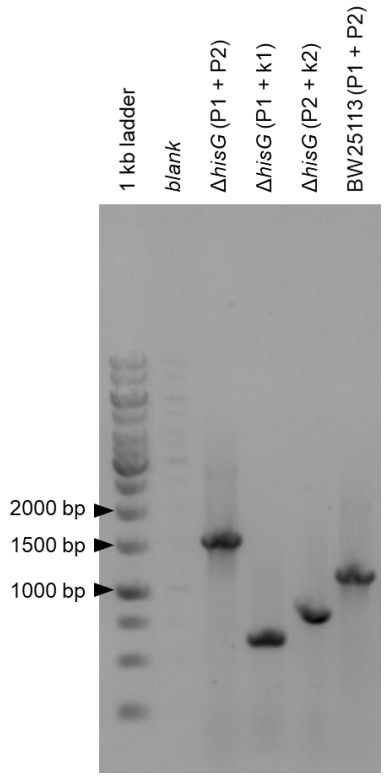

B

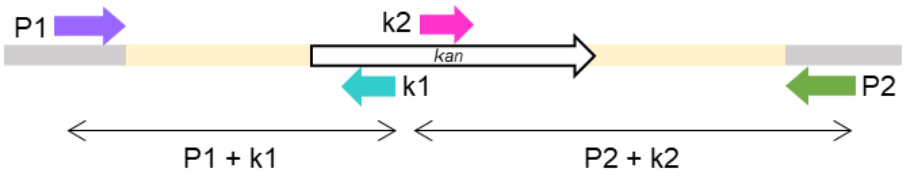

Figure 3.1: *ΔhisG* contains a *kan*^{r} insertion

(**A**) PCR analysis of BW25113 and *ΔhisG* to verify successful *hisG* disruption. Half of a 1 mm colony from a M63 agar plate was applied to the side of test tube prior to addition of master mix. The exact expected size of the fragments is unknown as the regions in yellow in panel B are not characterised. Primers are as given in Table 2.5; (**B**) Schematic describing the structure of *hisG* containing the *kan*^{r} disruption, as described in Datsenko and Wanner, 2000. Diagram is not to scale.

As the previous study only assessed growth on solid media (Nichols et al., 2011), the effect of Ni(II) stress on growth of *E. coli* Δ*hisG* in LB liquid medium was investigated. Parent BW25113 and Δ*hisG* mutant were grown with varying concentrations of Ni(II) (Figure 3.2). In the absence of additional Ni(II) (Figure 3.2A), there are slight differences in the shapes of the curves attributable to the apparent biphasic growth of BW25113 during exponential phase. BW25113 also reached an apparent higher final OD_{600} than Δ*hisG*, but this cannot be necessarily be attributed to a higher cell density due to the complex relationship between OD_{600} and cell size in stationary phase (Stevenson et al., 2016). The addition of Ni(II) had a greater effect on the growth of the Δ*hisG* strain. Doubling times and lag times were calculated from the growth curve data to confirm these differences (Table 3.1). This data is consistent with His biosynthesis being relevant to Ni(II) stress tolerance, even in rich media that can support His auxotrophy. HisG mutants impaired in feedback inhibition by His may display varying Ni(II) stress tolerance phenotypes through altered cytosolic His levels, compared to the wild-type strain.

3.2 Construction of *hisG* Mutant Library

To create a library of recombinants with mutations in *hisG*, a two-step overlap extension process was used to generate a *hisG* fragment carrying a randomised codon at the position of T252 ($hisG_{T252}$) (Figure 3.3 and Figure 3.4). A wild-type *hisG* fragment ($hisG_{WT}$) was generated as a control using P1 and P2 and the master mix composition and PCR protocol used in the first step of $hisG_{T252}$ generation.

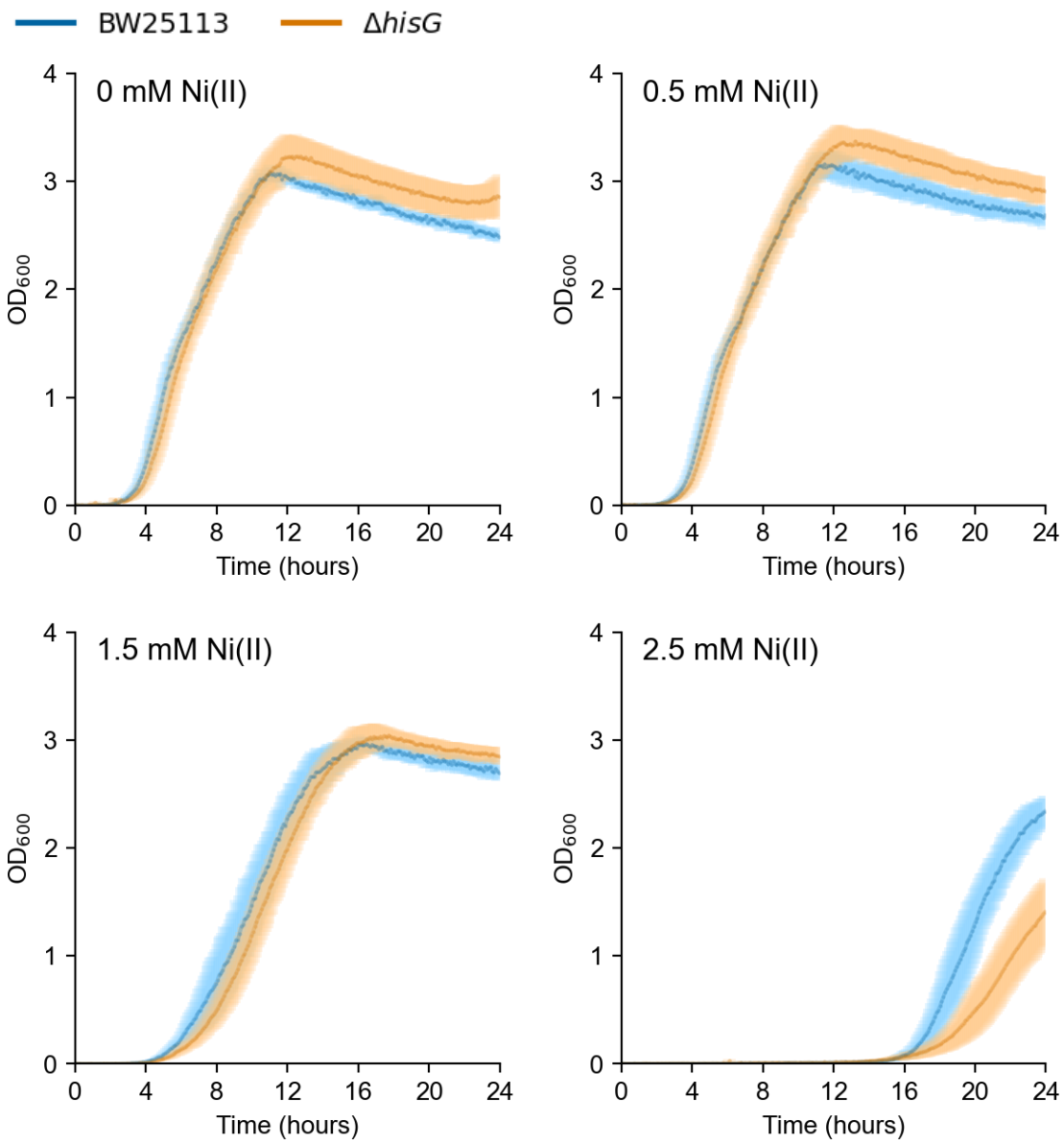

Figure 3.2: *ΔhisG* is more susceptible to Ni(II) toxicity than BW25113 in LB media
Growth curves set up as described in Section 2.6. Solid line is the average of biological triplicates. Shaded areas represent standard deviation. Analysis of doubling and lag times presented in Table 3.1.

Table 3.1: Lag and doubling times for BW25113 and *ΔhisG* in LB[a]

	Strains			
	Lag time[b]		Doubling time[c]	
[Ni] (mM)	**BW25113**	**Δ*hisG***	**BW25113**	**Δ*hisG***
0	3.48 ± 0.224	3.83 ± 0.287	0.78 ± 0.004	0.84 ± 0.023
0.5	3.45 ± 0.192	3.83 ± 0.287	0.86 ± 0.014	0.90 ± 0.025
1.5	5.69 ± 0.334	6.36 ± 0.471	0.99 ± 0.032	1.06 ± 0.006
2.5	17.19 ± 0.81	18.14 ± 0.952	0.78 ± 0.059	1.08 ± 0.056

a, Analysis of data from Figure 3.2 using the GrowthCurver R package (Appendix 2) (Sprouffske and Wagner, 2016). Values are the average and standard error of the triplicates.
b, the period of time when $OD_{600} < 0.15$.
c, the time required to double OD_{600} during the exponential phase of growth

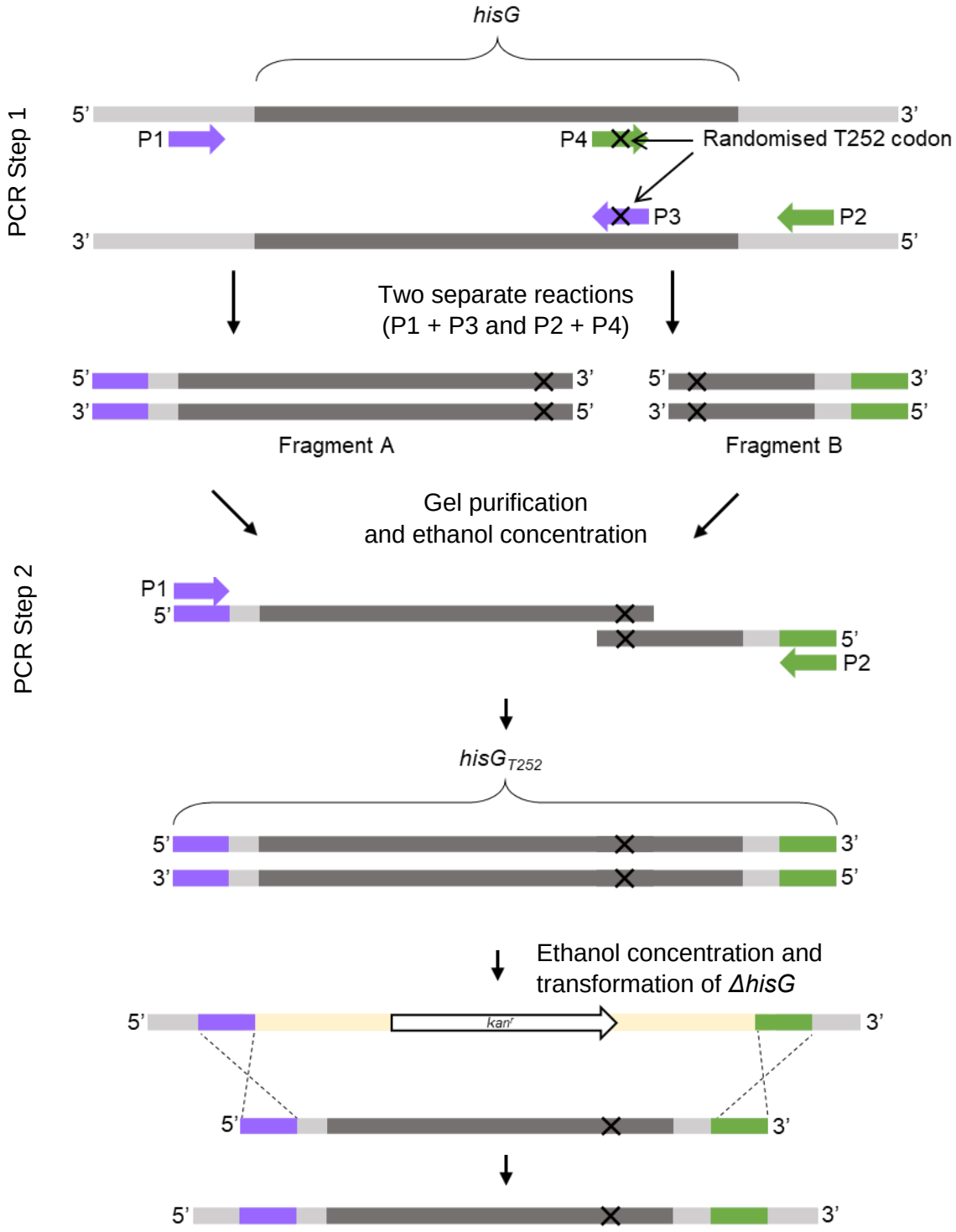

Figure 3.3: The stepwise construction of *hisG*$_{T252}$ recombinant *E. coli* strains
Step 1 produced Fragments A and B at concentrations of 32.4 ng/µL and 9.1 ng/µL, respectively, following gel purification and concentration. A and B were diluted back to 2 pM/µL with ddH_2O prior to use in step 2. The full-length fragments were concentrated, reconstituted in 5 µL ddH_2O to final concentrations of 852 ng/µL for *hisG*$_{WT}$ and 94 ng/µL for *hisG*$_{T252}$ and stored at -20 °C prior to use in transformation. Primers are described in Table 2.5; master mix composition as described in Table 2.6; PCR protocol as described in Table 2.7. Diagram not to scale.

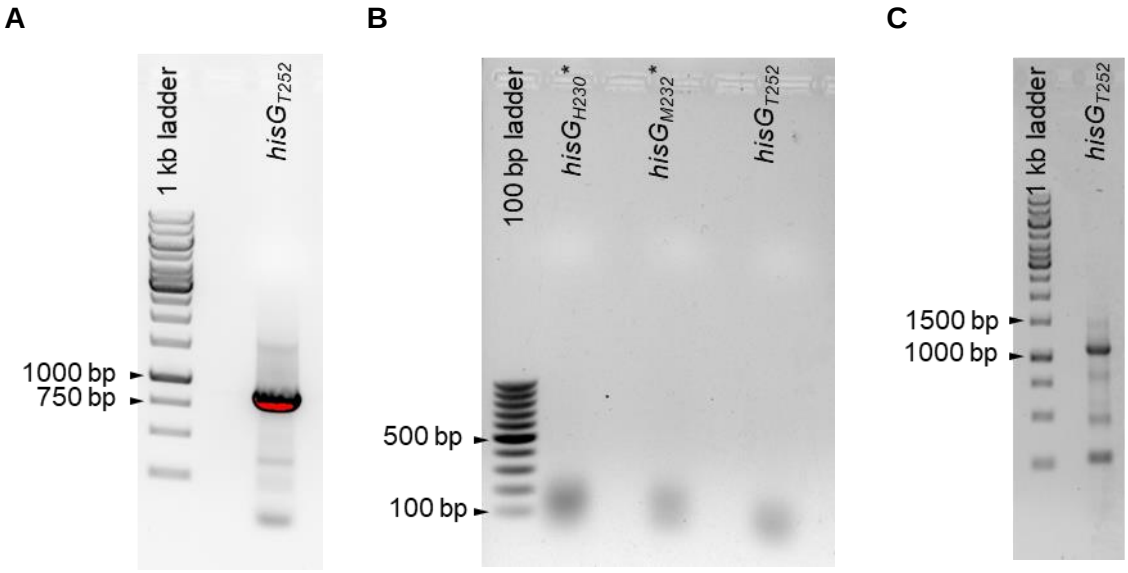

Figure 3.4: Gel analysis confirms the size of DNA fragments used to construct *hisG$_{T252}$*

(**A**) Preparative gel analysis of Step 1 reaction to generate the longer 5' *hisG* fragment A (Primers 1 and 3, Figure 3.3; expected size 887 bp); (**B**) Preparative gel analysis of Step 1 reaction to generating the shorter hisG$_{T252}$ fragment B (Primers 2 and 4, Figure 3.3; expected size 258 bps. **hisG*$_{M230}$ and *hisG*$_{H232}$ Fragments B were not used further in this work; (**C**) Analytical gel demonstrating generation of full length *hisG$_{T252}$* fragment (expected size 1117 bp) from 0.25 pM of Fragments A and B. These images are unmodified and the red colour represents signal saturation.

Transformation of *E. coli* Δ*hisG* with $hisG_{T252}$ or $hisG_{WT}$ DNA fragments (Figure 3.3) was used to generate a pool of recombinants. Successful recombination was identified using the following basic screens:

(1) Recombinant cells were grown on minimal medium agar plates to select for His-producing transformants. After this initial selection, single colonies were picked and re-streaked again on minimal agar to prepare LB freezer stocks. A total of 30 $hisG_{T252}$ colonies (T1-T30) and 8 $hisG_{WT}$ colonies (WT1-WT8). Recombinants T16 and T18 did not grow in LB after re-streaking and were omitted from any further analysis.

(2) An aliquot of the LB culture was also spotted on an LB agar plate supplemented with 25 μg / mL kanamycin (Figure 3.5) to screen for loss of the kan^r cassette through lack of growth. Only WT5 was insensitive to Kan and was excluded from any further analysis.

(3) Colony PCR was then performed using Primers 1 and 2 to verify restoration of the *hisG* locus (1117 bp). All recombinants analysed in this step (Figure 3.6) showed the correctly sized band.

3.3 Preliminary Screening for Ni(II) Sensitivity in Minimal Medium

An initial screen of the recombinant strains for Ni(II) sensitivity in M63 minimal liquid medium was performed. Growing strains in minimal medium requires them to produce His, potentially highlighting any differences in His biosynthesis between recombinants and their Ni(II) tolerance (Figure 3.7).

The preliminary screen used a protocol slightly modified from Section 2.6. Inoculum cultures were grown for 6-8 hours before dilution to the same starting OD_{600}. This meant that variations in growth stage of the inoculum sometimes affected the appearance of the growth curve and explains the observed differences of WT2 growth between runs. For example, Figure 3.7D would imply that WT2 is extremely sensitive to Ni(II) stress at the concentrations tested, but instead this is attributed to poor growth during the day. Nevertheless, these curves were integral in screening for broad differences in Ni(II) tolerance to identify potentially interesting $hisG_{T252}$ recombinants (Figure 3.7).

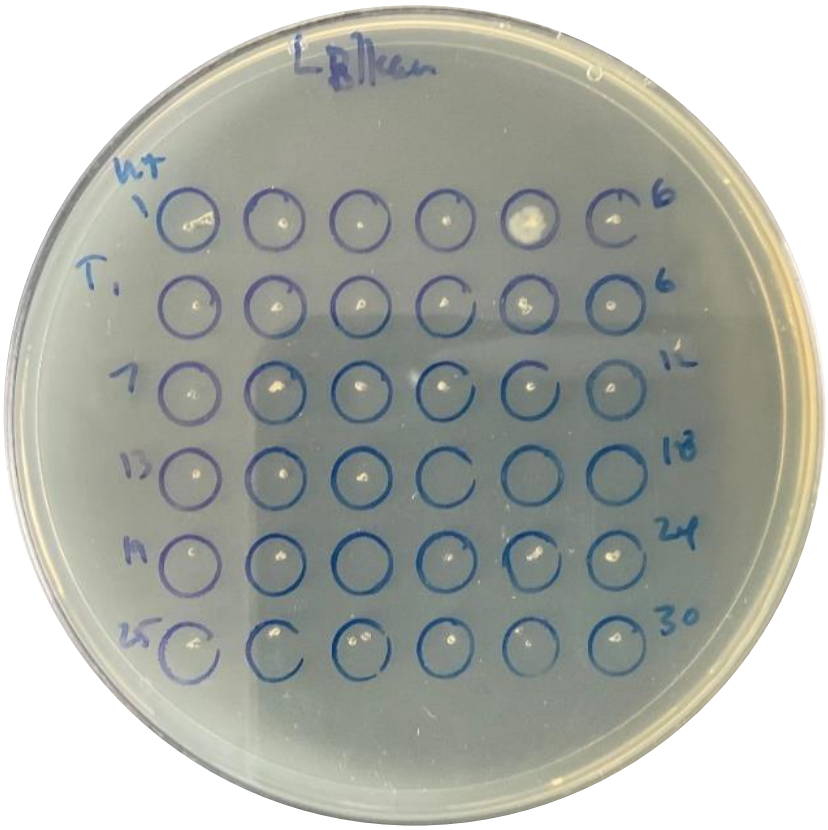

Figure 3.5: Kanamycin resistance is lost after *hisG* locus is restored
Liquid cultures (2.5 µL) of recombinants WT1-6 (top row) and T1-30 (rows 2 to 6) were spotted on an LB agar plate supplemented with 25 µg/mL kanamycin and grown for 24 h (30 °C). The small dots in the center of each circle are due to agar penetration during sample application.

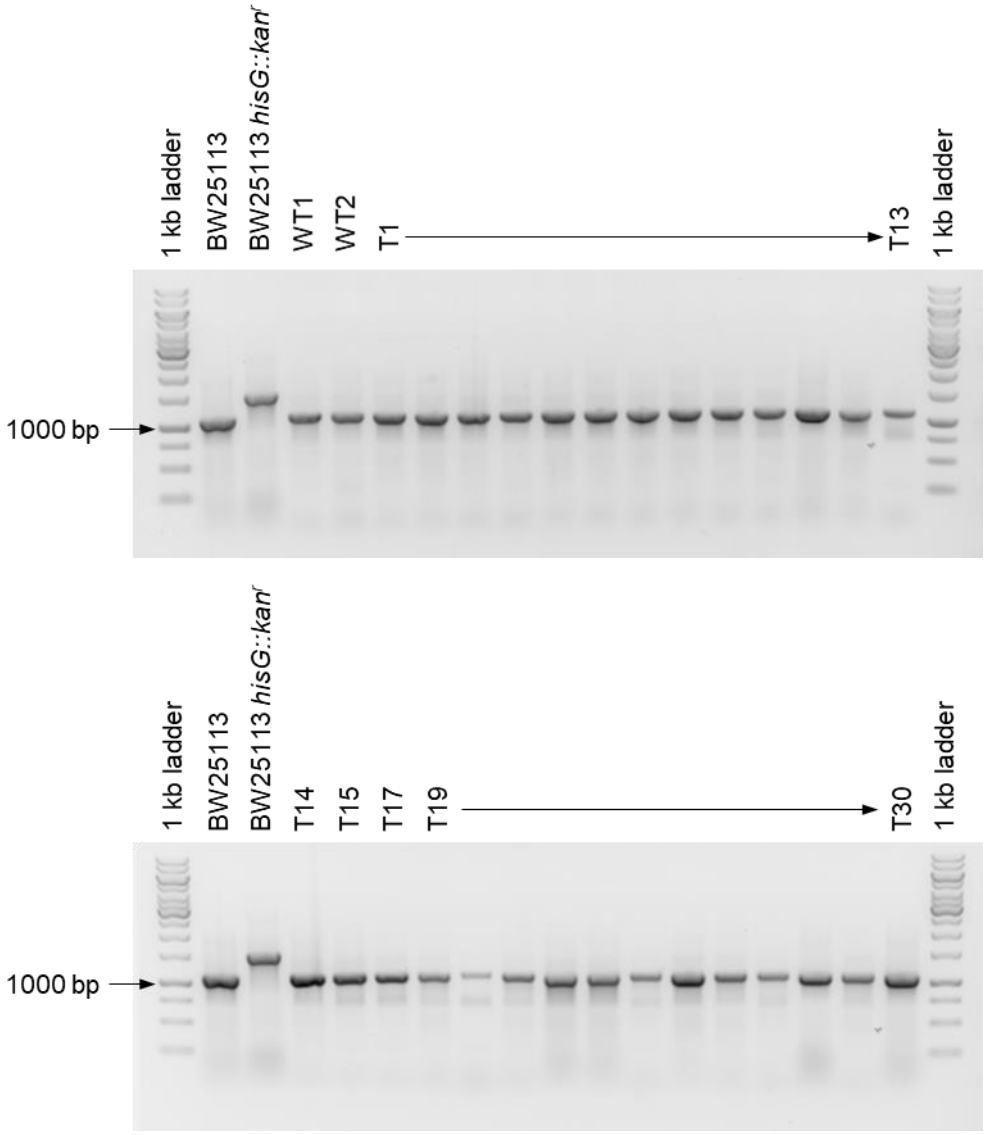

Figure 3.6: PCR analysis of recombinants confirms restoration of *hisG* locus
Half of a 1 mm colony from a M63 agar plate was applied to the side of test tube prior to addition of master mix. Expected BW25113 fragment size: 1117 bps. Expected *ΔhisG* fragment size: ~1500 bps. Used Primers 1 and 2 (Table 2.5); master mix composition as described in Table 2.6; PCR protocol as described in Table 2.7.

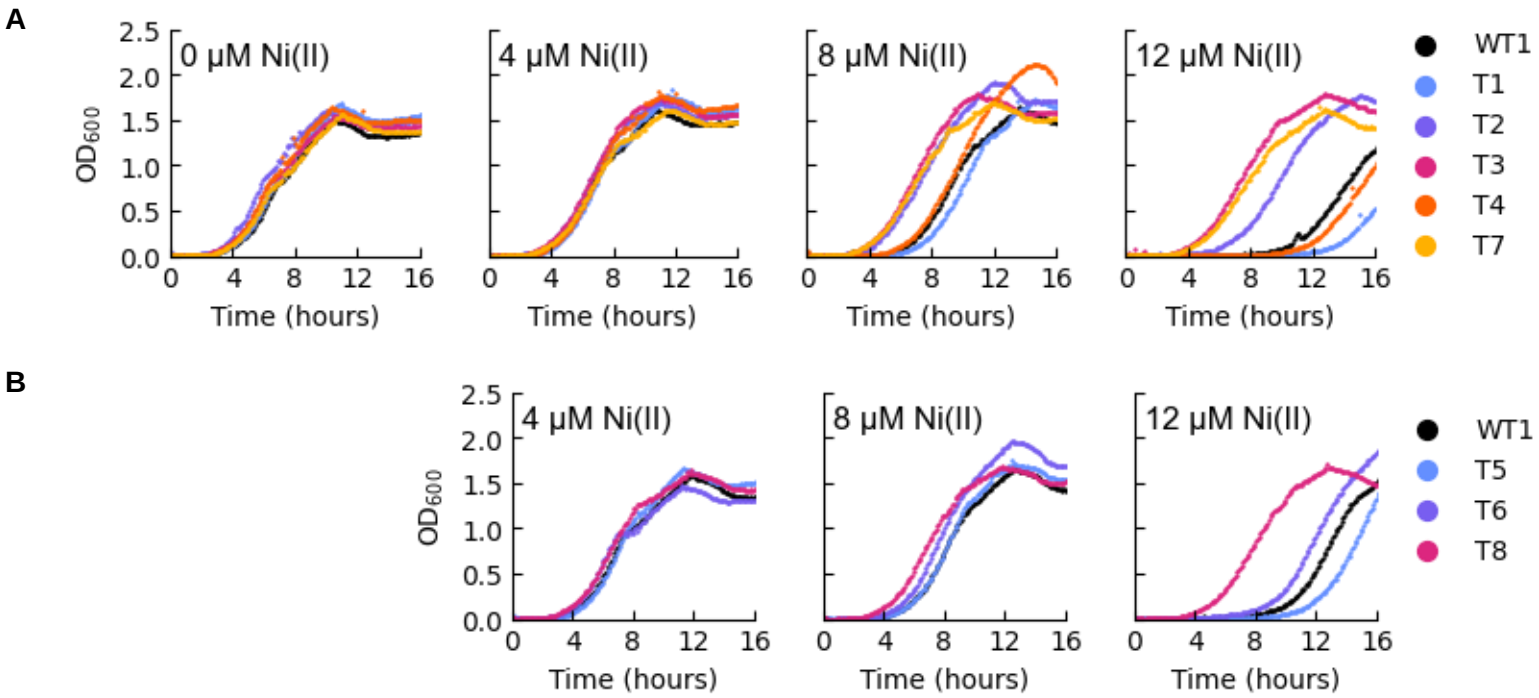
A
0 μM Ni(II)
4 μM Ni(II)
8 μM Ni(II)
12 μM Ni(II)
OD600
Time (hours)
WT1
T1
T2
T3
T4
T7
B
4 μM Ni(II)
8 μM Ni(II)
12 μM Ni(II)
OD600
Time (hours)
WT1
T5
T6
T8

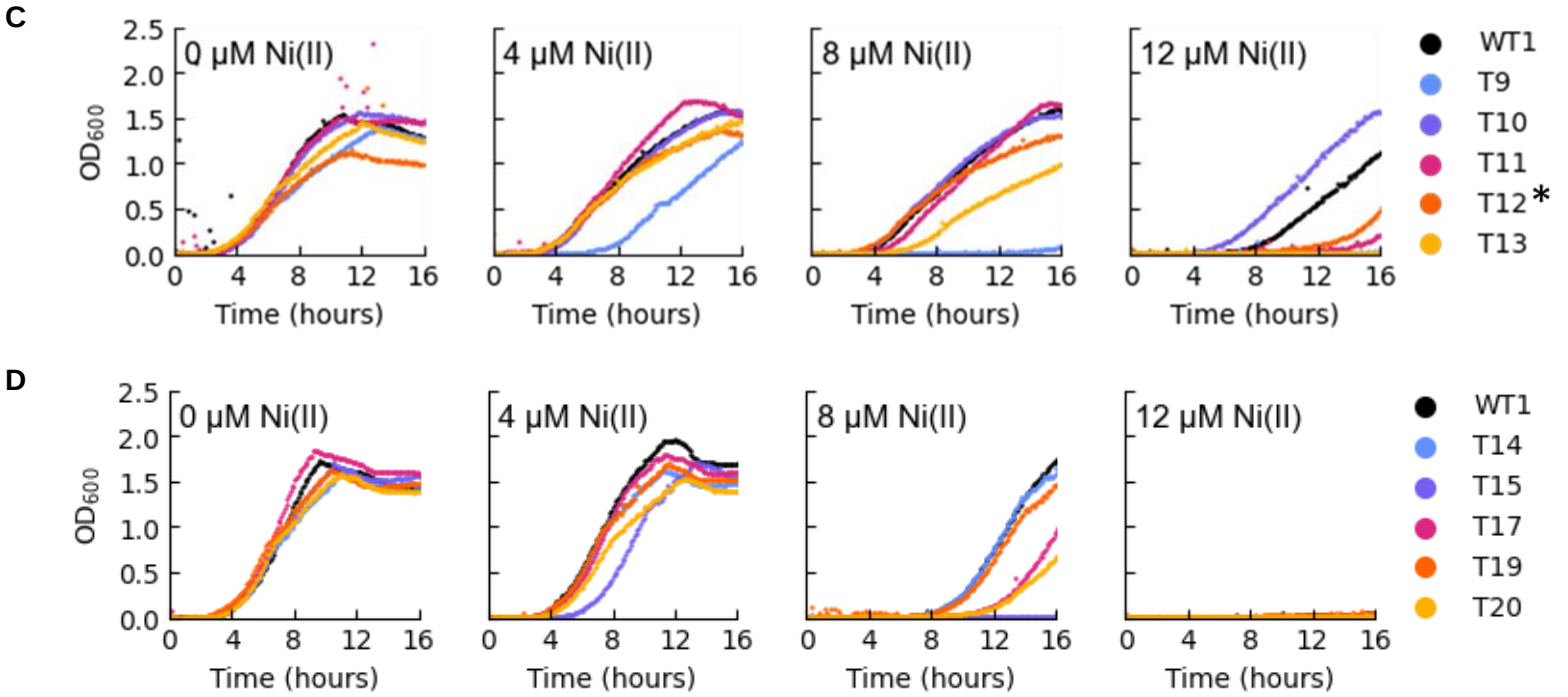
C
0 µM Ni(II)
4 µM Ni(II)
8 µM Ni(II)
12 µM Ni(II)
OD600
Time (hours)
WT1
T9
T10
T11
T12*
T13
D
0 µM Ni(II)
4 µM Ni(II)
8 µM Ni(II)
12 µM Ni(II)
OD600
Time (hours)
WT1
T14
T15
T17
T19
T20

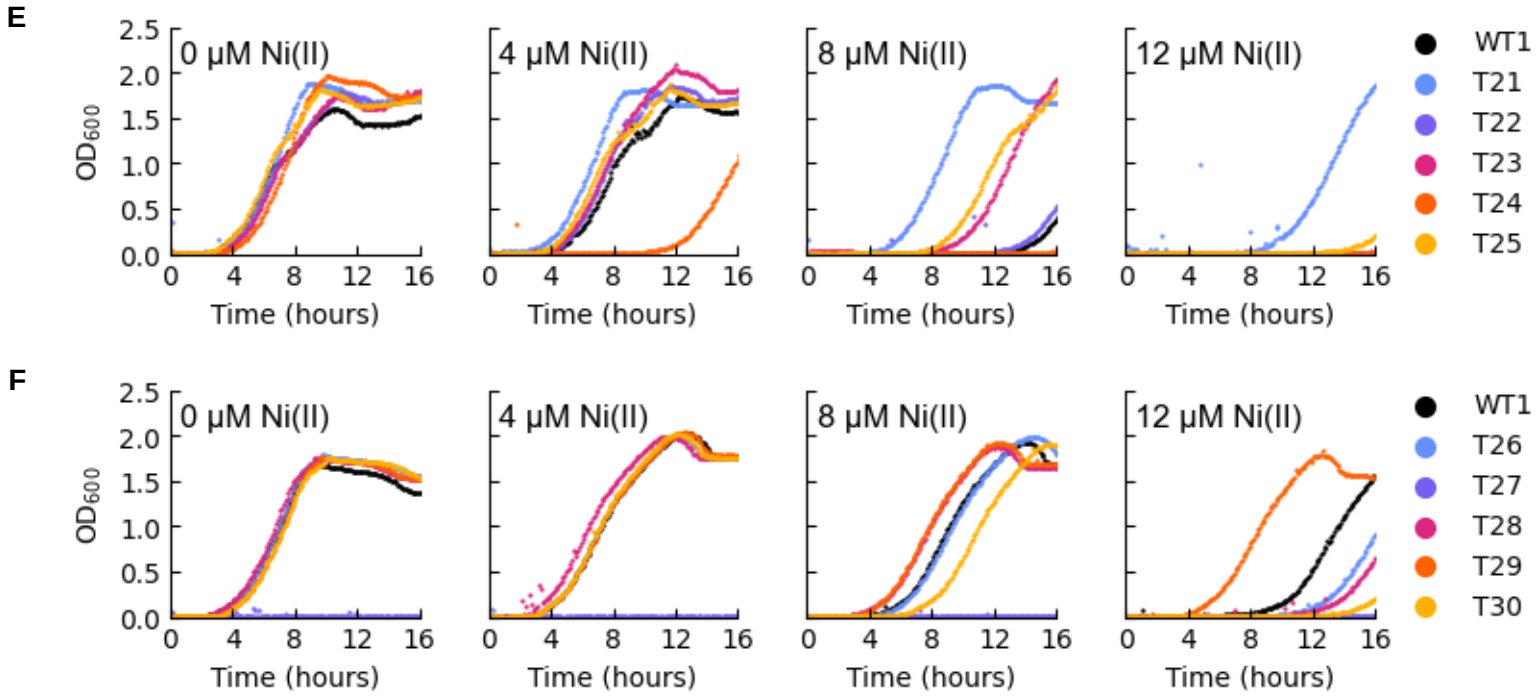

Figure 3.7: Preliminary analysis of Ni(II) sensitivity of recombinants carrying *hisG*$_{T252}$ reveals a range of sensitivities in M63 media
Growth curves set up as described in 2.6. Each lettered panel is from an individual growth assay. Each point is a reading from a single well under the specified condition.

Several strains were apparently more tolerant of Ni(II) stress (T2, T3, T7, T8, T10, T21, T23, T25 and T29) thus potentially expressed higher cytosolic His levels (e.g., Figure 3.7A at 12 μM Ni(II)). Conversely, several strains showed increased sensitivity to Ni(II) stress (T9, T11, T12, T13, T15, T24, T27 and T30). Among these strains, it was noted that T12 (Figure 3.7C, marked with an asterisk) had a lower final OD_{600} in the absence of any added Ni(II), that might be linked to its apparent increased Ni(II) sensitivity.

3.4 DNA Sequence Analysis of *hisG* Mutations

In parallel with the preliminary growth assay, the *hisG* gene was sequenced of 34 recombinants (30 $hisG_{T252}$ and 4 $hisG_{WT}$; Table 3.2). An additional seven recombinant sequences are present in Table 3.2 and the basis for their selection is described in Section 3.4.1. Of the recombinants transformed with the $hisG_{T252}$ fragment, 19 have a sequence change in the expected codon for T252 (ACT), 3 of which encode a synonymous change (ACT to ACC), leaving 16 recombinants with a missense mutation of the T252 codon. The frequency distribution of the 48 possible codons is listed in Table 3.3. The observed distribution of the observed codon changes is narrower and contains multiple instances of the same codon encoding the same amino acid (e.g., Arg, His, Pro, and Thr) when more than more codon is possible. Additionally, the high frequency of an unchanged codon (ACT) in the set of sequenced transformants suggests that one or more components of the PCR mutagenesis (e.g., annealing temperature) and transformation protocol enriched for specific codons.

Intriguingly, all possible bases were observed in the first (AGCT) and third (CGT) positions, while in the second position no T was observed in in any codon. Consequently, bulkier, hydrophobic residues were not observed in the recombinant pool (Ile, Leu, Met, Phe, and Val). Variants encoding Tyr and Trp were also absent, raising the possibility that these substitutions generate a his^- auxotroph. Site-directed mutations, and selection under less stringent conditions could be used to test this possibility.

Table 3.2: Sequence of *hisG* gene in recombinants transformed with *hisG*$_{WT}$ and *hisG*$_{T252}$

ID[a]	Mutation in T252	Mutation elsewhere in gene
WT1		D239D (gat → gac)
WT2[b]		
WT3		
WT6		E204G (gaa → gga)
T1[c]		
T2	**T252A (act → gcg)**	**N76D (aac → gac)**
T3	**T252N (act → aac)**	**F94L (ttt → ctt)** **A193A (gcc → gct)** **D211N (gac → aac)**
T4		D165G (gat → ggt)
T5		Q208R (caa → cga)
T6		A193V (caa → cga)
T7	**T252H (act → cac)**	**D199N (gat → aat)**
T8	T252H (act → cac)	D199N (gat → aat)
T9	**T252P (act → ccc)**	**S148P (tcc → ccc)**
T10	**T252D (act → gac)**	
T11		P59P (ccc → cct)
T12		**L17S (tta → tca)** **D140D (gac → gat)**
T13	T252P (act → ccc)	E186G (gaa → gga)
T14		E78G (gaa → gga)
T15	**T252S (act → tcg)**	**L150F (tta → ttc)**
T17		D113V (gat → gtt) L51L (ctg → ttg)
T19		R105R (cgt → cgc)
T20		R126H (cgt → cat) R262C (cgc → tgc)

T21		L34P (ctt → cct) A41V (gcg → gtg)
T22	T252R (act → cgg)	L39L (ctg → cta)
T23	T252H (act → cac)	R126C (cgt → tgt) I196T (att → act)
T24	T252T (act → acc)	D113G (gat → ggt) Q141R (cag → cgg)
T25		D140D (gac → gat)
T26	T252P (act → cct)	
T27	T252T (act → acc)	
T28	**T252R (act → cgg)**	**G118G (ggc → ggt)**
T29	T252A (act → gcc)	L245F (ctg → ttc)
T30	T252R (act → cgg)	L7V (tta → gta) L120P (ctc → ccc)
T31	T252N (act → aac)	P246L (cca → cta)
T32	T252T (act → acc)	D113G (gat → ggt) Q141R (cag → cgg)
T33	T252H (act → cac)	R22G (cgc → ggc) N180S (aac → agc)
T34		**I58T (att → act)**
WT9		**S14P (tcc → ccc)**
WT10		**I58V (att → gtt)**
WT12		**F101L (ttc → ctc)**

a, "T" indicates recombinant was transformed with *hisG*$_{T252}$; "WT" indicates recombinant was transformed with *hisG*$_{WT}$.
b, retained to use as a standard.
c, no changes in nucleotides detected.

Table 3.3: Frequency of point mutations in T252

Residue	Expected frequency in *hisG*$_{T252}$	*hisG*$_{T252}$ codon(s)	Actual appearances[a]	
Ala	3 / 48	gcc, gcg, gct	2	1 × gcc
				1 × gcc
Arg	4 / 48	agg, cgc, cgg, cgt	3	3 × cgg
Asn	2 / 48	aac, aat	2	2 × aac
Asp	2 / 48	gac, gat	1	1 × gac
Cys	2 / 48	tgc, tgt		
Gln	1 / 48	cag		
Glu	1 / 48	gag		
Gly	3 / 48	ggc, ggg, ggt		
His	2 / 48	cac, cat	4	4 × cac
Ile	2 / 48	atc, att		
Leu	4 / 48	ctc, ctg, ctt, ttg		
Lys	1 / 48	aag		
Met	1 / 48	atg		
Phe	2 / 48	ttc, ttt		
Pro	3 / 48	ccc, ccg, cct	3	2 × ccc
				1 × cct
Ser	5 / 48	agc, agt, tcc, tcg, tct	1	1 × tcg
Thr	3 / 48	acc, acg, act[b]	3	3 × acc
Trp	1 / 48	tgg		
Tyr	2 / 48	tac, tat		
Val	3 / 48	gtc, gtg, gtt		
STOP	1 / 48	tag		

a, out of 32 transformants carrying *hisG*$_{T252}$, including T31-T34 (see section 3.4.1).
b, act encodes the wild-type protein. Recombinants with this codon are omitted from this table.

Table 3.2 lists additional mutations observed in codons elsewhere in *hisG*. The lower fidelity Go*Taq* DNA polymerase was intentionally used in fragment generation due to the possibility of non-synonymous changes elsewhere in *hisG* that might lead to interesting phenotypes. However, the number of unique base changes (43 total, 40 in the longer 5' fragment) corresponds to a higher than expected error frequency (1.1×10^{-3} bp). Unexpectedly, these changes identified *hisG* variants of considerable interest in this study, which will be discussed in the next section.

Overall, 12 recombinants (in bold, Table 3.2) were identified of interest using the initial Ni(II) sensitivity screen (Section 3.3) and the sequence information.

3.4.1 Identification of Putative His Feedback Hypersensitive Mutants

The initial observation of T12 Ni(II) sensitivity (Figure 3.7C) was notable, as such variants were not anticipated to be easily identified in the T252 pool. Consequently, the T12 colony morphology was re-examined, as lower His might correspond to smaller colonies whilst growing on M63 agar. Interestingly, T12 displayed a distinct colony morphology; the colonies were flatter, larger, and possess a wrinkled surface (Figure 3.8), consistent with literature descriptions of *Salmonella* carrying *hisG* mutations encoding HisG variants hypersensitive to feedback inhibition by His (Roth, Antón and Hartman, 1966). Similar *E. coli hisG* mutants have been reported, but their colony morphology was not described (O'Donovan and Ingraham, 1965). *Salmonella* and *E. coli hisG* are 95.7% identical.

On this basis, the original $hisG_{T252}$ and $hisG_{WT}$ transformant plates were re-examined and any wrinkled colonies were re-streaked. A further 4 $hisG_{T252}$ (T31 – T34) and 5 $hisG_{WT}$ (WT9 – WT14) transformants were identified in this way and along with T12 screened in multiple ways to confirm the possible hypersensitive feedback phenotype, which would be consistent with increased Ni(II) sensitivity.

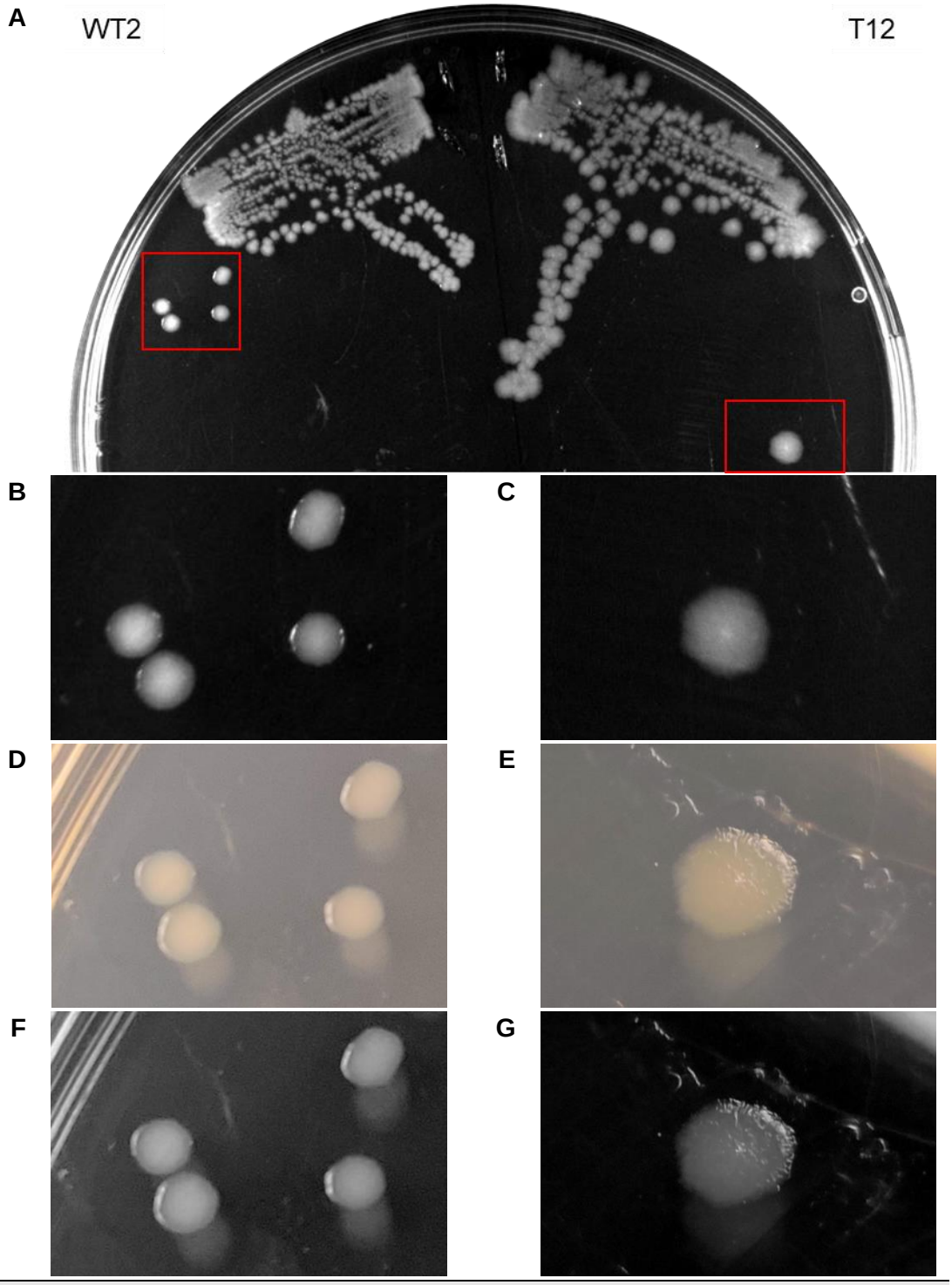

Figure 3.8: The recombinant T12 has a distinctive colony morphology on solid M63 media

(**A**) Plate with WT2 and T12; (**B**, **D**, **F**) Close-up of a WT2 colony; (**C**, **E**, **G**) Close-up of a T12 colony. (**A** - **C**) taken using BioRad Gel Doc XR+ Gel Documentation system. (**D** - **G**) taken using a phone camera. (**F**) and (**G**) are duplicates of (**D**) and (**E**), converted to 16-bit greyscale using ImageJ (Schneider, Rasband and Eliceiri, 2012). 48 hours growth on M63 agar at 37 °C.

A feedback hypersensitive of *E. coli hisG* mutation enzyme is unable to grow on solid glucose-salts medium below 20 ℃, and this defect can be complemented by addition of His or Hol to the growth medium (O'Donovan and Ingraham, 1965; Sterboul, Kleeman and Parsons, 1977). Screening the candidate variants, along with WT2 as a control, revealed that T12, WT9, WT10 and WT12 did not grow on M63 media at 20 ℃ (Figure 3.9A and B) without supplementation. T31, T33 and T34 displayed very low levels of growth. T32, WT11, WT13, and WT14 grew similarly to WT2 and were discarded. As an additional check, growth in liquid media with and without His and Hol was assessed (Figure 3.10). It appears that His and Hol restore the growth profile seen in WT2. In the presence of 500 μM His and 2 mM Hol, T12 and WT9 are indistinguishable from WT2. However, T34, WT10 and WT12 still have a slightly extended lag time.

Previous studies suggested that differences between WT2, T34, WT10 and WT12 could be due to an adenine deficiency (Sterboul, Kleeman and Parsons, 1977; Johnston and Roth, 1979). AICAR, an intermediate in His biosynthesis (Figure 1.7), is one route to purine (adenine) synthesis in *E. coli* and other bacteria. However, adenine supplementation appeared to be toxic (Figure 3.11). The basis for this unexpected toxicity, which is not observed when Hol is also present, was not explored further but may exacerbate the existing *hisG* hypersensitive phenotype.

Literature suggests that the wrinkled colony morphology is due to the de-repression of the *his* operon in response to a semi-functional HisG (Moyed, 1961; Ng, Ingraham and Marr, 1962; O'Donovan and Ingraham, 1965; Murray and Hartman, 1972). SDS-PAGE was used as an initial analysis of protein expression profiles to compare potential changes in the expression of the His operon enzymes (Table 3.4) in the presence and absence of Hol (Figure 3.12). Gels were analysed (Section 2.8) using ImageJ (Schneider, Rasband and Eliceiri, 2012) to generate intensity profiles for each condition that were then compared (Figure 3.13) to identify any bands whose expression was reduced in the presence of Hol. Three bands of interest were identified at ~ 50 kDa, ~ 33 kDa and ~ 25 kDa (Table 3.4), which could correspond to HisD, HisG and HisA/I/H, respectively. The bands of interest are most intense in T34 without Hol supplementation.

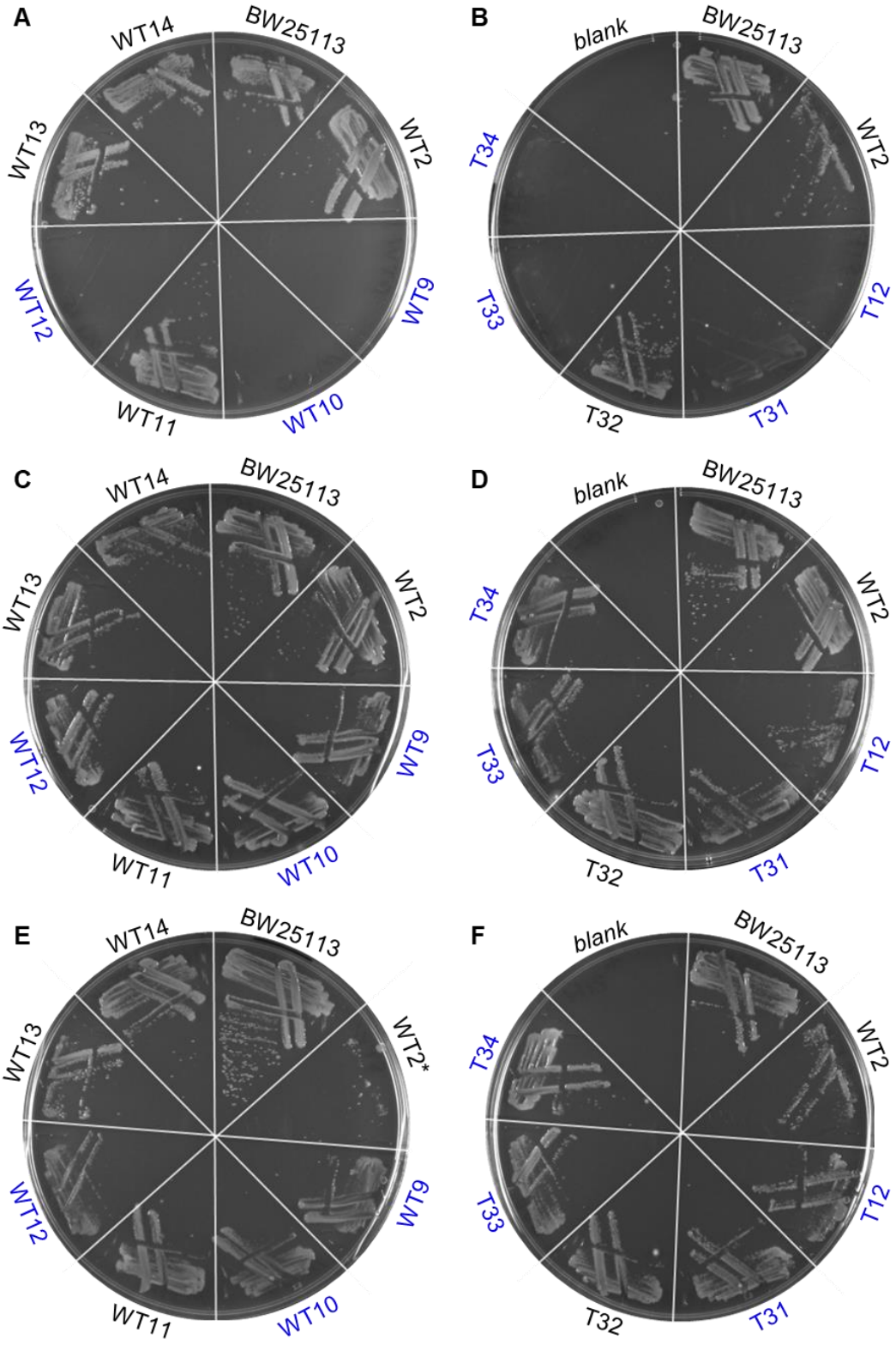

Figure 3.9: Growth of putative hypersensitive recombinants on solid M63 media at 20 °C is rescued by His and Hol

(**A, B**) No additional supplement; (**C, D**) 500 µM His; (**E, F**)1 mM Hol. Recombinants of interest labelled with blue text. *Low WT2 growth assumed to be due to poor re-streak. White lines have been overlaid on these images to help distinguish between plate sections. Plates grown for 5 days.

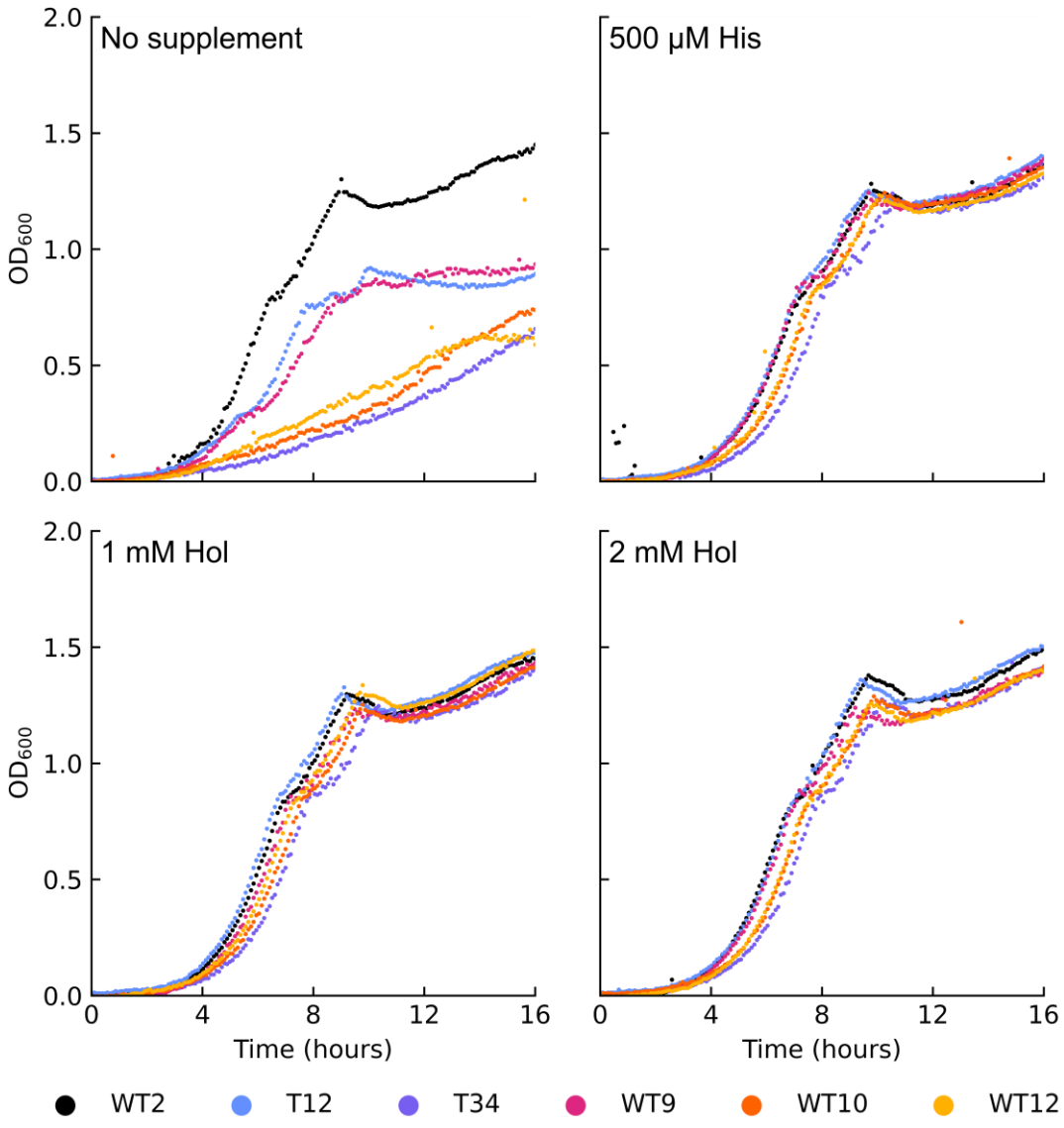

Figure 3.10: Poor growth of putative hypersensitive recombinants in M63 media is complemented by His and Hol

Growth curves set up as described in Section 2.6. Each point is a single reading.

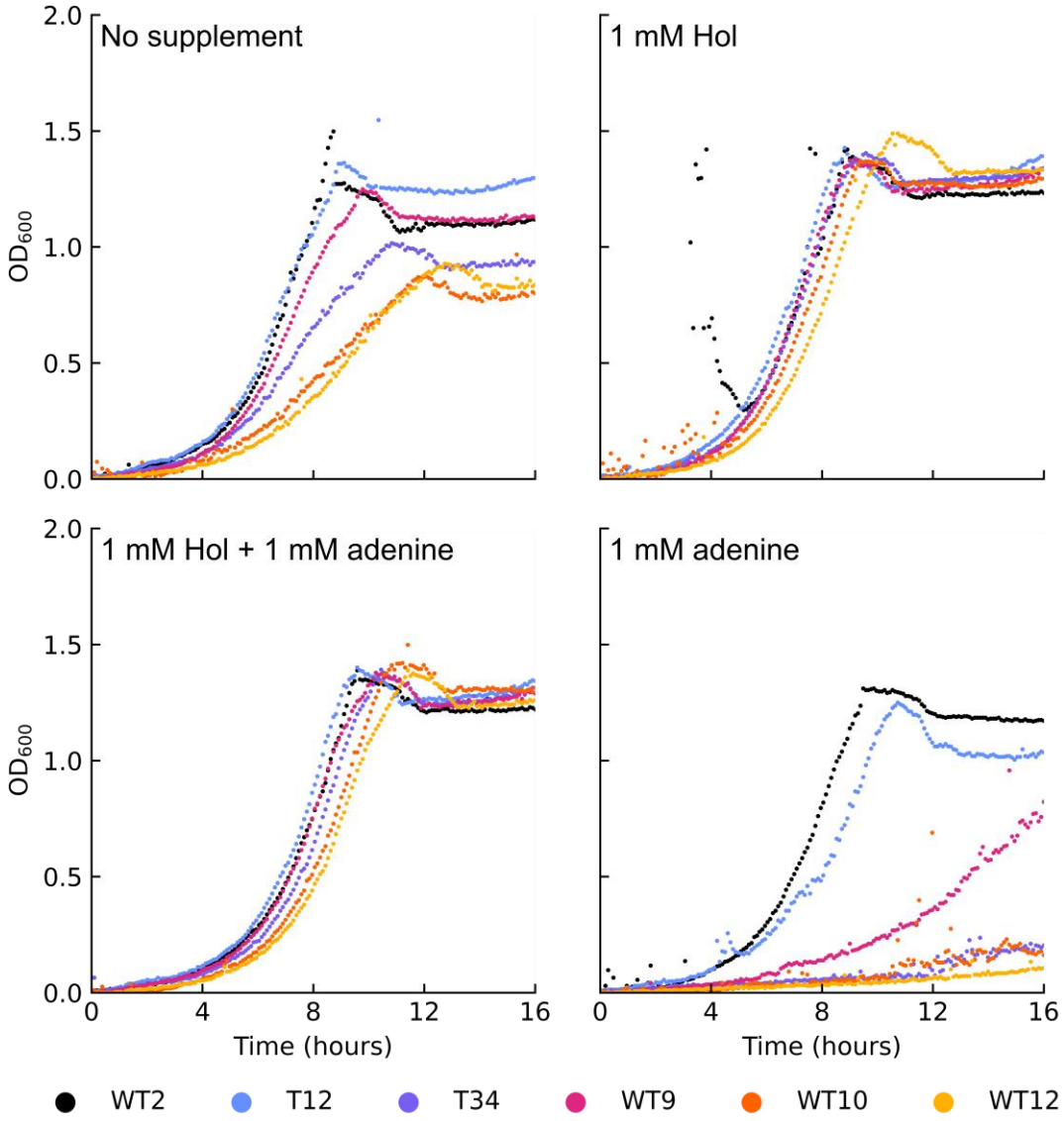

Figure 3.11: Poor growth of putative hypersensitive recombinants in M63 media is not complemented by adenine

Growth curves set up as described in Section 2.6. Each point is a single reading.

Table 3.4: Weight of *his* operon enzymes

Enzyme[a]	Weight (kDa)	UniProt ID[b]
HisG	33.4	P60757
HisI	22.8	P06989
HisA	26.0	P10371
HisH	21.7	P60595
HisF	28.5	P60664
HisB	40.2	P06987
HisC	39.4	P06986
HisD	46.1	P06988

a, ordered by step in His biosynthesis.
b, The UniProt Consortium et al., 2021.

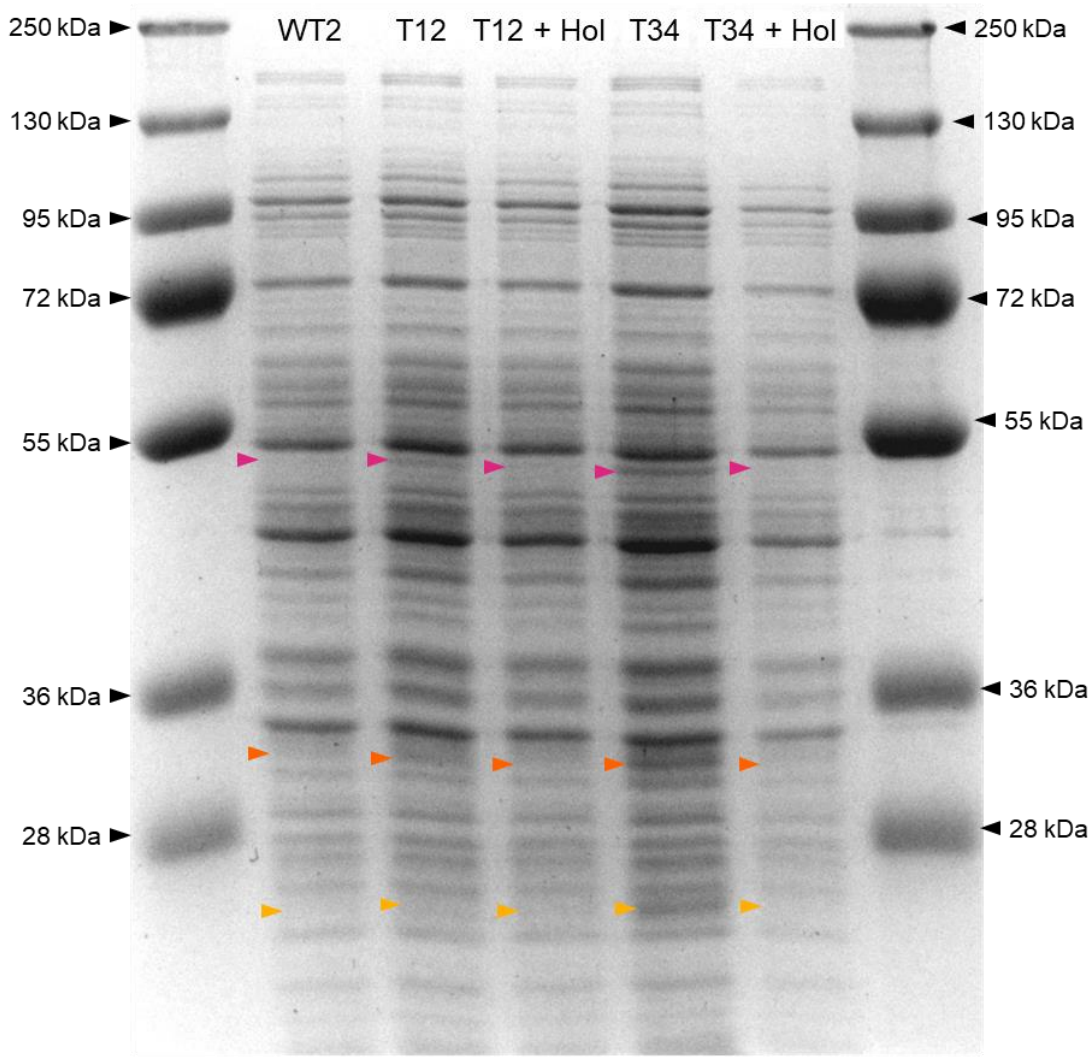

Figure 3.12: Analysis of His operon de-repression in putative hypersensitive mutants T12 and T34.

SDS-PAGE analysis of liquid cultures on a 13 % (v/v) acrylamide gel, as described in Section 2.8. Pink, orange, and yellow arrows indicate bands of sizes ~50 kDa, ~33 kDa, and ~25 kDa, respectively.

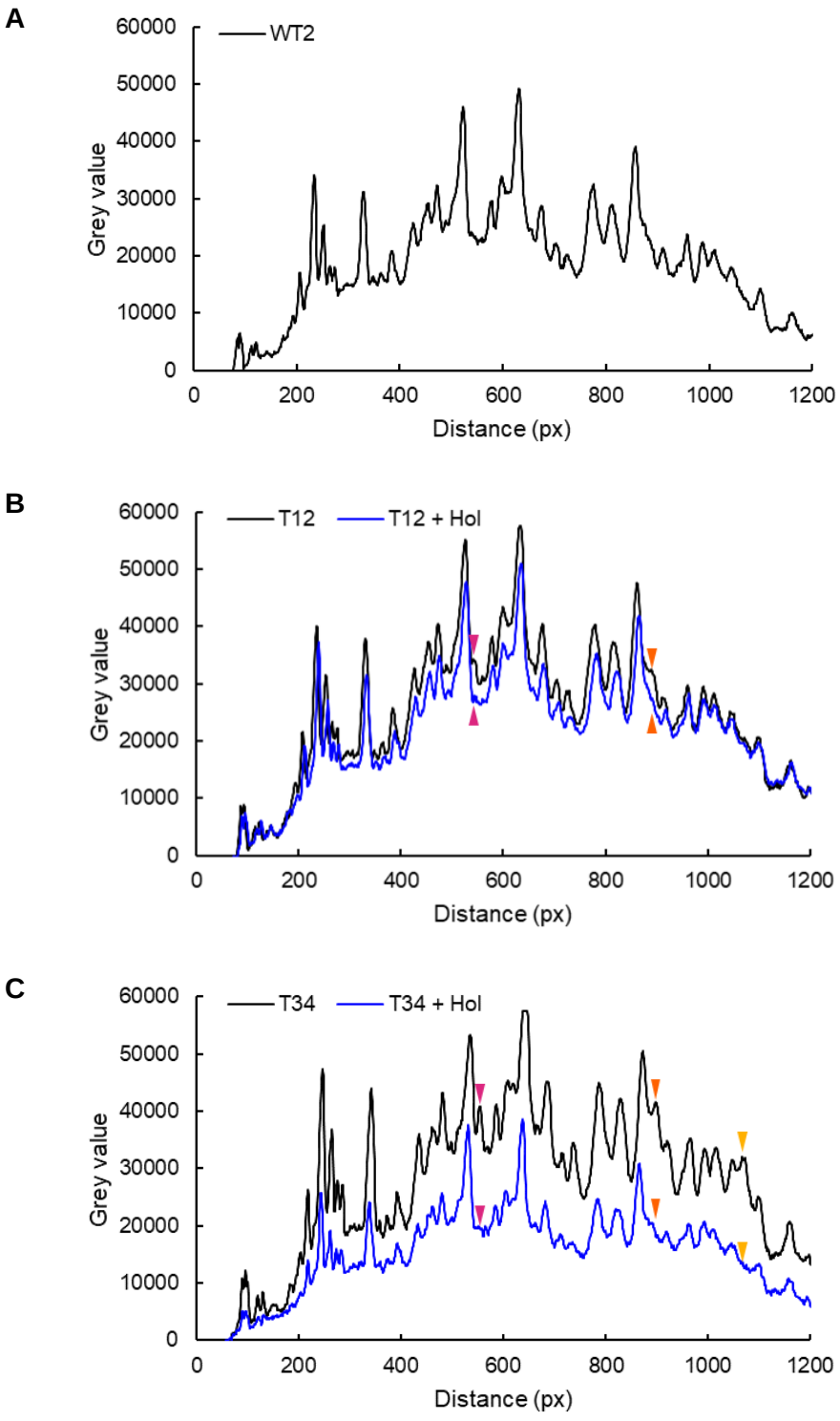

Figure 3.13: Analysis of SDS-PAGE band intensities supports Hol-dependent suppression of His enzyme overexpression.

(**A**) WT2; (**B**) T12 without and with Hol supplementation; (**C**) T34 without and with Hol supplementation. Arrows indicate peaks corresponding to bands of interest in Figure 3.12. Gel analysed using ImageJ (Schneider, Rasband and Eliceiri, 2012) as described in Section 2.8.

3.4.2 Structural Mapping of Hypersensitive Mutations

T12, T33, T34, WT9, WT10 and WT12 all carry mutations in *hisG* close to the active site in the N-terminal domain (Table 3.2). The mutations in T12, T34, WT9, WT10 and WT12 are all in highly conserved residues (Figure 3.14). The point mutation in T33 was not in a highly conserved residue, so further analysis of this recombinant was not pursued here.

These *hisG* mutations are distinct from the previously mapped *Salmonella* hypersensitive mutations, which are located within the C-terminal regulatory domain (Sheppardz, 1964; Sterboul, Kleeman and Parsons, 1977; Hoppe et al., 1979). One *Salmonella* His auxotroph carrying a point missense mutation in the N-terminal domain was later identified and sequenced (Miller and Barnes, 1986), but is different from those here. Nonetheless, as the colony morphology and temperature sensitivity are still consistent with the description of *Salmonella* carrying a feedback hypersensitive HisG, T12, T34, WT9, WT10 and WT12 will be referred to as being putative feedback hypersensitive from this point forwards. However, it is possible that these enzymes could have impaired catalytic activity, leading to constitutively low His levels independent of hypersensitive His feedback inhibition.

3.4.3 Putative Hypersensitive Recombinants Filament in Minimal Media

The *hisG* hypersensitive variant colony morphology (Figure 3.8) is reportedly linked to filamentation (Murray and Hartman, 1972; Frandscen and D'Ari, 1993). In an attempt to understand the extent of the filamentation and if the phenotype could be complemented with Hol, WT2 and T12 were grown in M63 media with and without Hol. Cells were grown to the mid-log to late-log phase, harvested and stained (Figure 3.15). T12 filaments in M63 media, but the wild-type phenotype is restored on the addition of 1 mM Hol.

As a consistently lower maximum OD_{600} was observed for these variants in liquid growth assays (Figure 3.7, Figure 3.10 and Figure 3.11), CFUs for WT2, T2, T12 and T34 were determined at apparent OD_{600} corresponding to mid-logarithmic growth (Figure 3.16). As a control in addition to WT2, a presumed feedback insensitive recombinant, T2 (T252A), was also analysed.

A

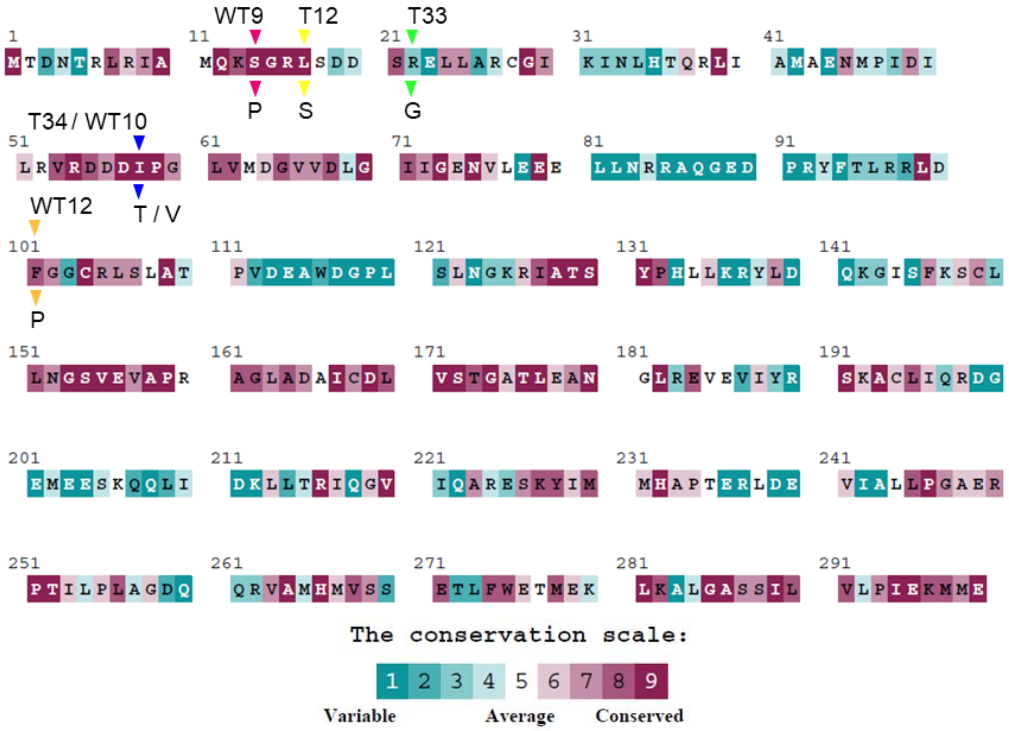

B

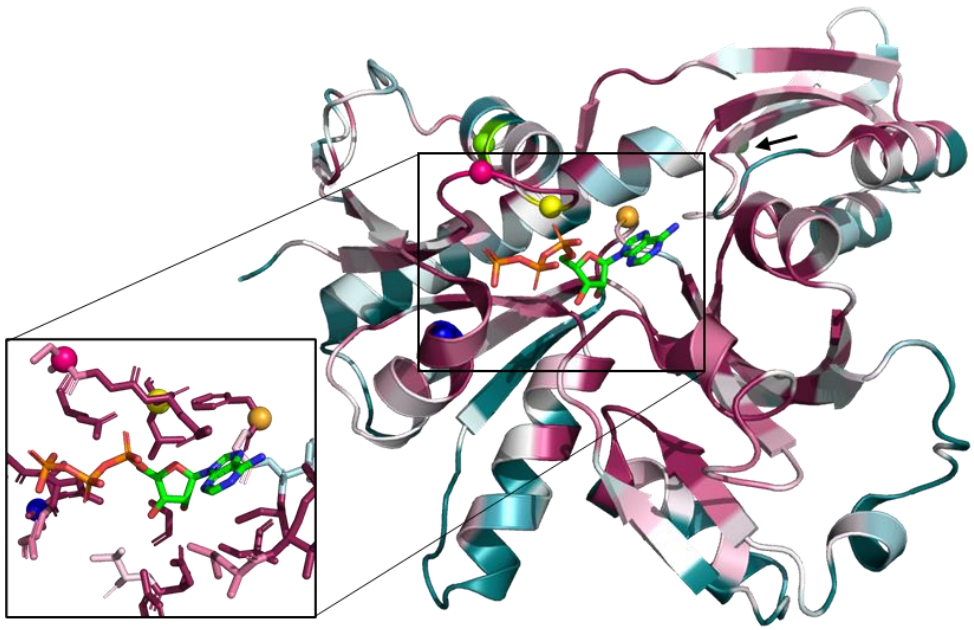

Figure 3.14: Mapping putative hypersensitive mutants onto the HisG structure
(**A**) *E. coli* HisG sequence. Amino acids colouring according to an estimate of the evolutionary conservation (ConSurf; Ashkenazy et al., 2016). (**B**) *C. jejuni* HisG monomer with ATP bound in the active site (Mittelstädt et al., 2016). Colouring according to the conservation scale. Putative hypersensitive N-terminal domain point mutations are shown as coloured spheres: S14: magenta; L17: yellow, R22: green; I58: blue; F101: orange. ATP (sticks) carbon atoms coloured in green. The location of T252 (dark green) is marked with a black arrow. Figure generated using PyMOL (Schrödinger and DeLano, 2020).

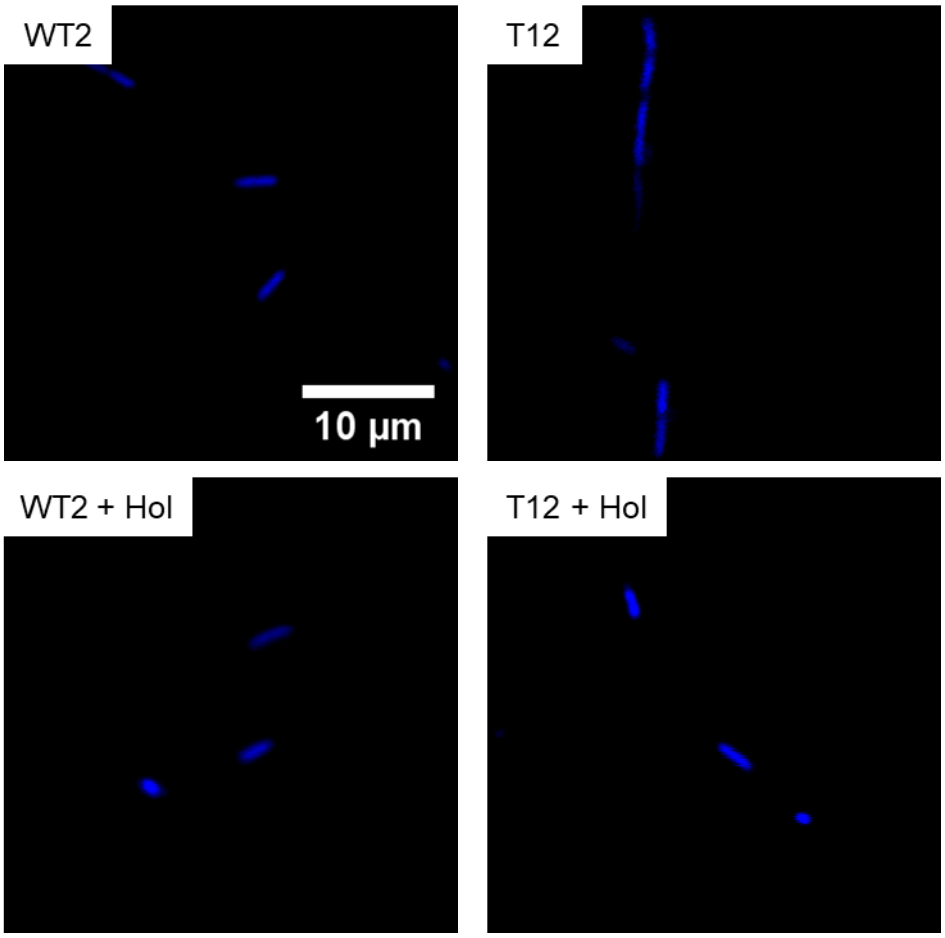

Figure 3.15: Filamentation of T12 in M63 media is complemented by Hol
WT2 and T12 grown in M63 media, with and without 1 mM Hol. Cells stained with a Hoechst dye. Images taken by Dominic Donkin, Pal group, Durham University.

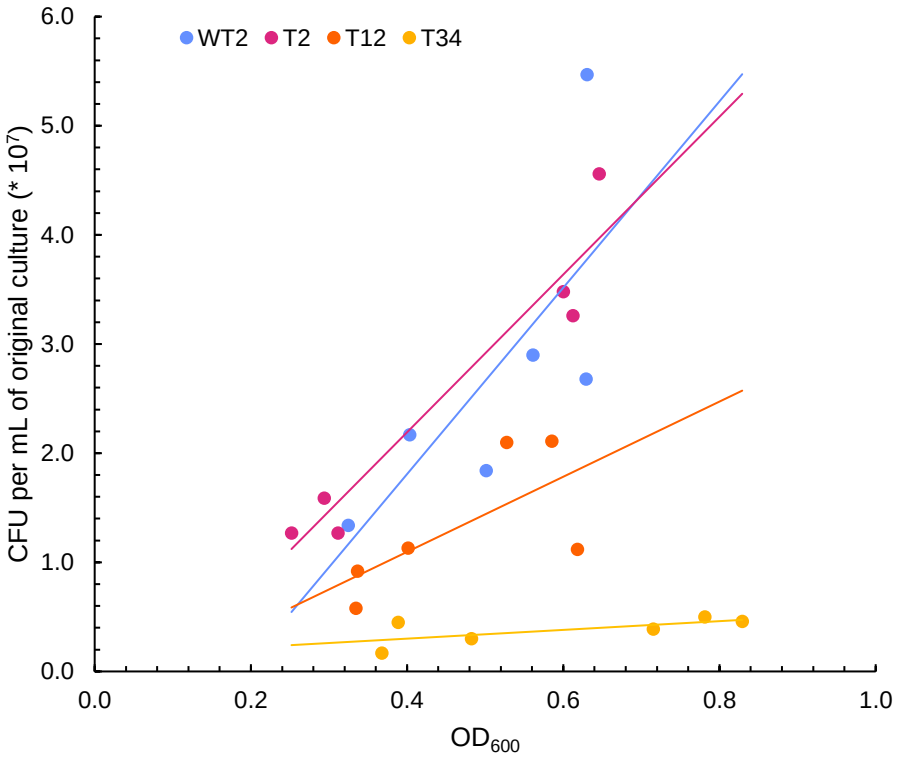

Figure 3.16: Filamentation of putative hypersensitive recombinants affects calibration of OD_{600} with CFUs

CFUs calculated as described in Section 2.10. OD_{600} measured using the Multiskan GO spectrophotometer. Data was plotted in Microsoft Excel and the "Linear Trendline" tool was used to determine the linear relationship between OD_{600} and CFUs. Trendline equations and R^2 values are as follows: WT2: $y = (9*10^7)x - 2*10^7$, $R^2 = 0.53$; T2: $y = (7*10^7)x - 7*10^6$, $R^2 = 0.93$; T12: $y = (3*10^7)x - 3*10^6$, $R^2 = 0.47$; T34: $y = (4*10^6)x + 1*10^6$, $R^2 = 0.45$. Each point is a single reading. These relationships will be used in Sections 3.7 and 3.8.

There was no difference in CFUs per mL between WT2 and T2. The CFUs per mL for T12 are similar to WT2 and T2 when $OD_{600} \approx 0.3 – 0.4$, but notably much lower when $OD_{600} \approx 0.5 – 0.6$. Additionally, the CFUs per mL for T34 are consistently lower than T12. These observations suggested that T34 has a more severe phenotype than T12, and there is variability within this class of recombinants.

3.4.4 Five Putative Hypersensitive Recombinants Have Been Carried Forwards for Further Testing

Overall, the characterisation of the five putative hypersensitive recombinants being carried forwards is summarised in Table 3.5.

3.5 Recombinants Show Differing Levels of Ni(II) Sensitivity in Defined Minimal Media

Using the preliminary Ni(II) sensitivity screen (Section 3.3) and sequence information (Section 3.4), a set of recombinants was selected for further Ni(II) sensitivity testing. Recombinants were split into two categories of interest: those carrying point mutations at position 252 and those described as putative hypersensitive recombinants in Section 3.4.1. The growth of each recombinant in M63 minimal media was compared with the wild-type recombinant WT2 as a standard. Growth curves were performed in triplicate as described using different Ni(II) concentrations (Figure 3.17, Figure 3.18 and Appendix 2), using three independent starter cultures for each strain, to quantify changes in Ni(II) sensitivity. An increased tolerance to Ni(II) stress would be characterised by a faster doubling time (rate of OD_{600} doubling in the exponential phase) and/or a decreased lag time (time to reach OD600 = 0.15), and the opposite behaviours for decreased tolerance to Ni(II) stress.

The lag and doubling of each recombinant were calculated from the replicate growth curves (Table 3.6, Table 3.8 and Table 3.7, Table 3.9 respectively).

Table 3.5: Properties of putative feedback hypersensitive *hisG* mutants

ID	Mutation in *hisG*	Growth at 20 ℃	Mutation in conserved NTD residue
T12	**L17S**	**No**	**Yes**
T31	*T252N/P256L*	Weak	No
T32	*D113G/Q141R*	Yes	No
T33	*T252H/R22G/N180S*	Weak	No
T34	**I58T**	**Weak**	**Yes**
WT9	**S14P**	**No**	**Yes**
WT10	**I58V**	**No**	**Yes**
WT11	*Not sequenced*	Yes	*n/a*
WT12	**F101L**	**No**	**Yes**
WT13	*Not sequenced*	Yes	*n/a*
WT14	*Not sequenced*	Yes	*n/a*

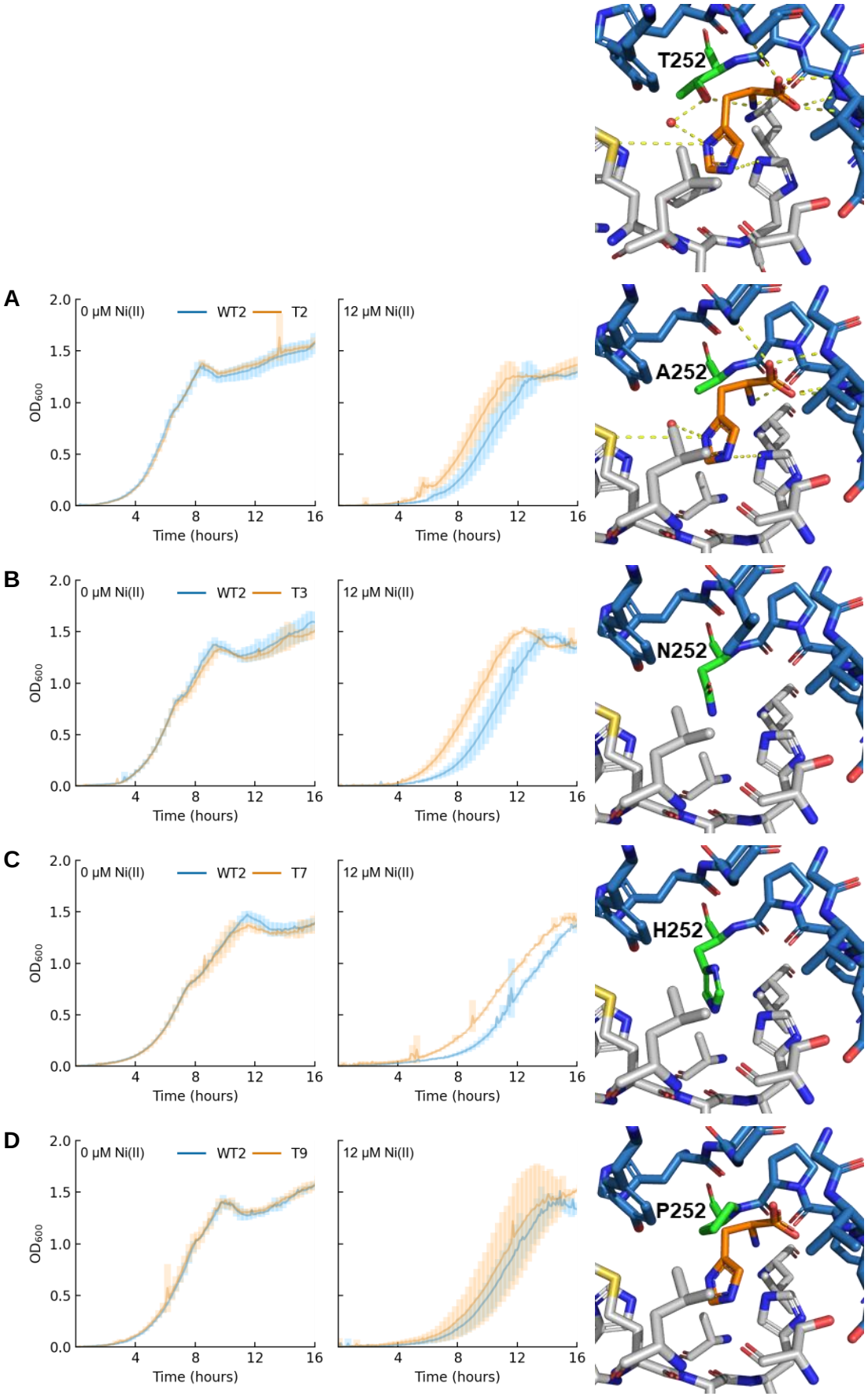
T252
A
0 μM Ni(II)
WT2
T2
12 μM Ni(II)
OD600
Time (hours)
A252
B
0 μM Ni(II)
WT2
T3
12 μM Ni(II)
OD600
Time (hours)
N252
C
0 μM Ni(II)
WT2
T7
12 μM Ni(II)
OD600
Time (hours)
H252
D
0 μM Ni(II)
WT2
T9
12 μM Ni(II)
OD600
Time (hours)
P252

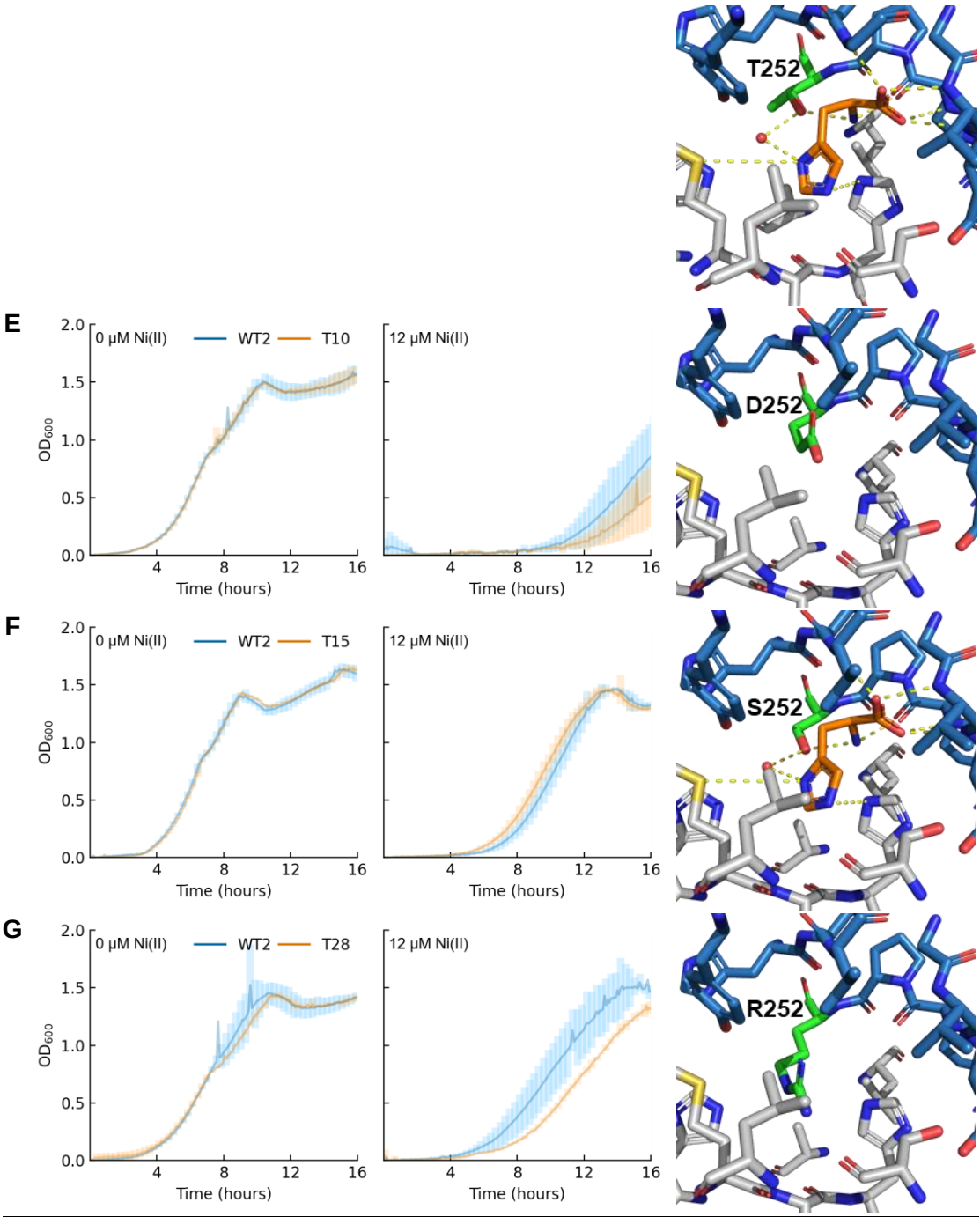

Figure 3.17: Recombinants carrying point mutations in T252 tend to be more tolerant of Ni(II) stress compared to a wild-type recombinant

(**A**); T2; (**B**); T3; (**C**); T7; (**D**); T9; (**E**); T10; (**F**); T15; (**G**); T28. Growth curves set up as described in 2.6, studying the response to chronic Ni(II) stress. Solid line is the average of biological triplicates. Shaded areas represent standard deviation. Accompanying structure is a representation of the His binding site of HisG (Mittelstädt et al., 2016). Figure generated using PyMOL (Schrödinger and DeLano, 2020).

Table 3.6: Lag times[a] for recombinants carrying a point mutation in T252 (Figure 3.17)

	0 µM Ni(II)		12 µM Ni(II)	
HisG variant	**WT2**	**Variant**	**WT2**	**Variant**
T2	3.74 ± 0.096	3.83 ± 0.000	7.12 ± 0.815	6.07 ± 0.399
T3	4.12 ± 0.166	4.12 ± 0.096	7.41 ± 0.652	5.69 ± 0.363
T7	4.50 ± 0.000	4.47 ± 0.241	8.47 ± 0.308	6.64 ± 0.277
T9	4.50 ± 0.096	4.34 ± 0.146	7.83 ± 0.744	7.38 ± 1.412
T10[b]	4.09 ± 0.111	4.15 ± 0.055	11.66 ± 1.683	13.13 ± 1.888
T15	4.12 ± 0.000	4.25 ± 0.055	7.32 ± 0.473	6.55 ± 0.221
T28	4.28 ± 0.111	4.15 ± 0.293	6.45 ± 0.732	7.70 ± 0.146

a, Lag time is defined as the period of time OD_{600} remains below 0.150. Values shown are the average and standard deviation from the triplicate samples.
b, data is assumed to be of poor quality due to extremely extended lag phase of WT2 at 12 µM Ni(II).

Table 3.7: Doubling times[a] for Ni(II)-tolerant T252 variants (Figure 3.17)

	0 µM Ni(II)		12 µM Ni(II)	
HisG variant	**WT2**	**Variant**	**WT2**	**Variant**
T2	0.74 ± 0.021	0.74 ± 0.004	0.88 ± 0.069	0.87 ± 0.1
T3	0.81 ± 0.022	0.84 ± 0.049	0.88 ± 0.073	0.83 ± 0.023
T7	0.93 ± 0.011	0.91 ± 0.078	1.26 ± 0.064	1.41 ± 0.105
T9	0.77 ± 0.030	0.79 ± 0.015	1.02 ± 0.157	1.05 ± 0.239
T10[b]	0.86 ± 0.031	0.85 ± 0.023	1.24 ± 0.166	1.91 ± 1.032
T15	0.78 ± 0.014	0.75 ± 0.029	0.80 ± 0.033	0.82 ± 0.039
T28[c]	1.04 ± 0.039	1.13 ± 0.146	1.25 ± 0.080	1.51 ± 0.134

a, Doubling time was calculated using the GrowthCurver R package (Sprouffske and Wagner, 2016) using the three growth curves. Curve fitting by GrowthCurver is displayed in Appendix 2.
b, data is assumed to be of poor quality due to extremely extended lag phase of WT2 at 12 µM Ni(II).
c, calculated manually due to poor curve fitting, as described in Appendix 2.

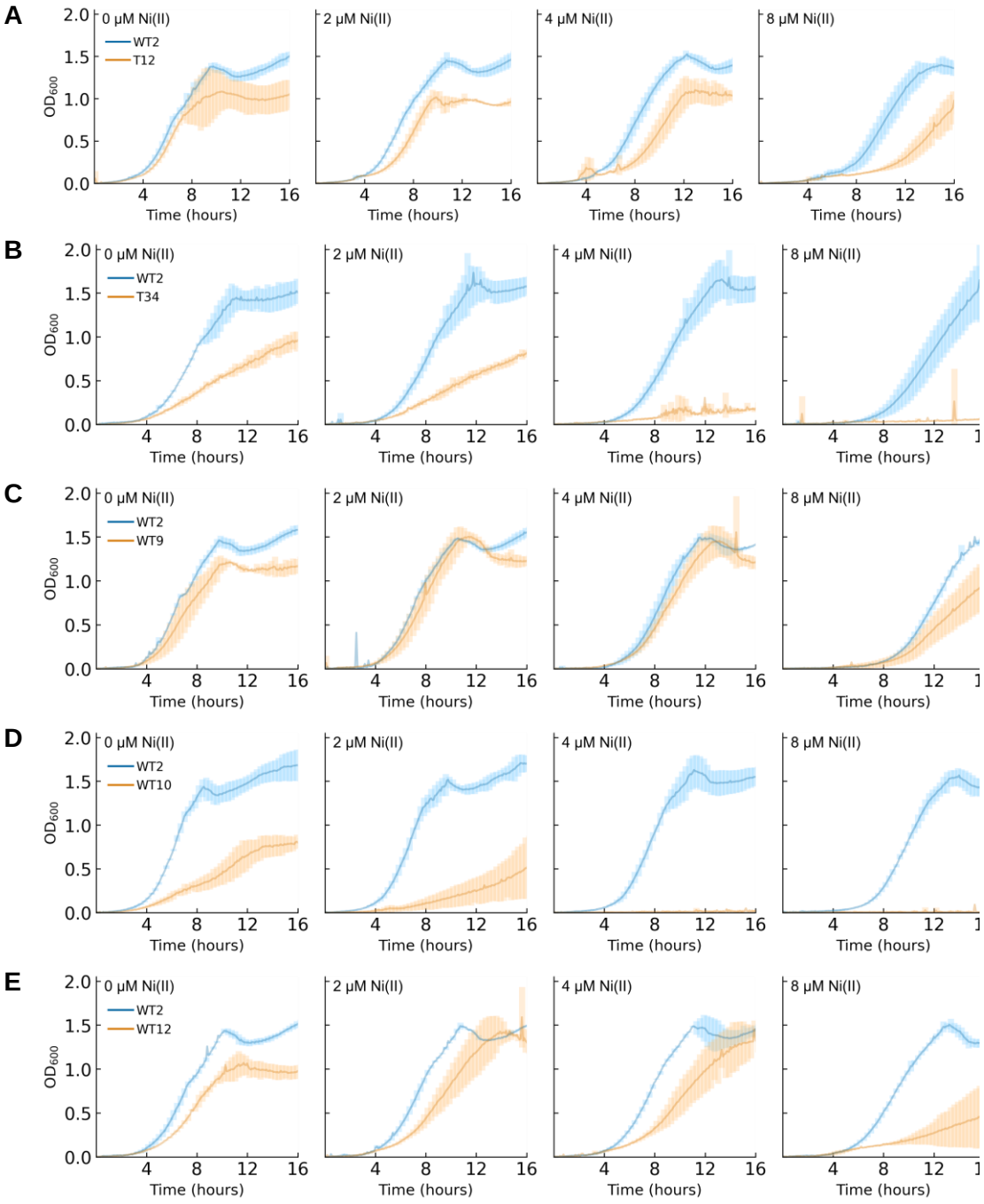

Figure 3.18: Putative hypersensitive recombinants are intolerant of Ni(II) stress compared to a wild-type recombinant

(**A**) T12; (**B**) T34; (**C**) WT9; (**D**) WT10; (**E**) WT12. Growth curves set up as described in 2.6, studying the response to chronic Ni(II) stress. Solid line is the average of biological triplicates. Shaded areas represent standard deviation. Analysis of doubling and lag times presented in Table 3.9 and Table 3.8, respectively.

Table 3.8: Lag times[a] for putative hypersensitive recombinants (Figure 3.18)

	0 μM Ni(II)		2 μM Ni(II)		4 μM Ni(II)		8 μM Ni(II)	
Recombinant	**WT2**	**Named recombinant**	**WT2**	**Named recombinant**	**WT2**	**Named recombinant**	**WT2**	**Named recombinant**
T12	4.06 ± 0.146	4.47 ± 0.111	4.57 ± 0.146	5.4 ± 0.241	5.02 ± 0.111	5.75 ± 2.049	6.84 ± 0.673	9.71 ± 0.638
T34	4.73 ± 0.146	5.40 ± 0.241	5.27 ± 0.254	6.48 ± 0.293		N/A[b]		N/A[b]
WT9	4.22 ± 0.096	4.73 ± 0.744	4.73 ± 0.146	5.02 ± 0.586	5.85 ± 0.507	6.10 ± 0.277	8.88 ± 0.199	9.58 ± 1.01
WT10	3.96 ± 0.055	5.46 ± 0.598	4.34 ± 0.199	11.02 ± 5.101		N/A[b]		N/A[b]
WT12	4.44 ± 0.293	5.11 ± 0.055	4.73 ± 0.199	5.69 ± 0.199	4.95 ± 0.111	6.07 ± 0.221	5.88 ± 0.146	8.75 ± 0.781

a, lag time is defined as the period of time OD_{600} remains below 0.15. Values shown are the average and standard deviation from the triplicate samples.
b, indicates the hypersensitive variant did not reach OD_{600} = 0.15.

Table 3.9: Doubling times[a] for putative hypersensitive recombinants (Figure 3.18)

	0 μM Ni(II)		2 μM Ni(II)		4 μM Ni(II)		8 μM Ni(II)	
Recombinant	**WT2[b]**	**Named recombinant**	**WT2**	**Named recombinant**	**WT2**	**Named recombinant**	**WT2**	**Named recombinant**
T12[b]	0.91 ± 0.006	0.93 ± 0.038	0.90 ± 0.041	1.54 ± 0.249	1.23 ± 0.068	2.56 ± 0.914	1.37 ± 0.178	2.55 ± 0.890
T34	0.92 ± 0.089	1.65 ± 0.113	0.88 ± 0.052	1.63 ± 0.154	N/A[c]		N/A[c]	
WT9[b]	0.93 ± 0.113	0.96 ± 0.092	0.73 ± 0.084	0.94 ± 0.179	1.06 ± 0.123	1.16 ± 0.051	1.20 ± 0.018	1.30 ± 0.280
WT10	0.75 ± 0.032	1.68 ± 0.326	0.73 ± 0.021	2.05 ± 0.181	N/A[c]		N/A[c]	
WT12[b]	0.79 ± 0.024	0.80 ± 0.058	0.80 ± 0.091	0.85 ± 0.077	1.16 ± 0.321	1.18 ± 0.586	1.38 ± 0.658	1.58 ± 0.159

a, doubling time was calculated using the GrowthCurver R package (Sprouffske and Wagner, 2016) using the three growth curves. Curve fitting by GrowthCurver is displayed in Appendix 2.
b, calculated manually (described in Appendix 2) due to poor curve fitting.
c, indicates the hypersensitive variant did not reach OD_{600} = 0.15.

3.5.1 Increased Tolerance to Ni(II) Stress

Recombinants with increased tolerance to Ni(II) (Figure 3.18) are characterised by decreased lag times relative to WT2 at 12 μM added Ni(II) (Table 3.8). T2, T3 and T7 appear to be the most tolerant of Ni(II) stress, with decreases in lag time of -14.8 %, -23.3 % and -21.5 %, respectively. At 0 μM Ni(II), all recombinants have a similar growth profile to WT2. Every curve (aside from WT2 in the T10 dataset) appears to have a small hump in the exponential phase between 6-8 hours (OD_{600} < 1.0), indicative of a potential growth shift in minimal media. This shift is absent for strains grown with Ni(II). Doubling times (Table 3.7) increased between 0 and 12 μM Ni(II), and there was no clear pattern of difference between HisG variants and WT2, in some cases the variant doubled more slowly despite having a shorter lag phase. This behaviour may reflect a link between Ni(II) tolerance and the energetic requirement for increased His biosynthesis.

The increased Ni(II) tolerant variants all had an amino acid change at T252 likely to render HisG less sensitive to feedback inhibition by His. The following different structure-function relationships can be inferred from structural modelling (Figure 3.18):

(1) Loss of an important hydrogen bond between T252 and His.
(2) Occlusion of the His binding site.
(3) Change in the conformation of other amino acids in the binding site, impacting backbone interactions with the His carboxyl group.

In each case, reduced affinity to His would lead to reduced feedback inhibition and higher cytosolic His levels and an increased tolerance to Ni(II) stress.

3.5.2 Decreased Tolerance to Ni(II) Stress

Recombinants with apparent hypersensitivity to His feedback, and thus reduced cytosolic His levels, have distinctive growth profile with a lower max OD_{600} in the absence of added Ni(II) (Figure 3.19). The addition of lower amounts of Ni(II) appears to complement this apparent defect in WT9 and WT12 (Ni(II) is used during anaerobic growth, which may occur at higher densities). Additionally, unlike WT2

and the Ni(II) tolerant variants, the growth curves of these hypersensitive variants do not appear to show a growth shift.

At 0 μM Ni(II), there is a clear difference between T12, WT9 and WT12, and T34 and WT10. T12, WT9 and WT12 display little change in doubling time, and an ~10 % increase in lag time. The doubling times of T34 and WT10 increase by 79.5 % and 125.1 %, respectively, compared to WT2. T34 and WT10 have an extremely Ni(II)-sensitive phenotype; they do not leave the lag phase above 4 μM Ni(II). T12, WT9 and WT12 all experience Ni(II)-dependent increases in doubling and lag time, with WT12 appearing more sensitive than T12, and T12 appearing more sensitive than WT9. WT12 grows poorly at 8 μM Ni(II). Overall, WT9 appears to be the "healthiest" putative hypersensitive recombinants.

3.6 Recombinants Carrying Point Mutations in T252 Secrete Histidine

Previous studies of His overexpression have generated strains capable of His secretion into the growth medium. To test whether Ni(II)-tolerant HisG variants were capable of His secretion, a plate assay was developed. As a first step, the addition of His to a top layer of M63 agar containing the Δ*hisG* strain was shown to support growth (Figure 3.19, panels D, E, F and H). This effect was specific to L-His, as D-His did no support growth, ruling out a non-specific effect on nutrient availability. Hol supplementation did not support growth at the concentrations tested here.

To test for His secretion, overnight liquid cultures of the recombinants WT2, T3, T7, T9, T10 and T28 were spotted onto *hisG*-containing top agar (Figure 3.20). As expected, WT2 did not rescue growth of Δ*hisG*, based on the absence of any visible growth halo around the WT2 growth spot. In contrast, T3, T7, T10 and T28 (Figure 3.20B and D), but not T2 and T9, secrete enough His to rescue growth of Δ*hisG* in the immediate vicinity of the growth, as evidenced by a small halo (< 1 mm) of growth in the top agar. For some strains (T10), the putative His secretion appears to be growth phase dependent, as spotting cells during exponential phase did not produce a halo (Figure 3.20C versus D).

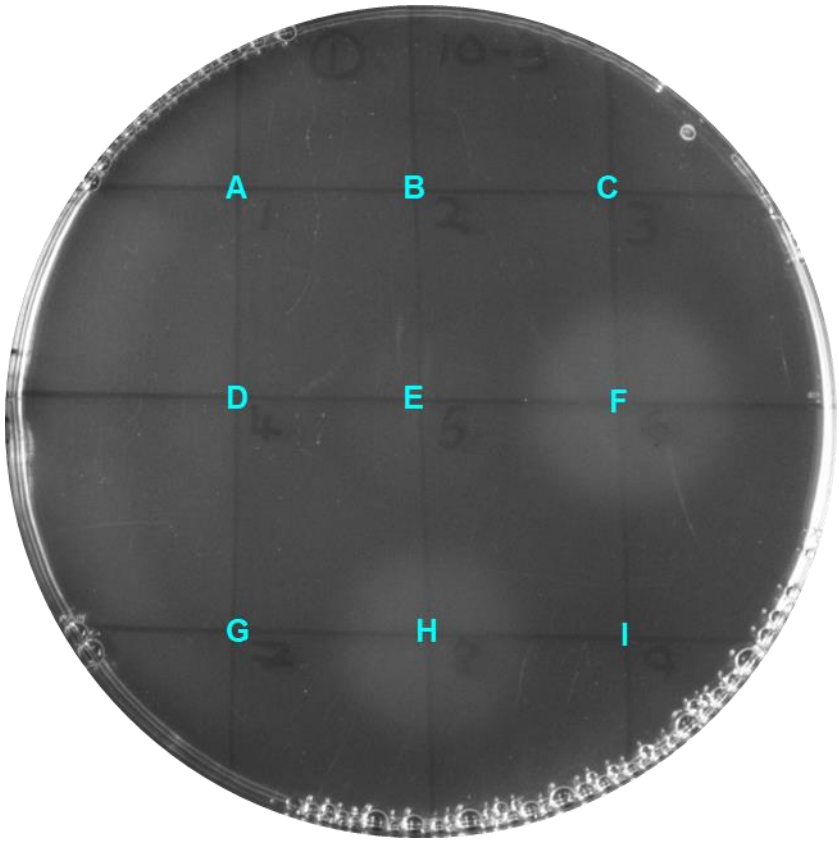

Figure 3.19: Growth of *ΔhisG* in minimal agar is rescued by His supplementation

M63 minimal agar (1 % (w/v)) with a top layer containing *ΔhisG*, prepared as described in Section 2.9. 5 µL of the following were spotted on the marked points: (**A**) M63 media; (**B**) 1 mM D-His; (**C**) 1 mM Hol; (**D**) 500 µM L-His; (**E**) 1 mM L-His; (**F**) 2 mM L-His; (**G**) blank; (**H**) 5 mM L-His; (**I**) blank. Images taken using the BioRad Gel Doc XR+ Gel Documentation system.

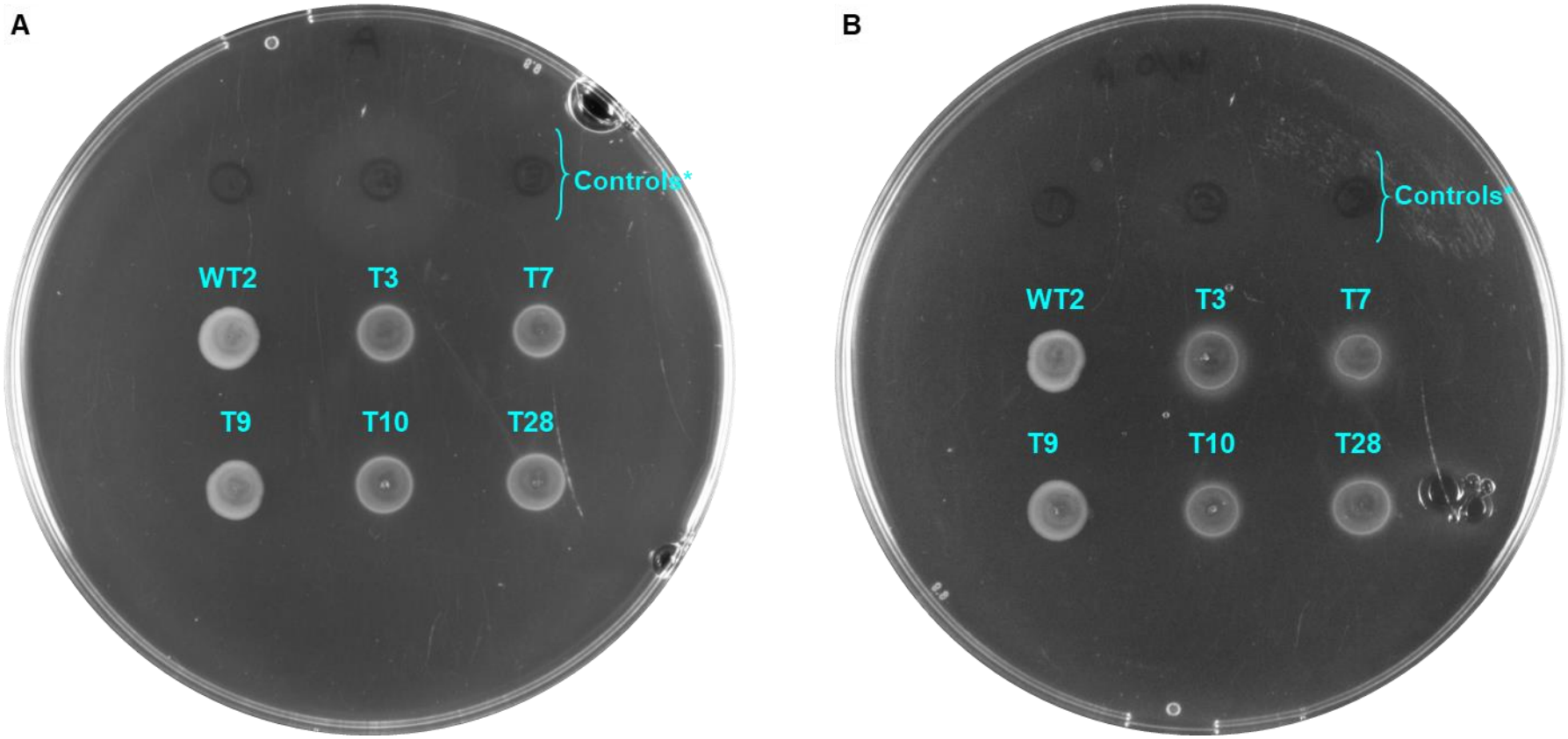
A
Controls*
WT2
T3
T7
T9
T10
T28
B
Controls*
WT2
T3
T7
T9
T10
T28

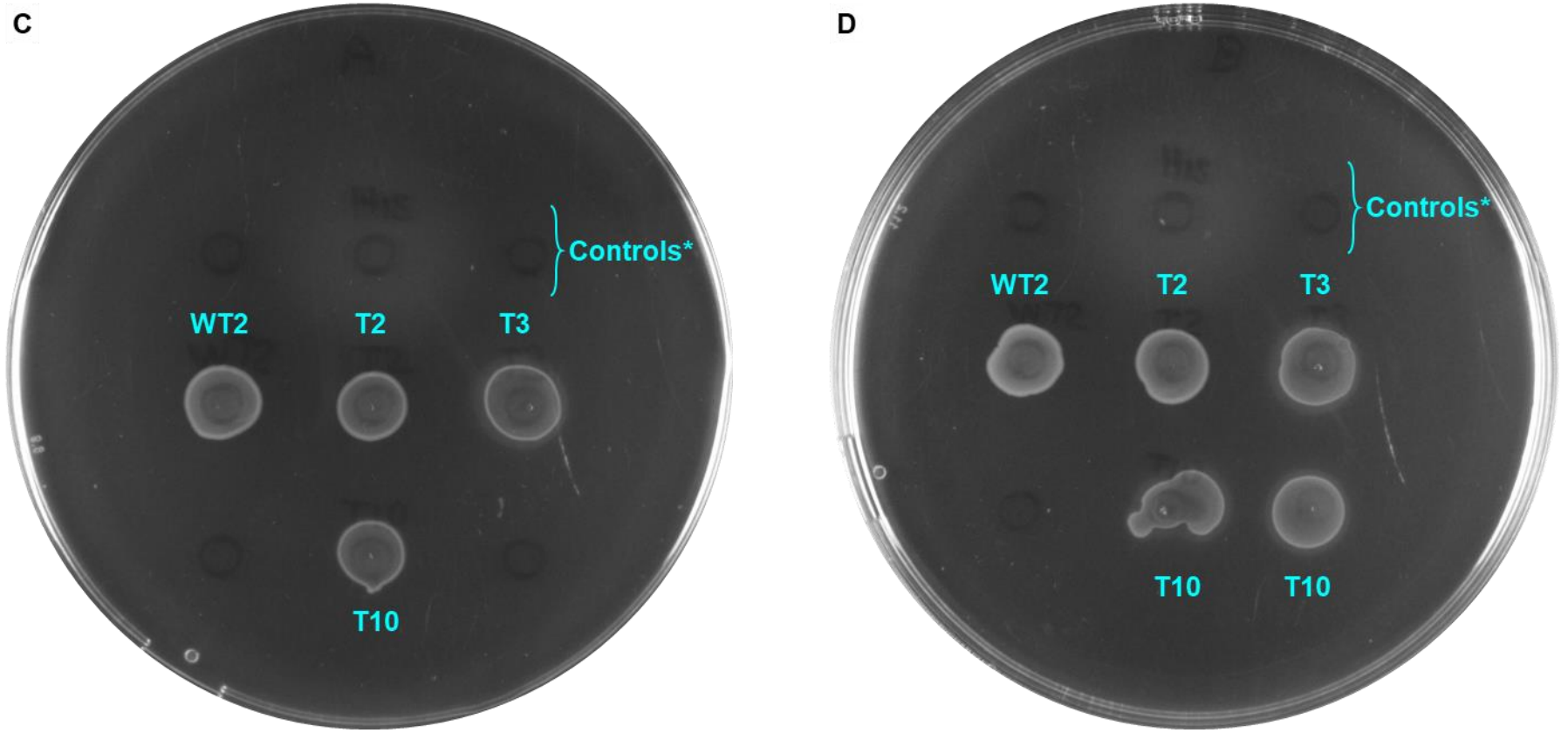

Figure 3.20: Growth of *ΔhisG* in minimal agar is rescued by recombinants carrying point mutations in T252

(**A**) Liquid cultures of recombinants presumed to be in the exponential phase (6-7 hours growth); (**B**) Liquid cultures of recombinants presumed to be in the stationary phase (overnight growth); (**C**) Liquid cultures of recombinants presumed to be in the exponential phase (6-7 hours growth); (**D**) Liquid cultures of recombinants presumed to be in the stationary phase (overnight growth). *From left to right, controls are: M63 media, 2 mM Hol, 2 mM D-His. Images taken using the BioRad Gel Doc XR+ Gel Documentation system.

In an attempt to complement the temperature sensitive growth defect of T12, T12 and our putative His secretors were spotted in close proximity on minimal plates and incubated for 4-5 days at 25 °C. However, these long incubation times resulted in excessive background growth. The plates were inconclusive and thus are not shown here.

3.7 Mutations in *hisG* Affect the Sensitivity of the RcnR-Dependent Transcriptional Response to Ni(II)

In the absence of Ni(II) (or Co(II)), RcnR represses the transcription of the RcnA efflux protein (Iwig, Rowe and Chivers, 2006). A P_{rcnA}-*lacZ* single-copy reporter construct was recombined into selected strains with *hisG* variants of interest by phage P1 transduction (Section 2.7). Assaying the Ni(II) and Co(II)-dependent LacZ activity of these recombinants can be used as a proxy for the metalation of RcnR. The effects of altered His levels on cytosolic Ni(II) and Co(II) buffering would be predicted to affect the extent of RcnR repression compared to the parent strain under the same growth conditions.

3.7.1 Single-Copy LacZ Reporter Activity in a Wild-Type Recombinant

The Ni(II)-dependent regulation of P_{rcnA}-*lacZ* was studied under acute and chronic Ni(II) stress to identify the best assay condition. Studying the acute response following metal addition allowed testing of higher Ni(II) concentrations whilst avoiding the slower growth rates associated with chronic Ni(II) stress at higher between 3.2 – 12.8 μM Ni(II) (Figure 3.21A), with a hyperbolic curve observed between 0 – 1 μM Ni(II) (Figure 3.21B). The variability in LacZ activity at 12.8 μM Ni(II) suggests this concentration is too high to be reliably used in this assay. Chronic Ni(II) stress (≤ 1.5 μM) resulted in higher LacZ activities (Figure 3.21C) but with an expression profile similar to that observed for acute Ni(II) stress over the same concentration range.

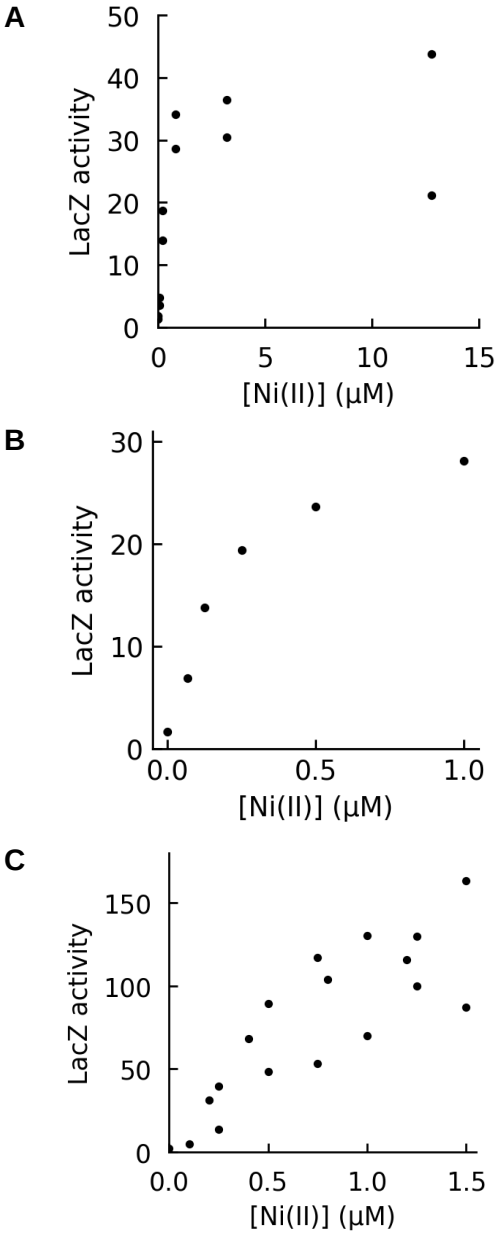

Figure 3.21: *P_{rcnA}-lacZ* is expressed in WT2 in response to Ni(II) stress

(**A, B**) P_{rcnA} expression under acute Ni(II) stress; (**C**) P_{rcnA} expression under chronic Ni(II) stress. Each point is a single sample. Multiple points at the same Ni(II) concentration are from runs on separate days. Cell growth and LacZ assays performed as described in Section 2.7.

Both of these approaches were used in the characterisation of recombinants. To allow Ni(II) insensitive recombinants (predicted higher cytosolic His) to be tested at higher concentrations of Ni(II), the acute response was studied between 0 – 3.2 μM Ni(II). In contrast, the acute response of the putative hypersensitive recombinants was initially studied over a lower Ni(II) concentration range (0 – 1 μM).

3.7.2 P_{rcnA} Expression is Lower in Recombinant Strains Predicted to Have Higher Cytosolic His

T3 (T252N), T7 (T252H) and T28 (T252R) have minimal Ni(II)-dependent P_{rcnA}-*lacZ* gene expression below 1 μM Ni(II), and when plotted, the curves may appear not to plateau (Figure 3.22). These are recombinants identified in Section 3.5.1 as secreting His into the media. The remaining Ni(II) resistant strains, T2 (T252A), T9 (T252P) and T10 (T252D), showed a similar qualitative behaviour with respect to Ni(II)-dependent P_{rcnA} expression (Figure 3.23). In this case, however, the profiles appear more hyperbolic with the highest activity ≥ 0.25 that of WT2. These observations are consistent with de-repression of His biosynthesis leading to increasing Ni(II) buffering and less Ni(II) availability to RcnR due to increased competition by His. Further, strains that secrete His have the lowest P_{rcnA} expression, potentially due to Ni(II)-buffering in the growth medium, preventing accumulation in the cell.

T3 was tested at higher concentrations of Ni(II) in an attempt to match Ni(II)-dependent gene expression to that of WT2. T3 (T252N) was tested from 4 to 16 μM Ni(II) (Figure 3.24A). P_{rcnA} expression still did not match WT2 and did not appear to plateau. Growth assay data collected as part of the LacZ assay shows that the doubling time of T3, unlike WT2, did not slow on the addition of Ni(II). The LacZ activity of WT2 decreases 12 μM to 16 μM Ni(II), presumably as Ni(II) toxicity beings to affect cell count. T28 was also tested at 4 – 16 μM Ni(II), but under chronic Ni(II) stress conditions. Once again, the expression of T28 still did not match that of WT2 (Figure 3.24C). It is possible there is sufficient His accumulation in the cytosol to buffer an excess of Ni(II). Alternatively, His secretion may reduce the extracellular availability of Ni(II).

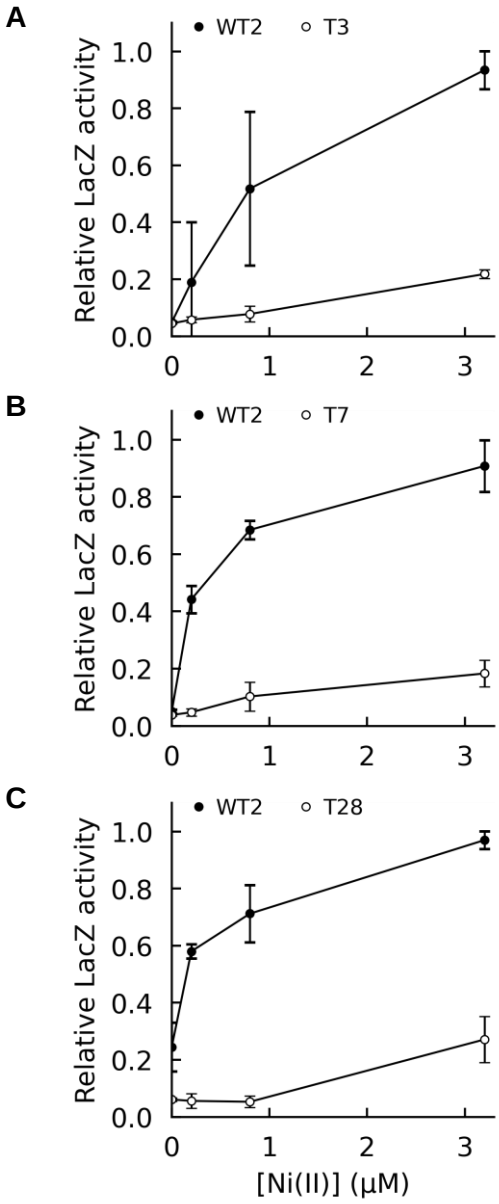

Figure 3.22: P_{rcnA} expression in candidate His secretor variants (T252N, T252H and T252R) in response to acute Ni(II) stress is lower than wild-type

(**A**) T3 (T252N); (**B**) T7 (T252H); (**C**) T28 (T252R). LacZ activity is shown relative to WT2 LacZ activity, carried out in parallel. Cell growth and LacZ assays performed as described in Section 2.7. Each point is the average of three independent cultures. Error bars represent standard deviation.

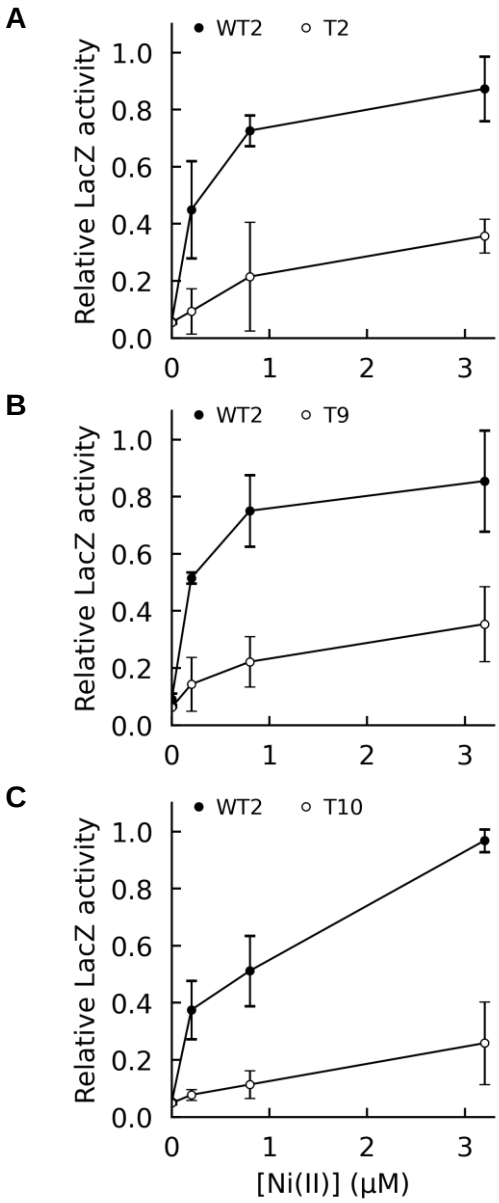

Figure 3.23: *P*$_{rcnA}$ expression in candidate elevated cytosolic His variants (T252A, T252P and T252D) in response to acute Ni(II) stress is lower than wild-type

(**A**) T2 (T252A); (**B**) T9 (T252P); (**C**) T10 (T252D). LacZ activity is shown relative to WT2 LacZ activity, carried out in parallel. Cell growth and LacZ assays performed as described in Section 2.7. Each point is the average of three independent cultures. Error bars represent standard deviation.

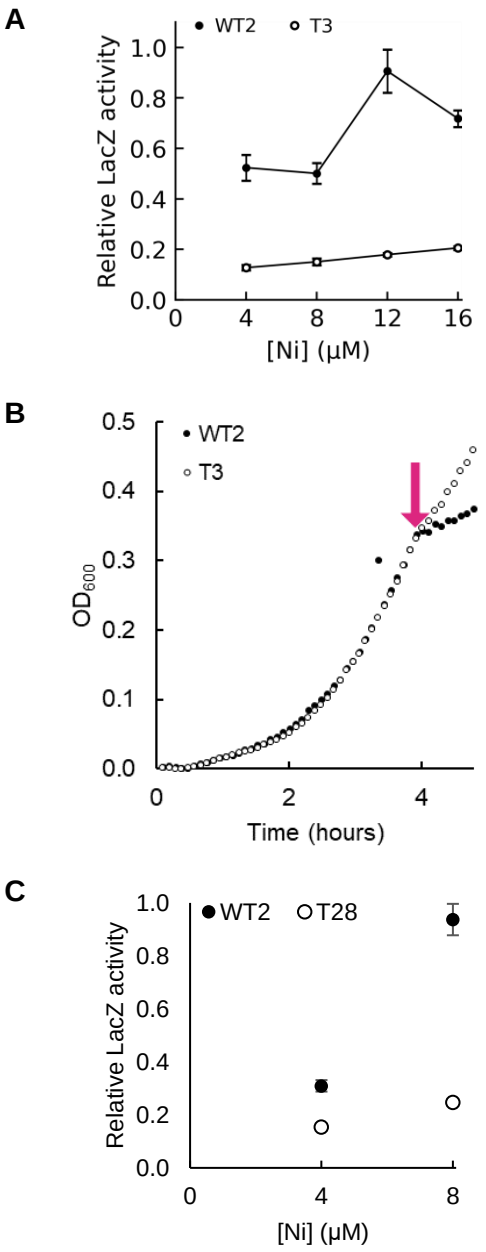

Figure 3.24: Ni(II)-dependent expression of P_{rcnA} cannot be fully de-repressed in His secreter recombinants

(**A**) P_{rcnA} expression of T3 (T252N) in response to acute Ni(II) stress. LacZ activity is shown relative to WT2 LacZ activity, carried out in parallel; (**B**) Growth curve data for panel A, 16 μM Ni(II). Magenta arrow indicates time of Ni(II) addition. Doubling times (calculated manually; see Appendix 2): one hour before Ni(II) added, WT2 = 4.14 h, T3 = 4.22 h; one hour after Ni(II) added, WT2 = 13.37 h, T3 = 4.21 h; (**C**) P_{rcnA} expression of T28 (T252R) in response to chronic Ni(II) stress. Data points at 12 and 16 μM Ni(II) have been excluded as cells did not reach the $OD_{600} \approx 0.35$ in assay timescales. LacZ activity is shown relative to WT2 LacZ activity, carried out in parallel. Each point is the average of three independent cultures. When shown, error bars represent standard deviation.

3.7.3 A T252S Point Mutation Does Not Affect Ni(II)-Dependent P_{rcnA} Response

T15 (T252S) carries a conservative Thr to Ser point mutation, which can presumably still H-bond with the His amino group (Figure 1.8E). This variant showed a small difference in Ni(II) sensitivity. Consistent with these prior observations, T15 displays similar levels of LacZ activity to WT2 using the acute response to Ni(II) stress (Figure 3.25A). There were also no differences when a broader range of Ni(II) concentrations (up to 12 μM) were tested (Figure 3.25B). Similarly, LacZ activity under chronic Ni(II) stress was not significantly different (Figure 3.25C). Hence, under these conditions, T15 is indistinguishable from WT2. Still, T252 is highly conserved across bacterial HisG enzymes (Figure 3.14), suggesting that Ser at this position may affect HisG activity in a way not detected in these assays that selects against Ser versus Thr.

3.7.4 Putative Hypersensitive Recombinants with Predicted Low Cytosolic His Show Variable P_{rcna} Expression in Response to Ni(II)

Five candidate recombinants [T12 (L17S), T34 (I58T), WT9 (S14P), WT10 (I58V) and WT12 (F101L)], each with a point mutations in a highly conserved residues of the N-terminal domain (Figure 3.14), showed increased sensitivity to Ni(II) (Figure 3.18). These presumed His feedback-hypersensitive recombinants are predicted to show enhanced P_{rcnA} response to Ni(II) at lower concentrations ($\leq$ 1 μM, where fractional WT2 P_{rcnA} expression $\leq$ 1.0) due to reduced cytosolic Ni(II) buffering by His.

Initially, T12 was tested under acute Ni(II) stress (Figure 3.26A) at a low range of Ni(II) concentrations. The LacZ activity of T12 was lower than WT2. This was unexpected as lower intracellular His levels should have a higher level of Ni(II)-dependent P_{rcnA} gene expression. Figure 3.26B shows T12, T34 and WT9 tested over a wider range of Ni(II) concentrations. Once again, the recombinants have a slightly lower level of Ni(II)-dependent P_{rcnA} gene expression, again inconsistent with the predicted His levels of these mutants based on their observed phenotypes.

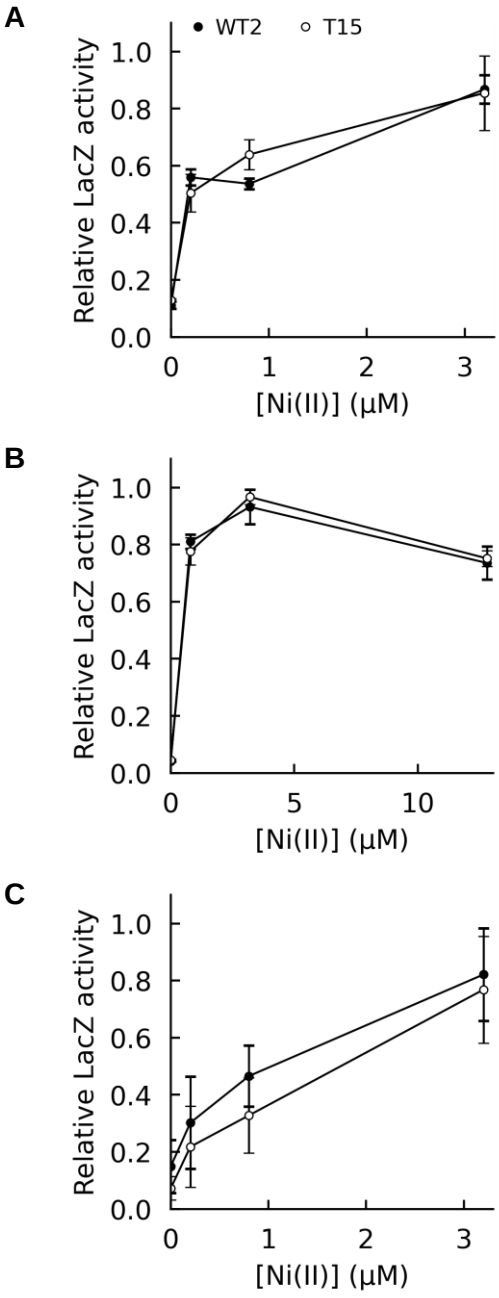

Figure 3.25: *P_{rcnA}* expression in the T15 (T252S) is similar to wild-type

(**A**) P_{rcnA} expression in response to acute Ni(II) stress (≤ 3.2 μM). (**B**) P_{rcnA} expression in response to acute Ni(II) stress (≤ 12 μM). (**C**) P_{rcnA} expression in response to chronic Ni(II) stress (≤ 3.2 μM). LacZ activity is shown relative to WT2 LacZ activity, carried out in parallel. Each point is the average of three independent cultures. When shown, error bars represent standard deviation.

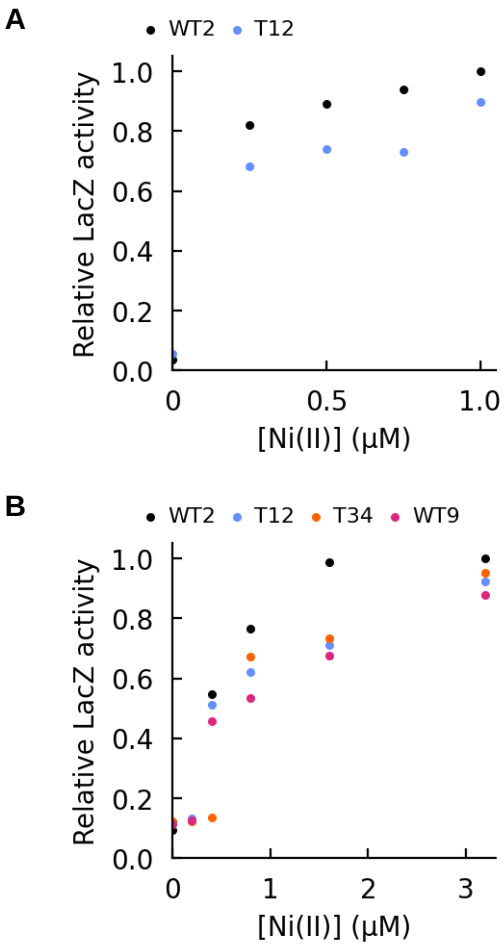

Figure 3.26: Some putative hypersensitive recombinants have a wild-type level of Ni(II)-dependent P_{rcnA}-*lacZ* expression

(**A**) T12 tested up to 1.25 μM Ni; (**B**) T12, T34 (I58V) and WT9 (S14P) tested up to 3.2 μM Ni(II). Cell growth and LacZ assays performed as described in Section 2.7. LacZ activity is shown relative to WT2 LacZ activity, carried out in parallel. Each point is a single reading.

The equation for calculating LacZ activity (Equation 2.2) uses OD_{600} as a proxy for cell count. However, filamentation observed in the putative hypersensitive recombinants appears to perturb the relationship between OD_{600} and CFUs (Figure 3.16). In an attempt to understand the P_{rcnA} expression profile of T12, its P_{rcnA} expression was corrected for CFUs (Figure 3.27). The correction results in T12 having approximately three times higher P_{rcnA} expression compared to WT2 at 1 μM extracellular Ni(II), equivalent to ~ 90 Miller Units. This level of P_{rcnA} expression is close to the chronic response in WT2 (Figure 3.21C). Additionally, as T12 cells filament in minimal media (Figure 3.15), it is probably there is a similar volume of cell present, albeit in a lower number of CFUs. It appears the previously established relationship between OD_{600} and CFUs cannot be directly applied to LacZ activity.

To further attempt to differentiate Ni(II)-dependent P_{rcnA} expression between WT2 and the putative hypersensitive recombinants, the chronic response to Ni(II) stress was tested. As T34, WT10 and WT12 were identified as being particularly sensitive to Ni(II) toxicity (Figure 3.19), these three recombinants were also supplemented with 50 μM Hol to aid growth. The supplementation should also help prevent severe filamentation, as T34 was identified in Section 3.4.1 as having a particularly low correlation between OD_{600} and CFUs. T12, T34, WT9, and WT12 all display a similar level of LacZ activity to the wild-type recombinant, while WT10 displays a higher level of LacZ activity. This phenotypic difference is particularly intriguing as WT10 and T34 contain a point mutation in the same residue (Table 3.2). Despite the change in assay conditions, the LacZ activity remains lower than predicted.

3.7.5 The P_{rcnA} Response to Co(II) is not Affected by Elevated Cytosolic His

RcnR also responds to Co(II) (Iwig et al., 2008). To test the effect of altered cytosolic His levels on Co(II) buffering, P_{rcnA} expression was tested in the T2 (T252A) variant strain in response to acute Co(II) stress. This variant shows little change in the Co(II)-dependent P_{rcnA} response compared to WT2 (Figure 3.30B). The Ni(II)-dependent P_{rcnA} response is shown for comparison (Figure 3.30A). This result suggests that cytosolic His is not a buffer of Co(II) ions.

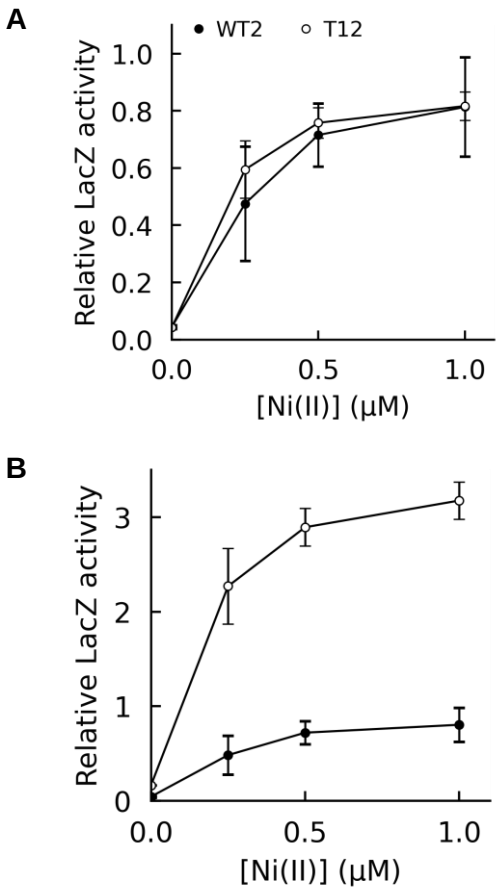

Figure 3.27: When corrected for CFUs, the relative Ni(II)-dependent P_{rcnA} expression of Class IV recombinant T12 is improbably high under chronic Ni(II) stress

(**A**) Relative LacZ activity of T12, with both WT2 and T12 adjusted for CFUs using the WT2 equation in Figure 3.16; (**B**) Relative LacZ activity with WT2 adjusted for CFUs using WT2 relationship and T12 with T12 relationship. LacZ assay performed as described in Section 2.7, studying the response to chronic Ni(II) stress. Each point is the average of three independent cultures. When shown, error bars represent standard deviation.

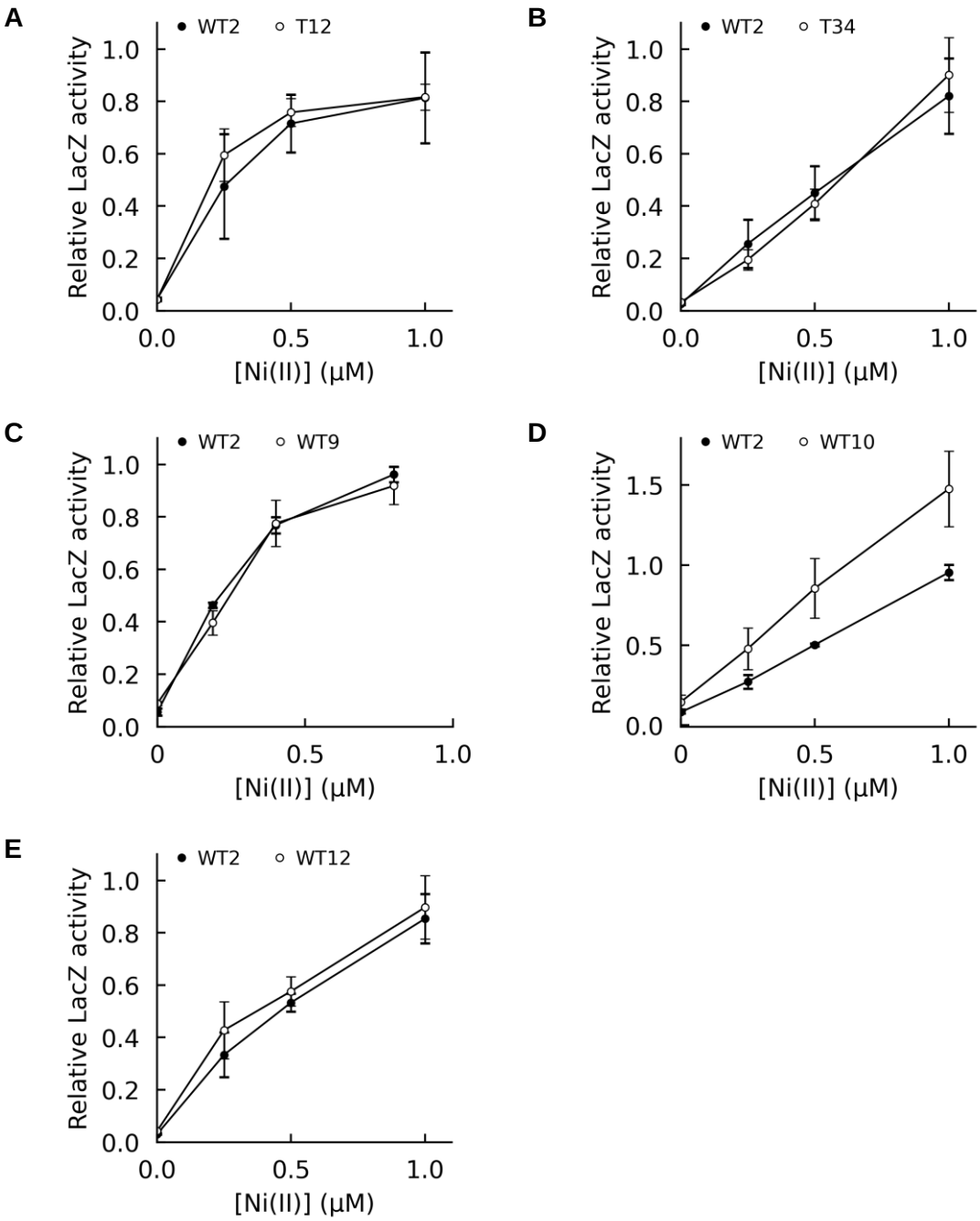

Figure 3.28: WT10 (I58T) has a higher level of Ni(II)-dependent P_{rcnA}-*lacZ* expression

(**A**) T12 (L17S); (**B**) T34 (I58V); (**C**) WT9 (S14P); (**D**) WT10 (I58T); (**E**) WT12 (F101L). LacZ activity is shown relative to WT2 LacZ activity, carried out in parallel. Cell growth and LacZ assays performed as described in Section 2.7. T34, WT10 and WT12 (and WT2, in these experiments) were supplemented with 50 μM Hol. Each point is the average of three independent cultures. When shown, error bars represent standard deviation.

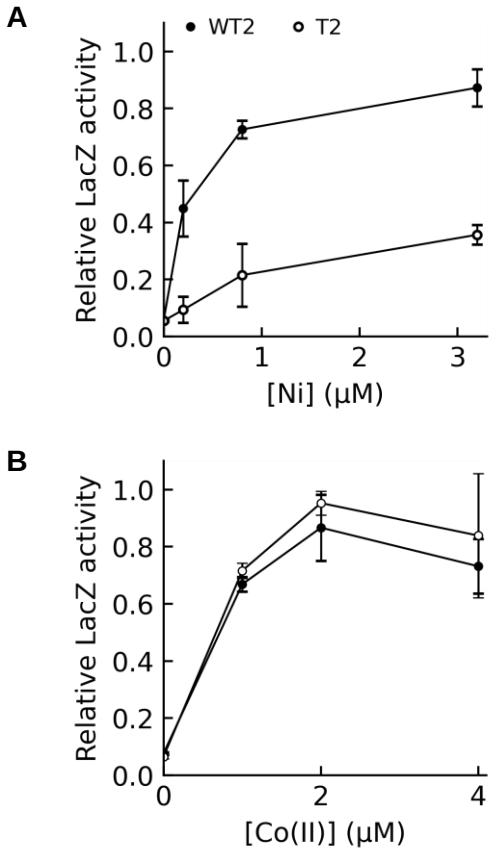

Figure 3.29: T2 (T252A) displays a similar level of Co(II)-dependent P_{rcnA}-*lacZ* expression relative to a wild-type recombinant under acute Co(II) stress

(**A**) Ni(II)-dependent P_{rcnA} expression assay; (**B**) Co(II)-dependent P_{rcnA} expression assay. Both assays performed as described in Section 2.7, studying the response to acute Ni(II) or Co(II) stress. LacZ activity is shown relative to maximal WT2 activity. Each point is the average of biological triplicates. Error bars represent standard deviation.

3.8 Ni(II) Content Varies Between Strains Under the Same Condition

A key parameter needed to properly compare P_{rcnA} expression levels across the various strains is the cytosolic Ni(II) content. It is also possible effects on His levels also affect Ni(II) content such that P_{rcnA} expression reflects a change in total cytosolic Ni(II) rather than available Ni(II) due to a change in buffering by His, or both.

The Ni(II) contents of previously assayed strains were measured using ICP-MS, growing cells under similar conditions as for the LacZ assay. Once the total Ni(II) content of a sample of known OD_{600} was determined, it was converted to Ni(II) atoms per CFU using the relationships between OD_{600} and CFUs outlined earlier (Figure 3.16). The data presented in Figure 3.30 uses the WT2-relationship for all recombinants, including those carrying a putative feedback-hypersensitive HisG. This is because an attempt to correct LacZ activity for CFUs in Section 3.7.4 did not produce meaningful data (Figure 3.27B). WT10 and WT12 are plotted separately to other recombinants as they were grown with 50 μM Hol (as in Section 3.7.4).

If the only effect on changes in Ni(II)-dependent P_{rcnA} expression was due to a change in Ni(II) buffering, then the Ni(II) content should be similar in each strain (approximately $9 * 10^5$ Ni(II) atoms per CFU). Non His-secreting strains appear to fit this relationship. However, for predicted His secretors (T3, T7 and T28) it appears that Ni(II) content is between 2.5 and 3.2-fold higher (Figure 3.30A). T10 was identified as potentially only secreting His in the stationary phase and has 1.5 times as much Ni(II) per CFU. These observations suggest that His secretion does not impact extracellular Ni(II) availability, at least in the context of chronic Ni(II) stress. The conservative T252S variant (T15) shows no significant difference in Ni(II) content, consistent with the LacZ result. The hypersensitive mutants grown with Hol (WT10 and WT12; Figure 3.30B) behave differently. WT10 shows the same Ni(II) content as WT2 consistent with reduced buffering and higher LacZ activity (Figure 3.28D). WT12 shows lower Ni(II) content, which in combination with reduced buffering could produce similar P_{rcnA} expression levels (Figure 3.28E).

Overall, the lack of a consistent relationship between Ni(II) content and LacZ suggest a more complex relationship between cytosolic Ni(II) and the levels of His produced by each strain.

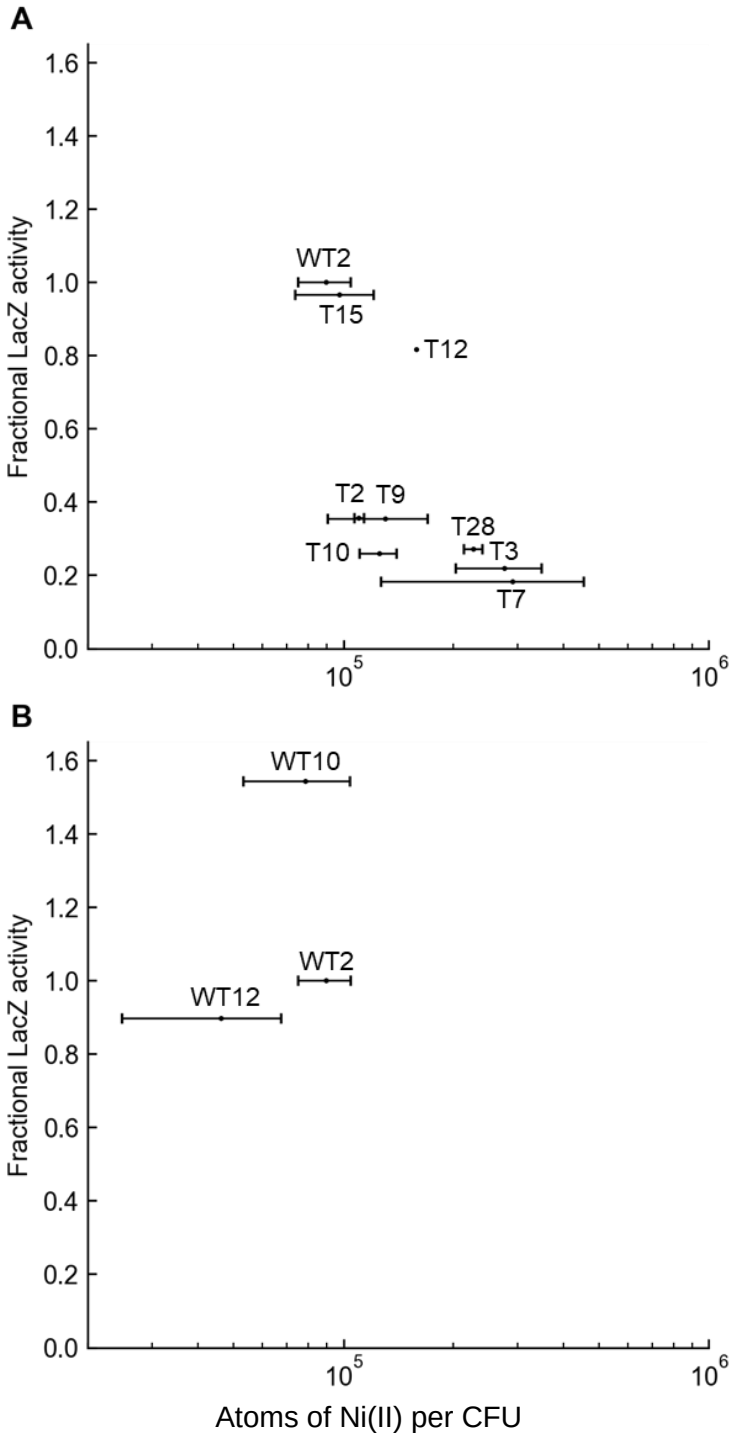

Figure 3.30: The Ni(II) content of recombinants varies with P_{rcnA} expression

(**A**) Ni(II) content of recombinants grown in M63 media with 3.2 µM Ni(II). T12 grown with 1 µM Ni(II); (**B**) Ni(II) content of WT10 and WT12 grown in M63 media with 1 µM added Ni(II) and 50 µM Hol. WT2 grown with 3.2 µM added Ni(II) without Hol supplementation and is included for comparison. ICP-MS analysis of Ni(II) content performed as described (Section 2.11). The relationship between OD_{600} and CFUs for WT2 (Figure 3.16) was used to calculate Atoms of Ni(II) per CFU for each recombinant. Attempts to correct T12 for CFUs resulted in high LacZ reporter activity (Figure 3.27B), so the correction was not applied to Ni(II) content. Each point is the average of three independent cultures (except WT2 and T2, n = 2 and T12, n = 1). When shown, error bars represent standard deviation.

3.9 Classification of Recombinants on the Basis of Ni(II) Sensitivity, His Secretion, LacZ Activity and Ni(II) Content

The various assays reported herein provide a way to group the T252 recombinants based on their behaviours (Table 3.10). Four classes of variant (I-IV) are used to categorise the recombinants. These classifications will be further analysed in the Discussion.

Table 3.10: Classification of recombinants on the basis of four phenotypes

Class	Ni(II) sensitivity[a]	Secrete His[b]	P_{rcnA} activity[c]	Ni(II) content[d]	Members
Class I	Insensitive	Yes	Minimal, may not plateau	Lower	T3 (T252N) T7 (T252H) T28 (T252R)[e]
Class II	Insensitive	No	Lower, appears to plateau	Lower	T2 (T252A) T9 (T252P) T10 (T252D)[f]
Class III	Similar to WT2	Unknown	Similar	Similar	T15 (T252S)
Class IV	Sensitive	Unknown	Varies	Varies	T12 (L17S) T34 (I58T) WT9 (S14P) WT10 (I58V) WT12 (F101L)

a, Section 3.5.
b, Section 3.5.1.
c, Section 3.7.
d, Section 3.8.
e, T28 has been placed in Class I based on His secretion and LacZ activity, despite apparent increased Ni(II) sensitivity (Figure 3.17G)
f, T10 has been placed in Class II based LacZ activity and Ni(II) content, even though it may secrete His (Figure 3.20B).

Chapter 4: Discussion

The correct metallation of proteins is essential to the survival of a cell. The identification of a critical role for metal buffering in the bacterial cytosol (Foster et al., 2017; Osman et al., 2019) has provided key insight into the mechanism(s) by which metallation is achieved and mismetallation prevented. A key thermodynamic component of cytosolic buffering is the presence of cellular components in sufficient quantity and with sufficient affinity to keep free (hydrated) metal levels below concentrations that could result in mismetallation (Equation 1.2). Small molecules are less flexible than proteins, and so multiple molecules could be involved in buffering depending upon the ligand identity and coordination geometry preferences of each metal. This thesis studied the effect of changing buffer molecule quantity; in other words, a perturbation of the equilibrium position of Equation 1.2 by mass action.

This thesis demonstrates that L-histidine (His) is a component of the cytosolic buffer for Ni(II) ions by creating site-directed mutants of HisG to eliminate feedback inhibition of His biosynthesis and thus elevated cytosolic His levels. *E. coli* strains encoding these HisG variants showed both reduced sensitivity to Ni(II) stress and a reduced Ni(II)-responsiveness by RcnR. While cytosolic His levels could not be measured, a bioassay was used to qualitatively identify mutants with elevated cytosolic His. Additionally, and usefully, the mutant construction strategy also generated mutations in *hisG* that appeared to lower His levels, leading to greater sensitivity to Ni(II) stress. The effect on Ni(II)-responsiveness by RcnR is not easily interpreted as these strains show filamentous growth morphology, which complicated data analysis that relied on accurate cell count.

4.1 Elevated His Levels Reduce Cytosolic Ni(II) Availability

Mutation of the His-binding site of HisG is known to result in elevated His levels due to the lack of feedback inhibition due to loss of allosteric regulation by His (Kulis-Horn, Persicke and Kalinowski, 2015; Wu et al., 2020). Of the mutants in T252 studied here, four classes were defined based on phenotypes linked to His levels. His secretion was linked to the presence of larger, polar, or charged residues

at position 252 (Class I variants His, Asn, Arg). These strains showed the least sensitivity to Ni(II) stress and the lowest level of Ni(II)-dependent P_{rcnA} expression compared to the wild-type strain. Indeed, the experimental data collected here suggest that Ni(II) is highly buffered in these strains and unlikely to be toxic via the normal mechanism of FbaA inhibition (Macomber, Elsey and Hausinger, 2011). Interpretation of these results may also need to consider the role of His secretion in binding Ni(II) ions in the growth medium and thus limiting their ability to enter the cell non-specifically under aerobic growth conditions. The cytosolic Ni(II) content of these strains was slightly higher than the wild-type strain, suggesting that a reduction in Ni(II) toxicity and RcnR responsiveness was not due to reduced Ni(II) content but instead due to increased buffering resulting in reduced thermodynamic availability.

In slight contrast, smaller residues (Class II variants Ala, Pro, and Asp) at position 252 did not result in detectable His secretion and additionally showed slightly more RcnR responsiveness to Ni(II). The combination of results for these two sets of mutants suggests that there is likely a limit for the cytosolic level of His and the latter class comes near to that limit but does not achieve it. The quantitative measurement of cytosolic His levels in these mutants, for example by LC-MS, will therefore inform this limit which has not been described in the literature.

One qualification when interpreting these data is the difference in exposure time to Ni(II) for the reporter assay compared to the Ni(II) content assay. P_{rcnA} expression was measured in response to acute Ni(II) stress (60 min), whilst Ni(II) content was monitored in cultures continually exposed to Ni(II). Under acute conditions cytosolic Ni(II) levels, and thus RcnR-dependent transcription, might not reflect homeostasis and be somewhat elevated. Similarly, secreted His could effectively buffer the added Ni(II) leading to decreased Ni(II) accumulation. However, preliminary data collected regarding P_{rcnA} expression in a Class I recombinant (T252N) under chronic Ni(II) stress shows LacZ activity (Figure 3.24C) similar to acute Ni(II) stress (Figure 3.24A). Hence, lowered P_{rcnA} expression in spite of an increased intracellular Ni(II) content can be attributed to His behaving as cytosolic buffer of Ni(II) with negligible effect on Ni(II)-accumulation. It is important to note that Ni(II) addition to the T252N mutant does have an effect on growth rate, indicating that it is not completely buffered by His, either intra- or extracellularly.

A further consideration when interpreting these data is that a lower level of RcnA expression might be expected from increased Ni(II)-buffering and thus cytosolic Ni(II) content would indeed be expected to be higher. This possibility could be explored by deleting *rcnA* in *hisG* variant strains. His overproducing strains should be relatively insensitive to loss of Ni(II)-efflux in response to Ni(II) stress compared to the wild-type strain and show even higher levels of Ni(II) accumulation.

No T252 mutants were obtained that showed an intermediate level of P_{rcnA} expression (e.g., 50-70 % of the wild-type strain). A likely candidate for such a mutant would be the Thr to Ser substitution. However, the T252S Class III variant behaved indistinguishably from the wild-type strain in the experiments carried out in this thesis. Ser can adopt a side-conformation that positions its side-chain hydroxyl nearly identically to T252 (Figure 3.17F), which would explain these results. However, T252 is highly conserved in a HisG sequence alignment (Figure 3.14), suggesting that Ser is not a physiologically suitable substitution. Measuring the cytosolic His levels and biochemical characterisation of the kinetic properties of this HisG variant (K_i for His) may reveal a quantifiable difference in the two enzymes. For example, there are multiple small molecules that regulate HisG activity (e.g., ppGpp and AMP, Section 1.6.2). These may be present in different amounts under different growth conditions, and act synergistically with His (K_i) in the Ser variant differently than in the wild-type enzyme. Alternatively, the Ser substitution could affect protein stability and/or translation under conditions not tested here in a way that selects for Thr at this position.

4.2 Mutants With Apparent Low Cytosolic His Exhibit Conflicting Phenotypes

The experimental design for generating HisG mutants was only going to yield strain with reduced His levels if a substitution of T252 mimic, at least in part, His binding to the regulatory domain. However, as a result of the intentional use of a lower fidelity DNA polymerase during fragment generation, several mutations separate from the T252 codon were found (Table 3.2). Serendipitously, one of these (T12) showed increased Ni(II)-sensitivity consistent with lower cytosolic His levels (and increased Ni(II)-inhibition of FbaA). Close inspection of the T12 colony morphology

(Figure 3.8) enabled identification of additional variants with mutations at codons other than T252 and all within the catalytic domain of HisG.

His-deficient strains of *Salmonella* and *E. coli* described in the literature mostly pre-date DNA-sequencing and the HisG enzymes are poorly biochemically characterised (Sheppardz, 1964; O'Donovan and Ingraham, 1965; O'Donovan, Kearney and Ingraham, 1965; Roth, Antón and Hartman, 1966; Hartman et al., 1971). Thus, a mechanistic understanding of how His biosynthesis is reduced in these strains is largely unknown. Filamentation was observed in strains of *E. coli* and *Salmonella* carrying a HisG hypersensitive to feedback inhibition by His (O'Donovan and Ingraham, 1965; Roth, Antón and Hartman, 1966). This hypersensitivity was determined through assays of HisG activity in cell lysates (O'Donovan and Ingraham, 1965). Filamentation arises as a result of *his* operon overexpression, specifically, the HisH-HisF enzyme complex, in an attempt to compensate for impaired His biosynthesis (Murray and Hartman, 1972; Frandscen and D'Ari, 1993; Flores and Casadesus, 1995; Cano et al., 1998). The colony morphology in the Class IV variants identified in this work was consistent with filamentation due to His operon overexpression. The subsequent tests of temperature dependent growth and the ability of histidinol and/or His to complement the filamentous phenotype and His operon overexpression are also consistent with the reported phenotypes and indicate the cytosol is apparently His-deficient.

The positions of the point mutations in Class IV HisG mutants is of general interest as almost all previous mutants are genetically mapped at best (Hartman et al., 1971). Formally, HisG would show lower catalytic activity, and thus lower cytosolic His, if a mutation mimicked His binding leading to a constitutively inhibited enzyme. Similarly, mutations at the binding sites for other inhibitors or in key catalytic residues could also result in lower pathway flux and lower His. All point mutations identified in this this study are located near the active site where PRPP, ATP, ADP, and AMP bind (Figure 3.14) suggesting that they may have lower HisG activity independent of His binding. Most of the mutated residues are highly conserved, potentially consistent with lowered activity due to perturbation of key interactions needed for substrate binding or catalysis (Section 3.4.2).

HisG activity assays are well documented in literature (Kulis-Horn, Persicke and Kalinowski, 2015; Wu et al., 2020). Detailed kinetic characterisation of the HisG variants from this study (including representatives of the Class I and II variants) will identify changes in substrate K_m (PRPP and ATP) and inhibitor K_i (His, AMP, ADP, and ppGpp) and make a valuable contribution to the literature of the regulation of His biosynthesis.

Discerning whether all Class IV HisG variants are similarly altered in their catalytic properties will also be important as phenotypic differences were evident between the strains.

(1) A difference in apparent filamentation (OD_{600} versus CFU; Figure 3.16).
(2) Differing sensitivities to Ni(II) stress (Figure 3.18).
(3) Differing Ni(II)-dependent P_{rcnA} expression profiles (Figure 3.28).

Filamentation in Class IV mutants correlated with lower CFUs per OD_{600} than the parent strain. Changes in cell morphology present a technical challenge, even before considering varying degrees of filamentation within Class IV. Studies on ampicillin-induced filamentation of LB-grown *E. coli* showed substantial deviation between OD_{600} and the number of cells (Stevenson et al., 2016). Notably, during exponential phase ($OD_{600} \geq 0.2$), as OD_{600} first increases, the cell count remains fairly constant (corresponding to an increase in cell mass/size). OD_{600} then decreases (as filaments divide into smaller cells), whereupon cell count and OD_{600} then both increase as filamentous bacteria both divide and grow as smaller cells. The extended lag times, slower growth rates and lower maximum OD_{600} of Class IV could be due in part to effects of cell morphology on OD_{600}. Nonetheless, these strains are all more sensitive to Ni(II) stress.

Cell morphology may also affect determination of P_{rcnA} activity as OD_{600} readings were used to quantify LacZ activity. Attempting to correct OD_{600} by using CFUs in this context data was unsuccessful and resulted in LacZ activity levels at least double those seen with the fully de-repressed wild-type strain (Figure 3.27). Previously, a multicopy P_{rcnA}-*lacZ* reporter in a Δ*rcnR* background showed the same activity as a fully Ni(II)-derepressed strain (Iwig, Rowe and Chivers, 2006). The relatively small OD_{600} range calibrated in this work (Figure 3.16) may not accurately reflect the true relationship between OD_{600} and CFUs. Correcting OD_{600} for cell

mass would probably yield a more robust correction. To reduce filamentation, the Ni(II)-dependent P_{rcnA} expression and Ni(II) content of T34, WT10 and WT12 was measured in the presence of 50 μM Hol, although the exact effect of this small quantity of Hol on filamentation and the relationship between OD_{600} and CFUs (and/or cell mass) in this scenario remains to be determined.

The Ni(II)-dependent P_{rcnA} expression profile of WT10 (I58V) is notable. Unlike the other Class IV mutants, this variant had higher LacZ activity compared to the parent strain. It is particularly interesting that T34 (I58T) did not show this increased activity, even though the two variants exhibited similar sensitivities to Ni(II) stress (Figure 3.18B and D). Both strains appear to grow particularly slowly and to a lower final density (albeit with the caveats mentioned above), suggesting mutations of this residue are most deleterious for HisG activity overall. An important control will be to re-transform the sequence fragments to verify that the difference in LacZ phenotype does not arise from outside *hisG* or results from the P1 transduction of the P_{rcnA}-*lacZ* reporter into the two variant strains (*hisG* is located 1.7 Mb from *lacZ*, well outside the typical 100 kb fragment size recombined in a P1 transduction. Indeed, all variants identified in this study should be re-transformed to ensure phenotypes are linked solely to the mutation in *hisG*.

Increased sensitivity to Ni(II) stress of *E. coli* grown with glucose arises from inhibition of fructose-1,6-bisphosphate aldolase II (FbaA) through displacement of a catalytic Zn(II) (Macomber, Elsey and Hausinger, 2011). Reduced cytosolic His levels would increase the likelihood of mismetallation of FbaA at lower extra-cellular Ni(II) concentrations. As Ni(II)-toxicity is reduced when *E. coli* are grown with glycerol as a carbon source (Macomber, Elsey and Hausinger, 2011), it would be useful to grow the variants under this condition to see if the toxicity is alleviated as it is in the parent strain. However, interpretation of this data could be complicated by the slower growth of wild-type *E. coli* on glycerol, which may be exacerbated by de-repression of *his* operon expression. Similarly, the filamentation of *E. coli* due to *his* operon overexpression (and potentially other unidentified physiological changes) may create a new, previously unknown site for Ni(II) mismetallation that supersedes the FbaA site regardless of growth condition. Also of note, *E. coli* grown with glycerol instead of glucose as a carbon source not only rely less on FbaA activity but have higher intracellular His (Bennett et al., 2009). A mechanistic basis for this

difference has not been put forward, which provides a further justification for examining growth of the variants from each Class with glycerol as a carbon source.

4.3 Future Directions

The quantification of intracellular His levels in different variants is the most important next step. His quantification can also be used to guide simulations of Ni(II)-dependent transcriptional responses using Dynafit (Kuzmič, 1996), which have previously established that His is able to compete with RcnR (and NikR) for metal ions (Scott, 2018; Bowers, 2020). Here, the Ni(II)-dependent DNA occupancy of RcnR in the presence of different concentrations of His has been simulated (Figure 4.1). The Ni(II) content and corresponding fractional DNA occupancy of RcnR based on LacZ assays have been overlaid. These simulations are supportive of Class I and II having elevated cytosolic His and thus greater thermodynamic competition for Ni(II) by the buffer compared to wild-type. The simulations suggest that cytosolic His concentrations are > 1 mM for the Class I mutants and around 1 mM for the Class II mutants, based on the observed LacZ activity as a function of Ni(II). A significant limitation of this interpretation is a lack of LacZ activities as a function of different Ni(II) content (i.e., different added Ni(II)). As an example, it is possible a lower intracellular Ni(II) content could still result in 100 % LacZ activity for WT2. Additionally, after the experimental work was completed, a biochemical analysis the labile Ni(II) pool in *E. coli* lysates was described (Brawley and Lindahl, 2021) and identified additional Ni(II) complexes with oxidised glutathione, aspartic acid and ATP. Apparently, none of these complexes were composed of mixed ligands and the authors did not consider this a possibility despite evidence for mixed Ni(II)-amino acid complexes (Blackburn and Jones, 1973). Additionally, ATP was not identified as a contributor to the biochemical buffering of the RcnR paralog InrS from cyanobacteria (Foster et al., 2017). Critically, mixed complexes of Ni(II) with His and other molecules will likely be needed for accurate simulations of RcnR (and NikR) DNA occupancy so the *in silico* modelling is presented in this thesis is a useful tool, but likely simplifies Ni(II)-ligand interactions in the cytosol, of which His is a critical component.

It will also be important to identify whether other metals also form cytosolic complexes with His in parallel to the measurement of His levels and modelling of mixed buffer complexes. Data collected in this thesis shows His is not a universal metal buffer, due to the absence of any change in the Co(II)-dependent response of RcnR with elevated His (Figure 3.29), consistent with the original study of Δ*his* mutants (Nichols et al., 2011) and Dynafit modelling (Bowers, 2020). It may prove interesting to test the Co(II)-responsive RcnR expression of Class IV recombinants. An analysis of metal-dependent transcriptional responses to first row transition metals in strains from each Class will help to identify these buffer complexes.

A final important set of experiments should focus on the effect of altered His levels on anaerobic Ni(II) homeostasis in *E. coli*, when [NiFe]-hydrogenases contribute to energy metabolism (Section 1.4) (Böck et al., 2006; Forzi and Sawers, 2007; Higgins, 2019). These experiments would reveal the extent to which Ni(II)-buffering by His occurs under anaerobic conditions when Ni(II)-binding proteins are present. Under these conditions, NikR is required to repress expression of the NikABCDE importer system. Class I and II mutants may demonstrate elevated P_{nik} expression if increased His effectively competes with NikR. It will be interesting to see how hydrogenase activity is affected in these mutants, and whether they accumulate cytosolic Ni(II) but cannot assemble active enzyme. Additionally, His secretion by Class I may also aid Ni(II) uptake in minimal medium as NikA recognises a Ni-(L-His)$_2$ complex (Chivers et al., 2012) for import into the cell. Conversely, in a His-deficient cytosol (Class IV mutants), premature activation of NikR may reduce Ni(II) accumulation due to repression of NikABCDE levels. However, the extra capacity for Ni(II)-binding by the Hyp metallochaperone system may mean that hydrogenase activity is observed at higher added Ni(II) concentrations, as observed in Δ*nikA E. coli*.

Regardless of the specific experiments and their outcomes, the mutants identified in this study have made a key contribution to our understanding of metal buffering in the bacterial cytosol.

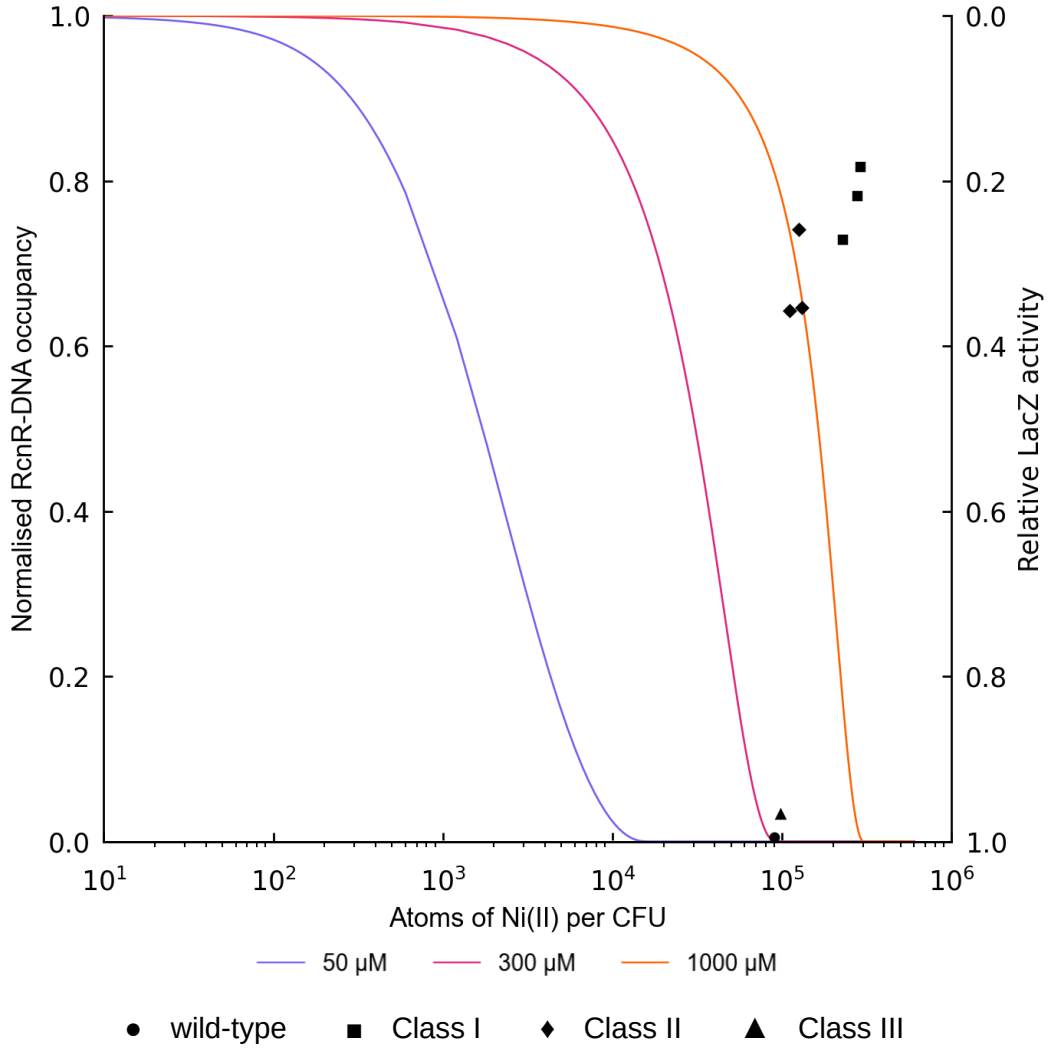

Figure 4.1: Dynafit modelling reveals predicted fractional DNA occupancy of RcnR

Dynafit script used to generate Normalised RcnR-DNA occupancy given in Appendix 3. Relative LacZ activity is as given in Section 3.7 and Number of Ni(II) Atoms per CFU is as given in 3.8.

Chapter 5: Appendices

Appendix 1

DNA Sequences

hisG

Sequence of the *E. coli hisG* gene (Médigue et al., 1993). Coding sequence displayed in black; upstream and downstream regions are displayed in blue. Regions Primers 1 and 2 anneal to are highlighted in purple and pink respectively; the region Primers 3 and 4 anneal to in grey (Table 2.5). T252 codon is underlined.

CATTCAGATCTTCCAGTGGTGCATGAACGCATGAGAAAGCCCCCGGAAGATCACCTTCCGGGGGCTTT
TTTATTGCGCGGTTGATAACGGTTCAGACAGGTTTAAAGAGGAATAACAAAATGACAGACAACACTCG
TTTACGCATAGCTATGCAGAAATCCGGCCGTTTAAGTGATGACTCACGCGAATTGCTGGCGCGCTGTG
GCATTAAAATTAATCTTCACACCCAGCGCCTGATCGCGATGGCAGAAAACATGCCGATTGATATTCTG
CGCGTGCGTGACGACGACATTCCCGGTCTGGTAATGGATGGCGTGGTAGACCTTGGGATTATCGGCGA
AAACGTGCTGGAAGAAGAGCTGCTTAACCGCCGCGCCCAGGGTGAAGATCCACGCTACTTTACCCTGC
GTCGTCTGGATTTCGGCGGCTGTCGTCTTTCGCTGGCAACGCCGGTTGATGAAGCCTGGGACGGTCCG
CTCTCCTTAAACGGTAAACGTATCGCCACCTCTTATCCTCACCTGCTCAAGCGTTATCTCGACCAGAA
AGGCATCTCTTTTAAATCCTGCTTACTGAACGGTTCTGTTGAAGTCGCCCCGCGTGCCGGACTGGCGG
ATGCGATTTGCGATCTGGTTTCCACCGGTGCCACGCTGGAAGCTAACGGCCTGCGCGAAGTCGAAGTT
ATCTATCGCTCGAAAGCCTGCCTGATTCAACGCGATGGCGAAATGGAAGAATCCAAACAGCAACTGAT
CGACAAACTGCTGACCCGTATTCAGGGTGTGATCCAGGCGCGCGAATCAAAATACATCATGATGCACG
CACCGACCGAACGTCTGGATGAAGTCATCGCCCTGCTGCCAGGTGCCGAACGCCCAACTATTCTGCCG
CTGGCGGGTGACCAACAGCGCGTAGCGATGCACATGGTCAGCAGCGAAACCCTGTTCTGGGAAACCAT
GGAAAAACTGAAAGCGCTGGGTGCCAGTTCAATTCTGGTCCTGCCGATTGAGAAGATGATGGAGTGAT
CGCCATGAGCTTTAACACAATCATTGACTGGAATAGCTGTACTGCGGAGCAACAACGCCAGCTGTTAA
TGCGCCCGGCGATTTCCGCCTCTGAAAGC

kan^r

Sequence of the *kan*^{r} cassette used in *ΔhisG* KO strain to disrupt *hisG* (Datsenko and Wanner, 2000). Sites where primers k1 and k2 (Table 2.5) anneal are highlighted in orange and blue, respectively.

TTAGAAGAACTCGTCAAGAAGGCGATAGAAGGCGATGCGCTGCGAATCGGGAGCGGCGATACCGTAAA
GCACGAGGAAGCGGTCAGCCCATTCGCCGCCAAGCTCTTCAGCAATATCACGGGTAGCCAACGCTATG
TCCTGATAGCGGTCCGCCACACCCAGCCGGCCACAGTCGATGAATCCAGAAAAGCGGCCATTTTCCAC
CATGATATTCGGCAAGCAGGCATCGCCATGGGTCACGACGAGATCCTCGCCGTCGGGCATGCGCGCCT
TGAGCCTGGCGAACAGTTCGGCTGGCGCGAGCCCCTGATGCTCTTCGTCCAGATCATCCTGATCGACA
AGACCGGCTTCCATCCGAGTACGTGCTCGCTCGATGCGATGTTTCGCTTGGTGGTCGAATGGGCAGGT
AGCCGGATCAAGCGTATGCAGCCGCCGCATTGCATCAGCCATGATGGATACTTTCTCGGCAGGAGCAA
GGTGAGATGACAGGAGATCCTGCCCCGGCACTTCGCCCAATAGCAGCCAGTCCCTTCCCGCTTCAGTG
ACAACGTCGAGCACAGCTGCGCAAGGAACGCCCGTCGTGGCCAGCCACGATAGCCGCGCTGCCTCGTC
CTGCAGTTCATTCAGGGCACCGGACAGGTCGGTCTTGACAAAAAGAACCGGGCGCCCCTGCGCTGACA
GCCGGAACACGGCGGCATCAGAGCAGCCGATTGTCTGTTGTGCCCAGTCATAGCCGAATAGCCTCTCC
ACCCAAGCGGCCGGAGAACCTGCGTGCAATCCATCTTGTTCAATCAT

P_{rcnA}-lacZ

Ni-dependent gene expression of recombinants generated in Section 2.5 was assayed via a single-copy *P_{rcnA}-lacZ* reporter introduced into each strain by P1 phage transduction. The sequence of the reporter is as below:

ggccgacagatgtgtccacgctggatgttgatgcaatggtggtacgcgaaaccactcaccgtttcagc
cgcttatcctttcaccgggcaatggtcgggcgacgtttgccgcttctgaaaaccgcctcgggcctgac
ctggctggccttttgcccggaacaagaccgcaaggaattaatcgaaatgttagcctcccgccccggtg
atgactatcaactggcacgggaaccgttaaagctggaagccattctggcgcgcgcgcgcaaagagggt
tacggacagaactaccgcggctgggatcaggaggagaagatcgcctctatcgccgtaccgctgcgcag
tgaacaacgggtgattggctgtctgaatctggtgtatatggcgagcgcaatgaccattgaacaggcag
cggaaaagcatcttccggcgctacaacgggtagcaaaacagatcgaagaaggggttgaatcgcaggct
attctggtggccggaaggcgaagcggcatgcatttacgttgacaccatcgaatggcgcaaaacctttc
gcggtatggcatgatagcgcccggGTGTAGGCTGGAGCTGCTTCGAAGTTCCTATACTTTCTAGAGAA
TAGGAACTTCGGAATAGGAACTTCAAGATCCCCTTATTAGAAGAACTCGTCAAGAAGGCGATAGAAGG
CGATGCGCTGCGAATCGGGAGCGGCGATACCGTAAAGCACGAGGAAGCGGTCAGCCCATTCGCCGCCA
AGCTCTTCAGCAATATCACGGGTAGCCAACGCTATGTCCTGATAGCGGTCCGCCACACCCAGCCGGCC
ACAGTCGATGAATCCAGAAAAGCGGCCATTTTCCACCATGATATTCGGCAAGCAGGCATCGCCATGGG
TCACGACGAGATCCTCGCCGTCGGGCATGCGCGCCTTGAGCCTGGCGAACAGTTCGGCTGGCGCGAGC
CCCTGATGCTCTTCGTCCAGATCATCCTGATCGACAAGACCGGCTTCCATCCGAGTACGTGCTCGCTC
GATGCGATGTTTCGCTTGGTGGTCGAATGGGCAGGTAGCCGGATCAAGCGTATGCAGCCGCCGCATTG
CATCAGCCATGATGGATACTTTCTCGGCAGGAGCAAGGTGAGATGACAGGAGATCCTGCCCCGGCACT
TCGCCCAATAGCAGCCAGTCCCTTCCCGCTTCAGTGACAACGTCGAGCACAGCTGCGCAAGGAACGCC
CGTCGTGGCCAGCCACGATAGCCGCGCTGCCTCGTCCTGCAGTTCATTCAGGGCACCGGACAGGTCGG
TCTTGACAAAAAGAACCGGGCGCCCCTGCGCTGACAGCCGGAACACGGCGGCATCAGAGCAGCCGATT
GTCTGTTGTGCCCAGTCATAGCCGAATAGCCTCTCCACCCAAGCGGCCGGAGAACCTGCGTGCAATCC
ATCTTGTTCAATCATGCGAAACGATCCTCATCCTGTCTCTTGATCAGATCTTGATCCCCTGCGCCATC
AGATCCTTGGCGGCAAGAAAGCCATCCAGTTTACTTTGCAGGGCTTCCCAACCTTACCAGAGGGCGCC
CCAGCTGGCAATTCCGGTTCGCTTGCTGTCCATAAAACCGCCCAGTCTAGCTATCGCCATGTAAGCCC
ACTGCAAGCTACCTGCTTTCTCTTTGCGCTTGCGTTTTCCCTTGTCCAGATAGCCCAGTAGCTGACAT
TCATCCGGGGTCAGCACCGTTTCTGCGGACTGGCTTTCTACGTGTTCCGCTTCCTTTAGCAGCCCTTG
CGCCCTGAGTGCTTGCGGCAGCGTGAGCTTCAAAAGCGCTCTGAAGTTCCTATACTTTCTAGAGAATA
GGAACTTCGAACTGCAGGTCGACGGATCCCCGGATaacggcagttttacaatcgcgttaataaattat
ttgatatatgaatccagcaccttcagaacgacatccagatcttcttcacgttttagctcatccccctg
gtgaacgatgtgttccgtcagatgacctttaatcacttcccgcatcagaccgtttaccgcgccacgga
tagcagcaatctgttgtaaaactgcagcgcattcgtgcggctcgtcgagcattttcttgagcgccacg
acctggccctgaatcttactggcacgcgctttcagtttctgtttatcacggattgtatgagacatggc
aacacctggttaacaagaatatgaaaaatcatagcactattaatctactgggggtagtatcaggtac
tgggggggagtagaatcagattgccgaattaatactaagaattattatcatgaccatgattacggatt
cactggccgtcgttttacaacgtcgtgactgggaaaaccctggcgttacccaacttaatcgccttgca

gcacatccccctttcgccagctggcgtaatagcgaagaggcccgcaccgatcgcccttcccaacagtt
gcgcagcctgaatggcgaatggcgctttgcctggtttccggcaccagaagcggtgccggaaagctggc
tggagtgcgatcttcctgaggccgatactgtcgtcgtcccctcaaactggcagatgcacggttacgat
gcgcccatctacaccaacgtgacctatcccattacggtcaatccgccgtttgttcccacggagaatcc
gacgggttgttactcgctcacatttaatgttgatgaaagctggctacaggaaggccagacgcgaatta
ttttgatggcgttaactcggcgtttcatctgtggtgcaacgggcgctgggtcggttacggccaggac
agtcgtttgccgtctgaatttgacctgagcgcatttttacgcgccggagaaaaccgcctcgcggtgat
ggtgctgcgctggagtgacggcagttatctggaagatcaggatatgtggcggatgagcggcattttcc
gtgacgtctcgttgctgcataaaccgactacacaaatcagcgatttccatgttgccactcgctttaat
gatgatttcagccgcgctgtactggaggctgaagttcagatgtgcggcgagttgcgtgactacctacg
ggtaacagtttctttatggcagggtgaaacgcaggtcgccagcggcaccgcgcctttcggcggtgaa

Appendix 2

Analysis of Growth Assay Data Using GrowthCurver R Package

Growth assays were performed as described in Section 2.6. Each growth assay used a 24-well plate, allowing WT2 and another recombinant to be analysed under four different conditions in triplicate. OD_{600} was measured every 5.75 minutes, resulting in large datasets for each assay. OD_{600} measurements were corrected for background and pathlength as described in Equation 2.1.

GrowthCurver fits the growth assay data to a standard form of the logistic equation common in ecology and evolution whose parameters (the growth rate, the initial population size, and the carrying capacity) provide meaningful population-level information with straight-forward biological interpretation (Sprouffske and Wagner, 2016). The logistic equation describes the population size, N_t, at time t using Equation 6.1 (where is N_0 population at $t = 0$, K is the maximum possible population, and r is the growth rate if no restrictions were imposed on total population size).

$$N_t = \frac{K}{1 + \left(\frac{K - N_0}{N_0}\right) e^{-rt}} \qquad 6.1$$

The doubling time (t_{DT}) can be extracted from these parameters using Equation 6.2.

$$t_{DT} = \frac{ln2}{r} \quad 6.2$$

More information can be found in the associated vignette: https://cran.r-project.org/web/packages/growthcurver/vignettes/Growthcurver-vignette.html

The Figures below show the raw data points (black circles) overlaid with the curve fitted to the data by GrowthCurver (red line). In all figures, columns 1-3 are WT2 and columns 4-6 are the named recombinant.

GrowthCurver Analysis of Class I, II and III recombinants

Class I (T3, T7, T28), II (T2, T9, T10) and III (T15) recombinants were grown with 0 μM (row A), 4 μM (row B), 8 μM (row C) and 12 μM (row D) Ni(II).

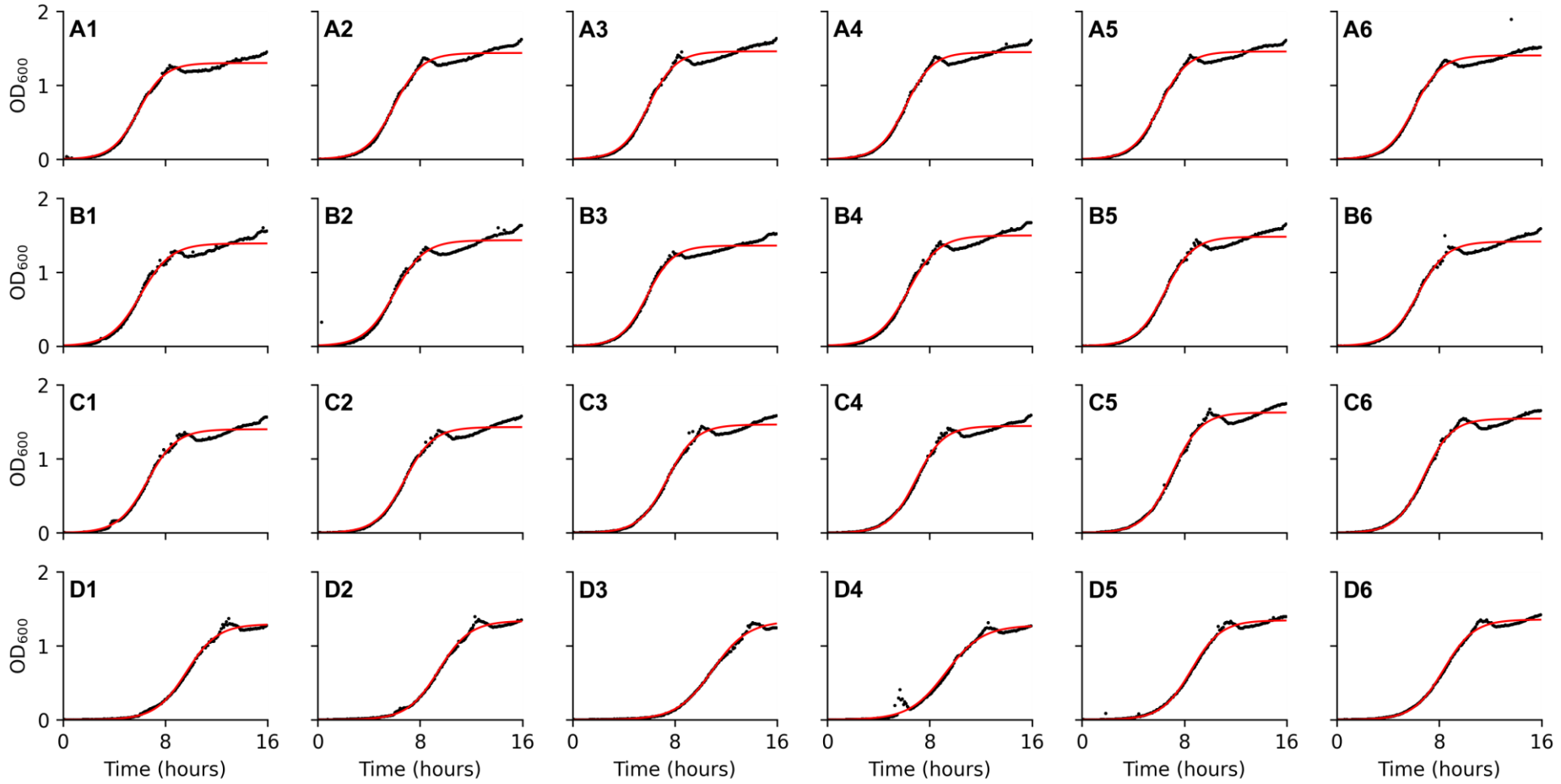

Figure 5.1: Analysis of T2 (T252A) growth using GrowthCurver R package

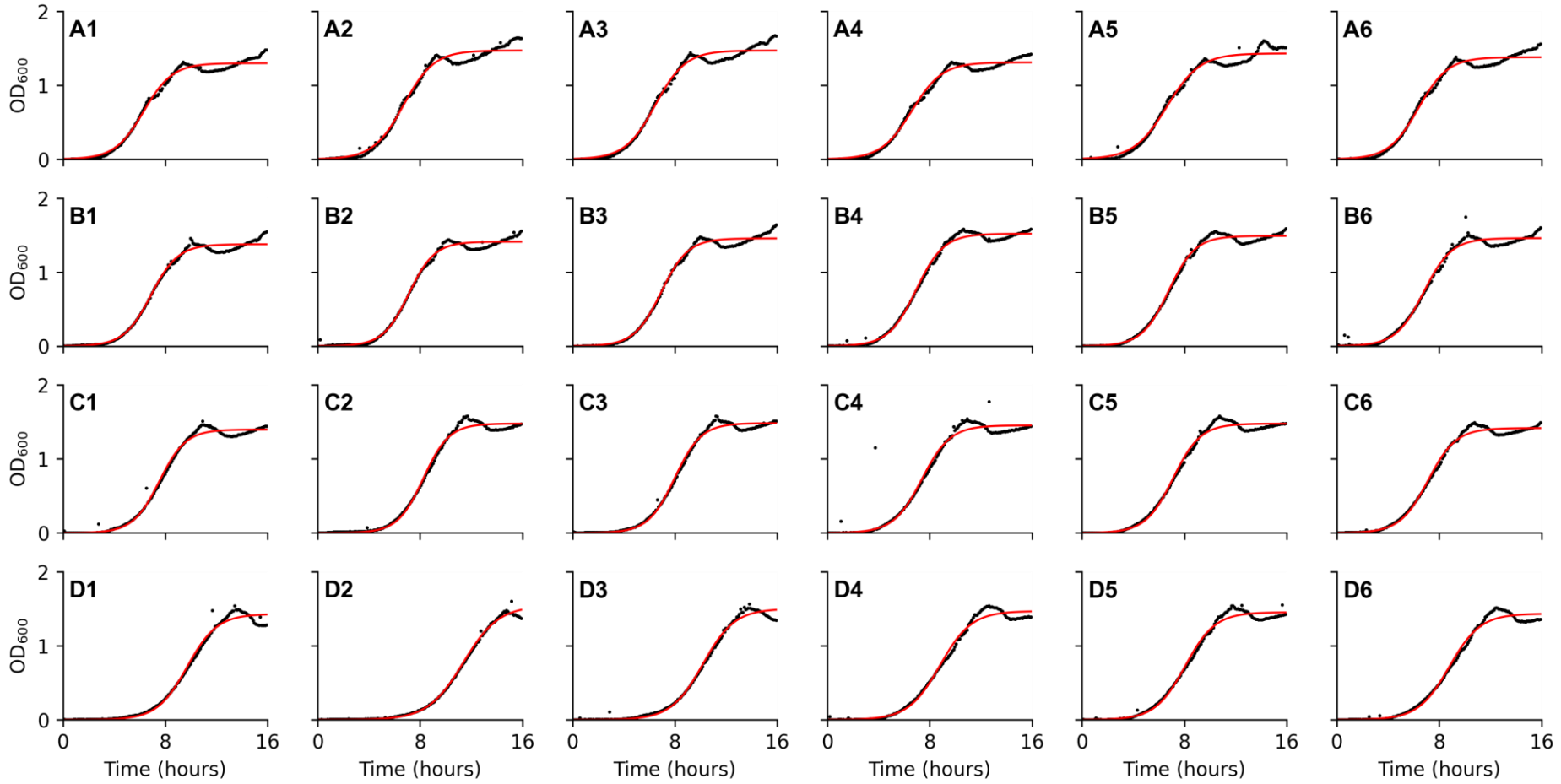

Figure 5.2: Analysis of T3 (T252N) growth using GrowthCurver R package

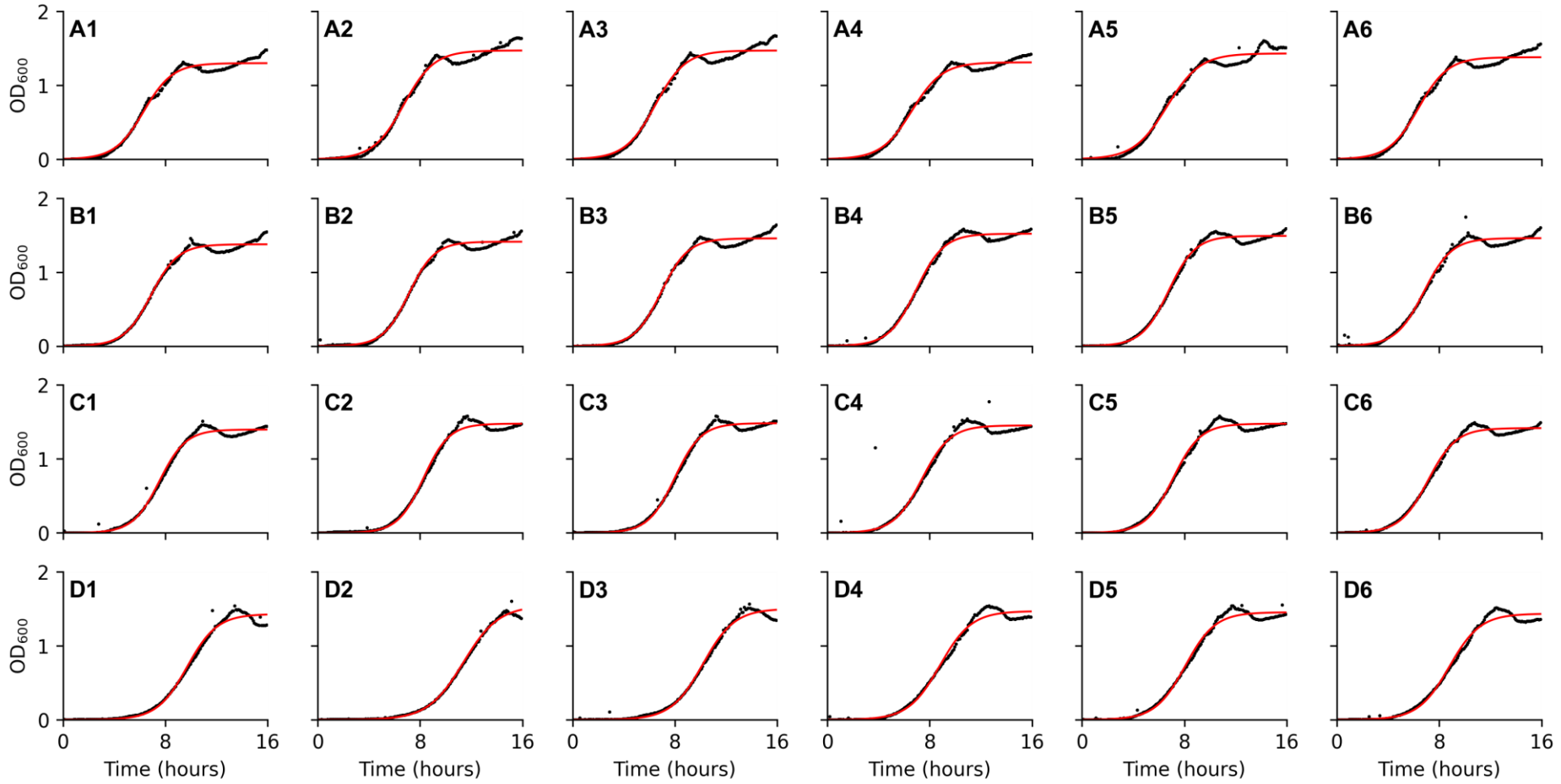

Figure 5.3: Analysis of T7 (T252H) growth using GrowthCurver R package

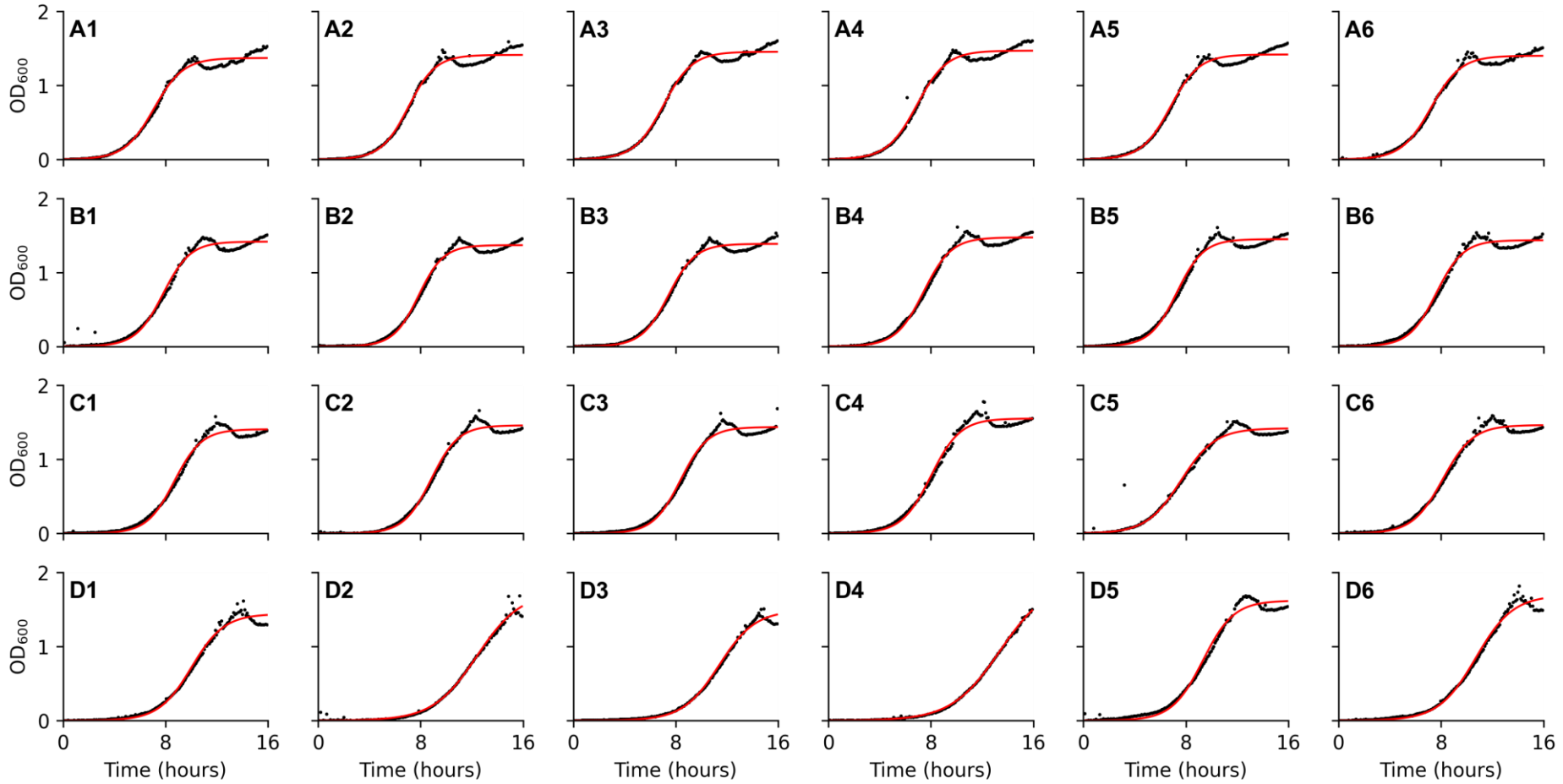

Figure 5.4: Analysis of T9 (T252P) growth using GrowthCurver R package

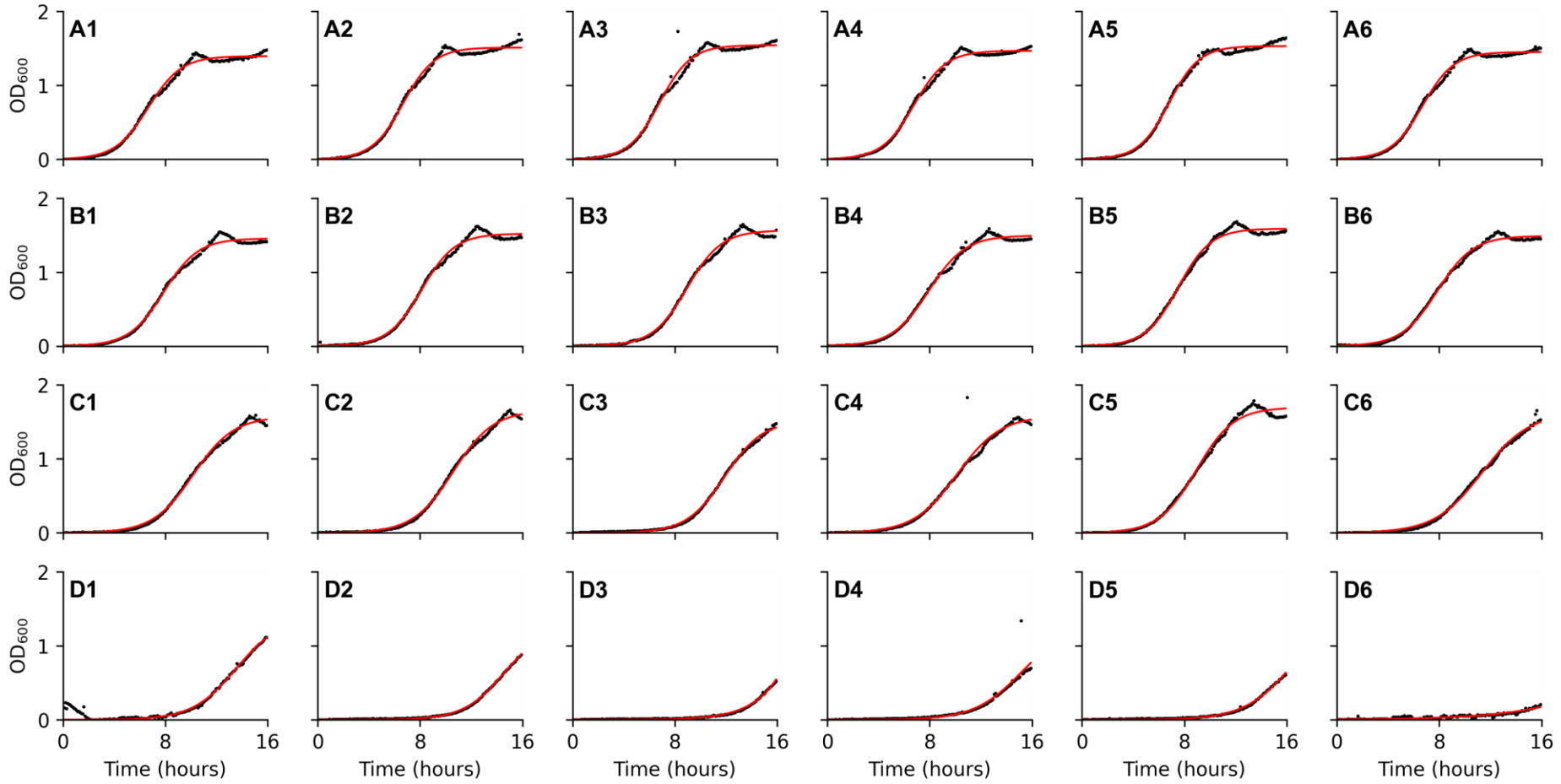

Figure 5.5: Analysis of T10 (T252D) growth using GrowthCurver R package

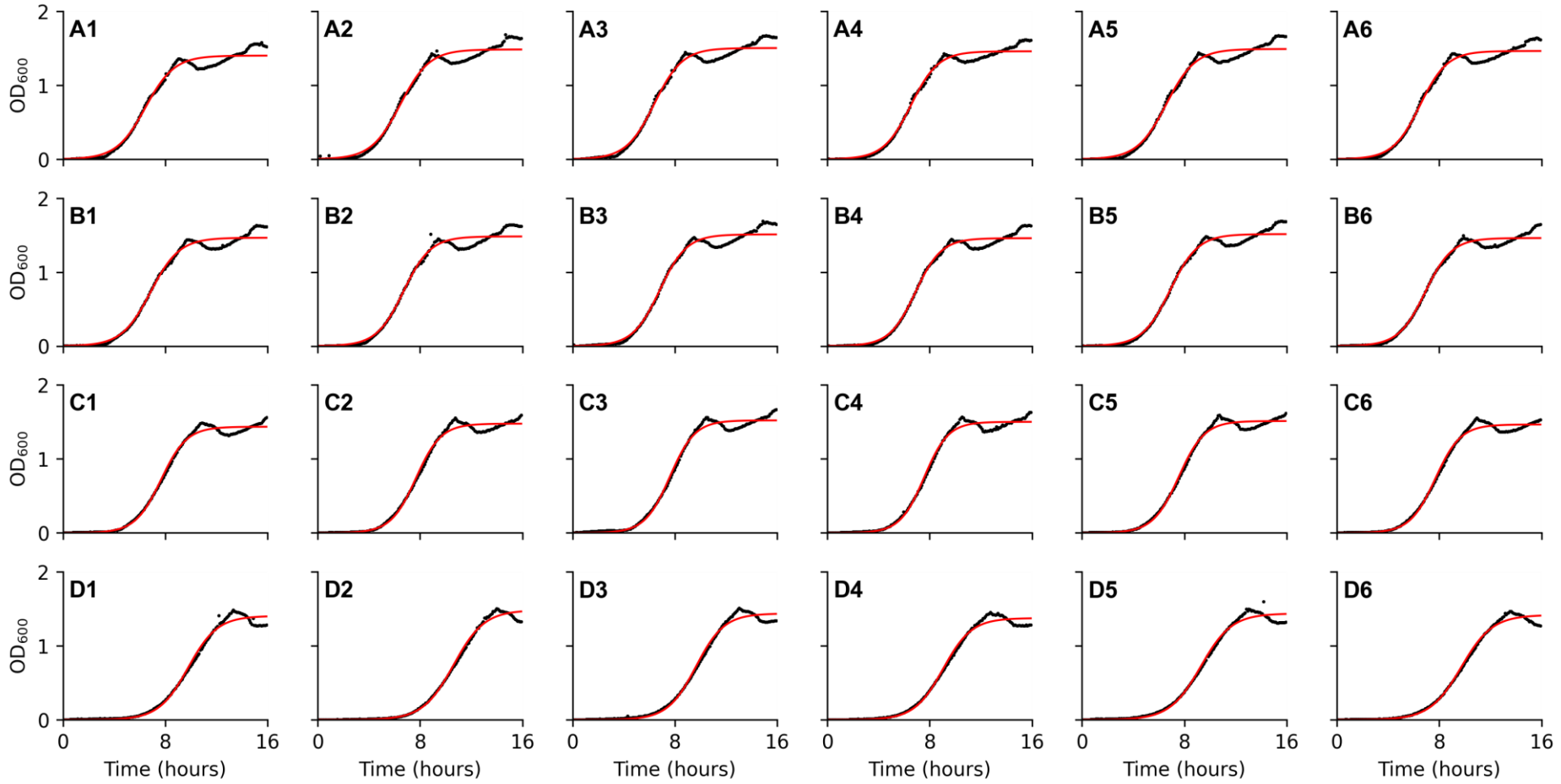

Figure 5.6: Analysis of T15 (T252S) growth using GrowthCurver R package

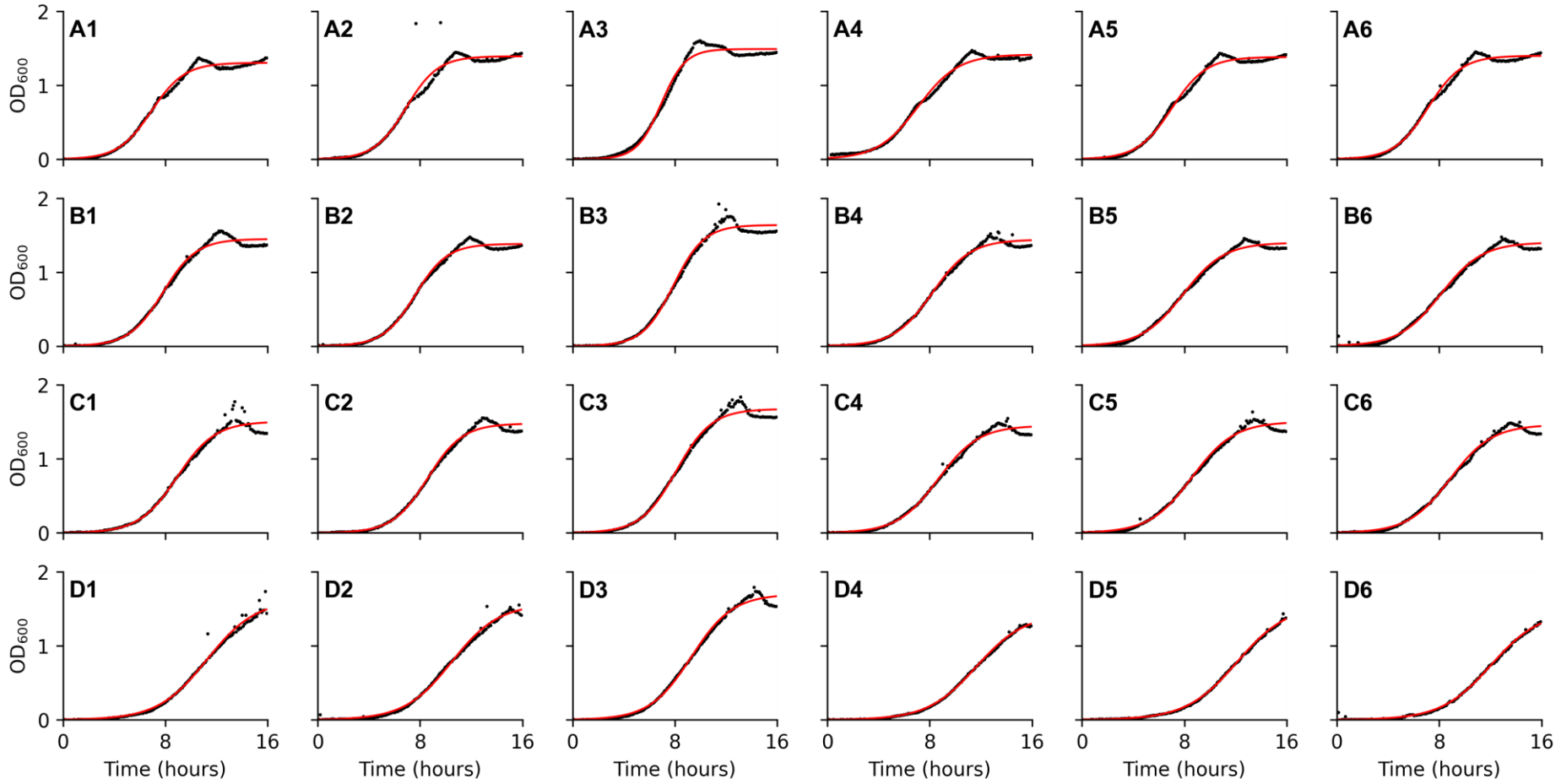

Figure 5.7: Analysis of T28 (T252R) growth using GrowthCurver R package

Class IV recombinants (T12, T34, WT9, WT10, WT12) were grown with 0 μM (row A), 2 μM (row B), 4 μM (row C) and 8 μM (row D) Ni(II).

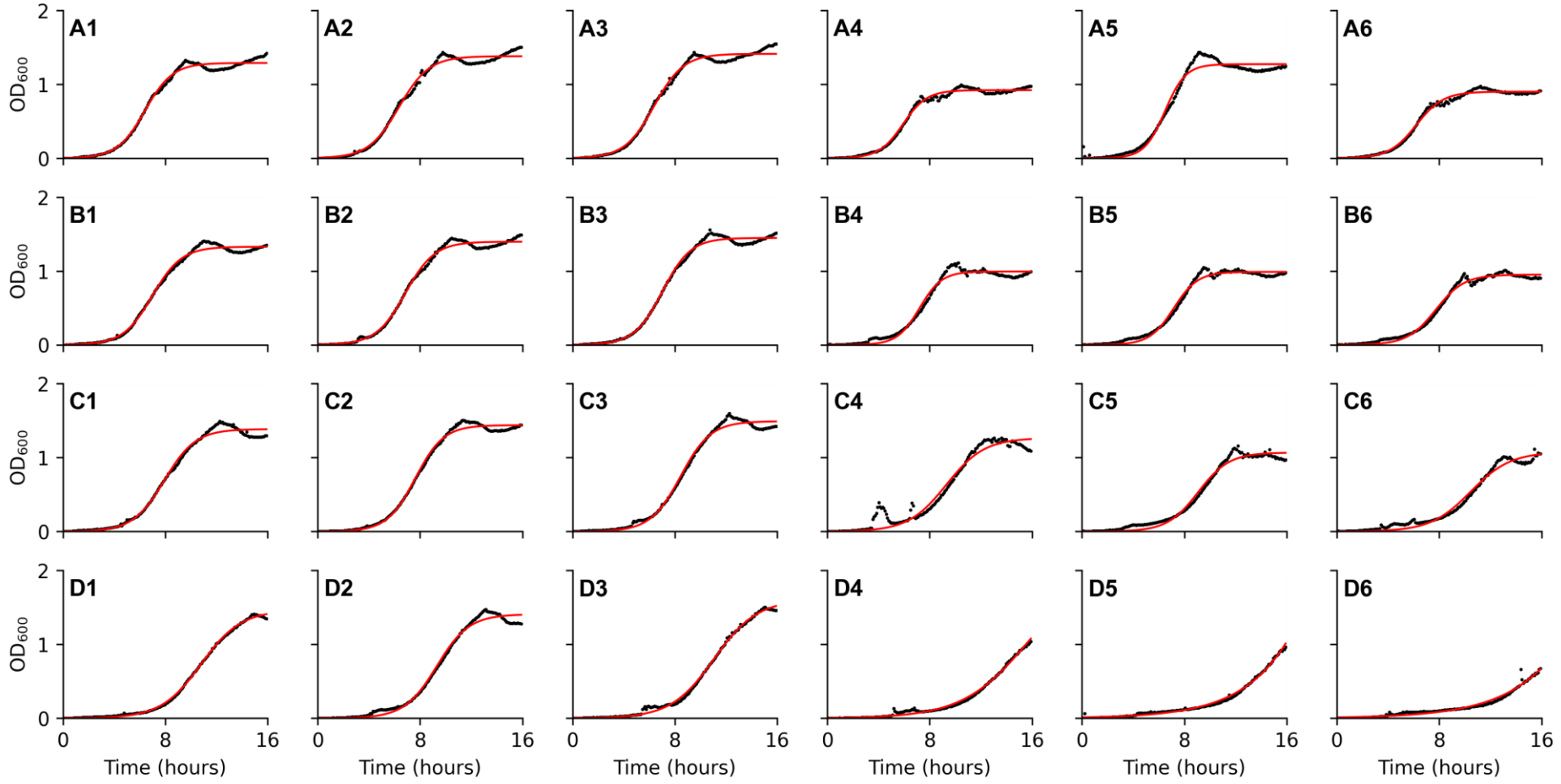

Figure 5.8: Analysis of T12 (L17S) growth using GrowthCurver R package

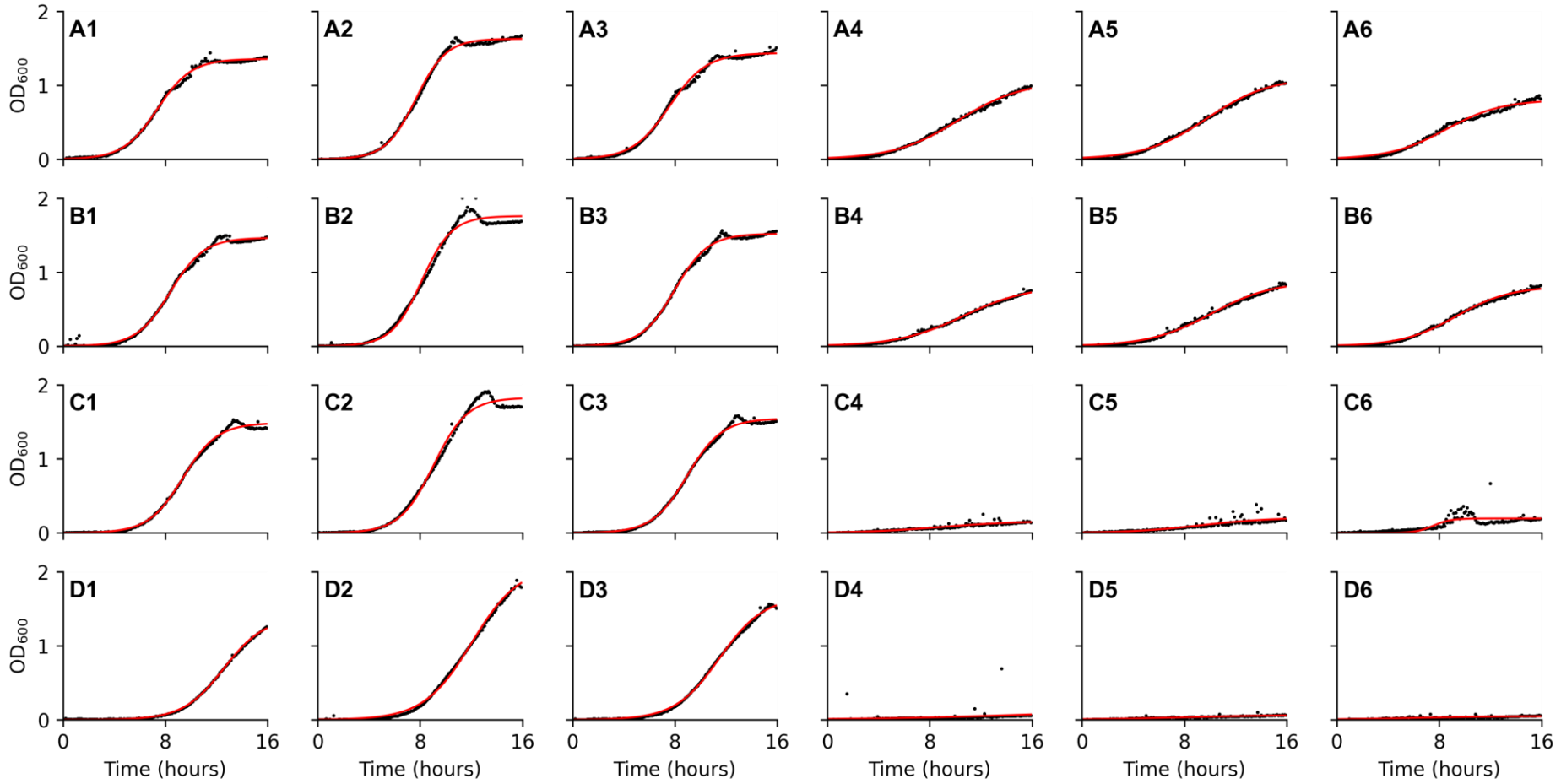

Figure 5.9: Analysis of T34 (I58T) growth using GrowthCurver R package

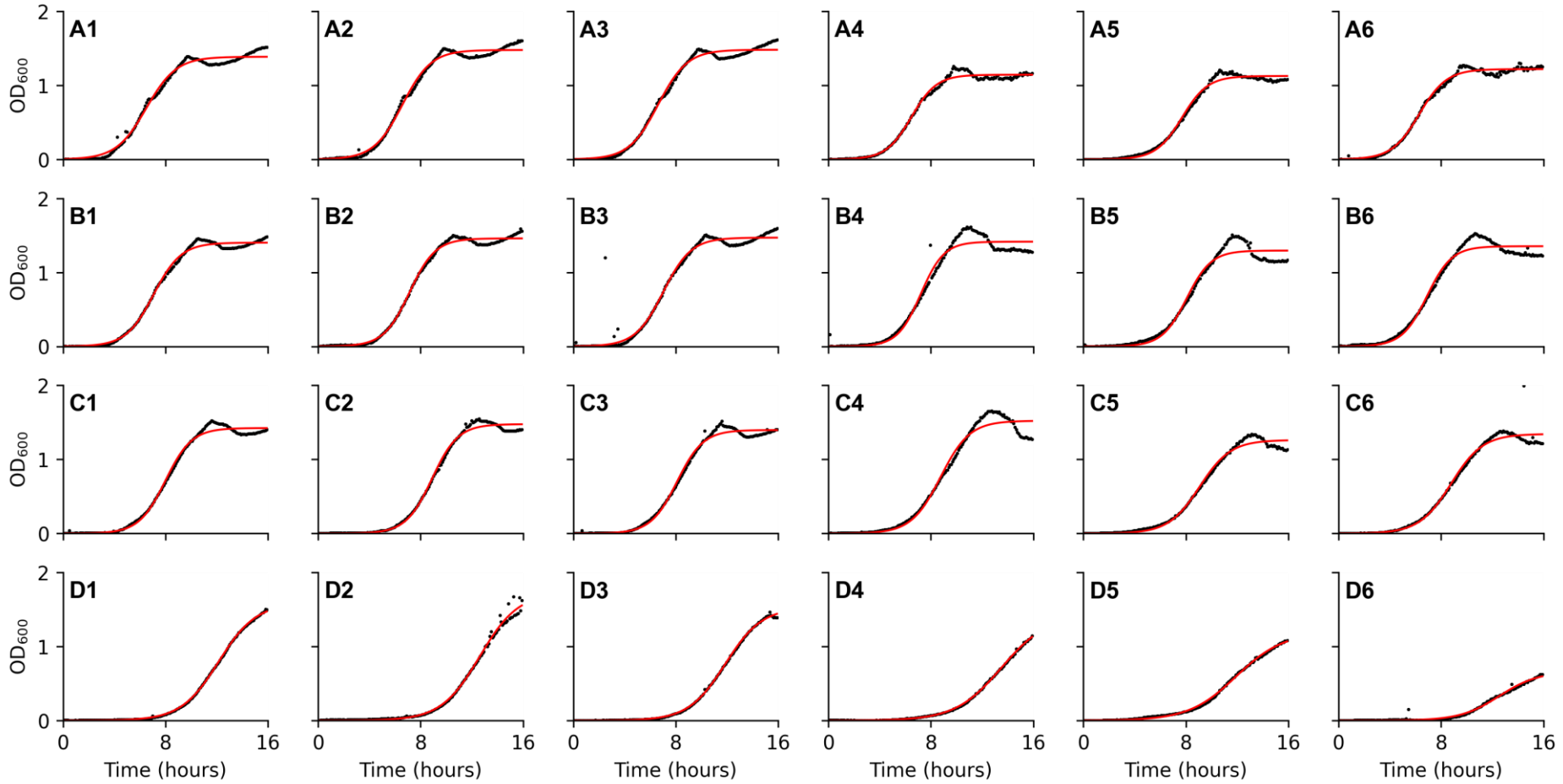

Figure 5.10: Analysis of WT9 (S14P) growth using GrowthCurver R package

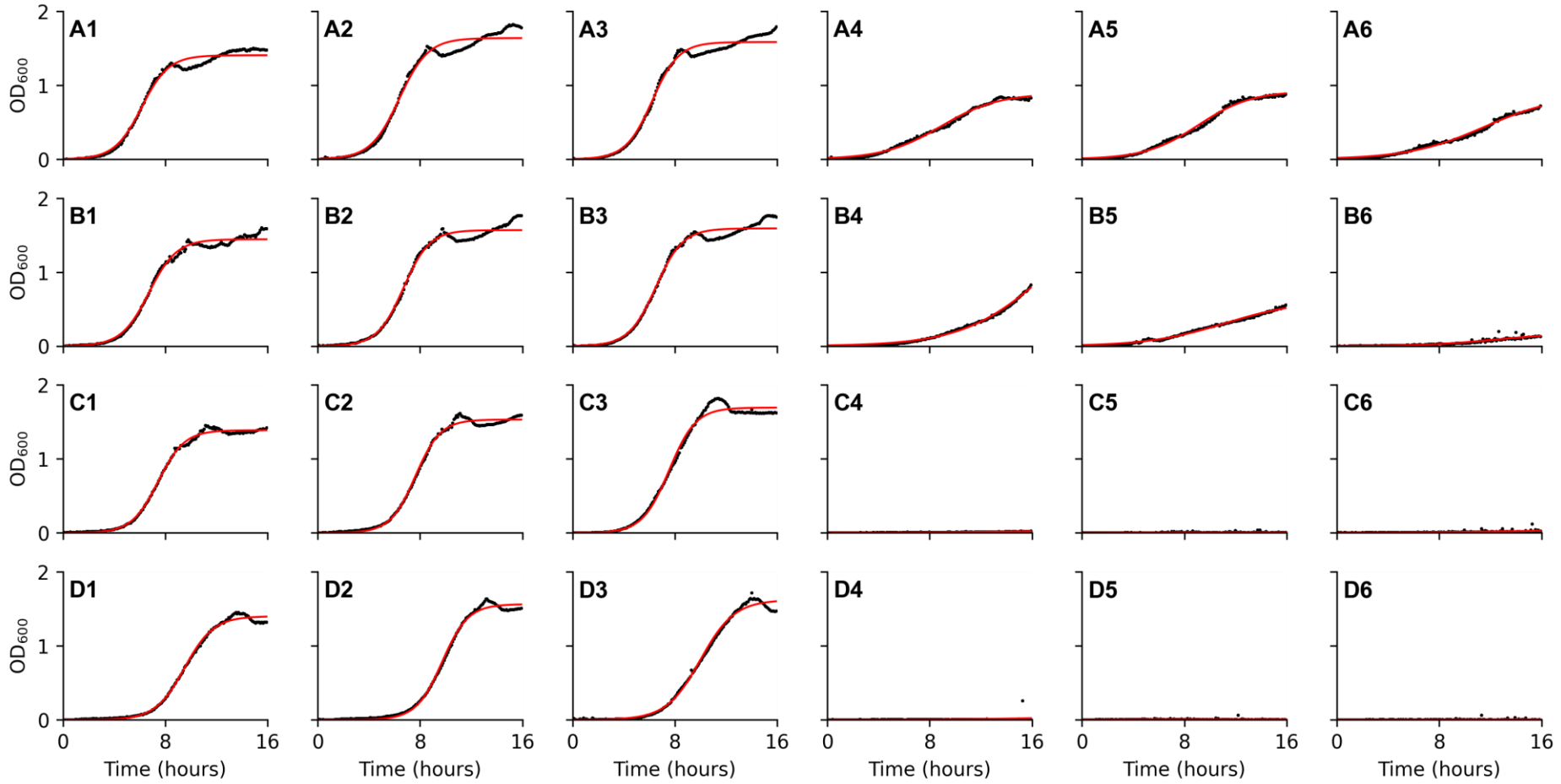

Figure 5.11: Analysis of WT10 (I58V) growth using GrowthCurver R package

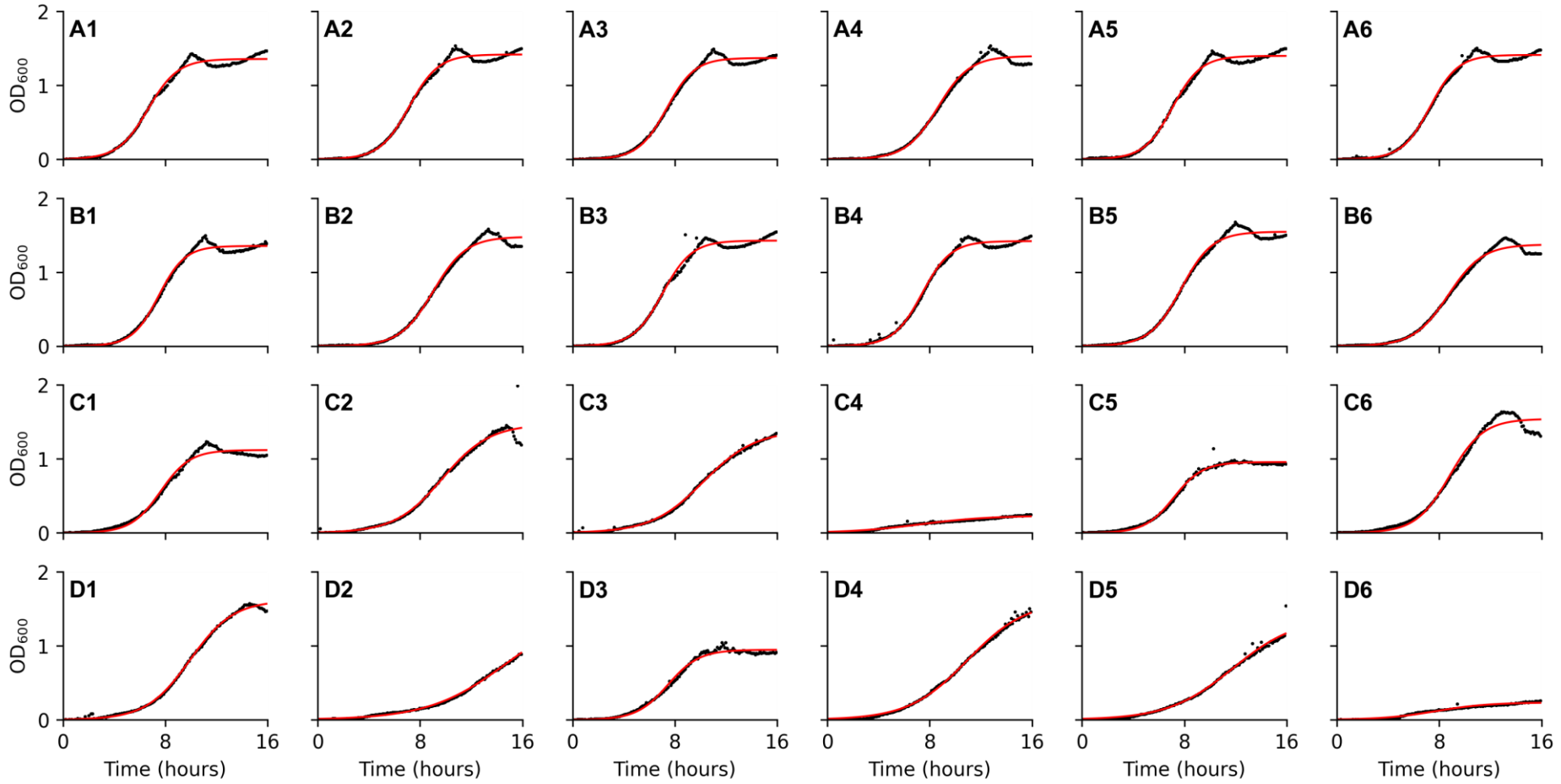

Figure 5.12: Analysis of WT12 (F101L) growth using GrowthCurver R package

Manual Calculation of Doubling Time

The growth assay data was plotted on a semi-log plot in Microsoft Excel. An exponential curve (Equation 6.3) was fitted to the linear slope using the Trendline tool.

$$y = Ae^{bx} \tag{6.3}$$

The variable b from this exponential curve was then converted to doubling time using Equation 6.4.

$$t_{DT} = \frac{ln2}{b} \tag{6.4}$$

Appendix 3

Dynafit Script for DNA Occupancy of RcnR in a His Buffer

This Dynafit script can be used to model the DNA occupancy of the Ni(II) and Co-responsive sensor RcnR as a function of Ni(II) concentration in the presence of the buffer molecules His and Asp (Scott, 2018; Bowers, 2020; Dr. P. T. Chivers, private communication). The output of these simulation is a normalised response for Ni(II) occupancy as a function of [Ni] in μM. Values for *Salmonella* RcnR affinities are listed in Figure 1.2. Dissociation constants for interactions between Ni(II) and His are listed in Figure 1.5. Comments are italicised. Red text indicates parameter was adjusted for the modelling in this report.

```
;; Components
; M = metal = Ni(II)
; H = His (buffer molecule)
; D = Asp (buffer molecule)
; RcnR = RcnR, a Ni(II)-responsive sensor
; Dr = DNA promoter

; working in uM

[task]
  task = simulate
  data = equilibria


[mechanism]
H + M <==> HM  : K1 dissociation            ; His Buffer
```

```
HM + H <==> H2M  : K2 dissociation        ; K2 is used for 2:1 His:Ni


;; RcnR
RcnR + M <==> RcnR.M : R1 dissociation
RcnR.Dr + M <==> RcnR.M.Dr : R2 dissociation
RcnR + Dr <==> RcnR.Dr : R3 dissociation
RcnR.M + Dr <==> RcnR.M.Dr : R4 dissociation

[constants]
;; dissociation constants for interactions between Ni(II), His and Asp
K1 = 0.0155        ; Zhang, Akilesh and Wilcox, 2000
K2 = 0.214         ; Zhang, Akilesh and Wilcox, 2000

;; RcnR
;; Sensor's affinity to Ni(II) and DNA in Salmonella
R1 = 0.00000237
R2 = 0.0000416
R3 = 0.025
R4 = 3.11

[concentrations]
RcnR = 0.16        ; The physiological concentration of the sensor
Dr = 0.00322       ; The physiological concentration of DNA promoter targets for the sensor

H = 1000           ; [His] - variable in different simulations

[responses]
RcnR.Dr = 1
RcnR.M.Dr = 310.6

[data]
 variable M
 plot logarithmic

mesh from 100 to 10000 step 10; range of [M]

 directory         ; define the directory
 extension         txt
 file              ; define file name

[output]
 directory         ; define the directory

[end]
```

References

ANDREINI, C. et al. (2008) Metal ions in biological catalysis: From enzyme databases to general principles. *Journal of Biological Inorganic Chemistry*, 13(8), pp. 1205–1218.

ASHKENAZY, H. et al. (2010) ConSurf 2010: Calculating evolutionary conservation in sequence and structure of proteins and nucleic acids. *Nucleic Acids Research*, 38(SUPPL. 2), pp. 529–533.

ASHKENAZY, H. et al. (2016) ConSurf 2016: an improved methodology to estimate and visualize evolutionary conservation in macromolecules. *Nucleic acids research*, 44(W1), pp. W344–W350.

AUSUBEL, F. (1996) *Short protocols in Molecular Biology, Third Edition*. 5th ed. AUSUBEL, F.M. et al. (eds.). John Wiley & Sons Inc.

BABA, T. et al. (2006) Construction of *Escherichia coli* K-12 in-frame, single-gene knockout mutants: the Keio collection. *Molecular Systems Biology*, 2, p. 2006.0008.

BENNETT, B.D. et al. (2009) Absolute metabolite concentrations and implied enzyme active site occupancy in *Escherichia coli*. *Nature Chemical Biology*, 5(8), pp. 593–599.

BEREZIN, C. et al. (2004) ConSeq: The identification of functionally and structurally important residues in protein sequences. *Bioinformatics*, 20(8), pp. 1322–1324.

BLACKBURN, J.R. and JONES, M.M. (1973) Stereoselectivity in the metal complex catalysed hydrolysis of amino acid esters -III. *Journal of Inorganic and Nuclear Chemistry*, 35(1968), pp. 1605–1620.

BLOOM, S.L. and ZAMBLE, D.B. (2004) Metal-selective DNA-binding response of *Escherichia coli* NikR. *Biochemistry*, 43(31), pp. 10029–10038.

BÖCK, A. et al. (2006) Maturation of Hydrogenases. *Advances in Microbial Physiology*, 51, pp. 1–71.

BOER, J.L., MULROONEY, S.B. and HAUSINGER, R.P. (2014) Nickel-dependent

metalloenzymes. *Archives of Biochemistry and Biophysics*, 544, pp. 142–152.

BOWERS, K.C.E. (2020) *Quantitative modelling to gain insight into bacterial small molecule cysotolic buffers of nickel*. Durham University.

BRAWLEY, H.N. and LINDAHL, P.A. (2021) Direct Detection of the Labile Nickel Pool in *Escherichia coli*: New Perspectives on Labile Metal Pools. *Journal of the American Chemical Society*, 142, pp. 18571–18580.

BRENNER, M. and AMES, B.N. (1971) The histidine operon and its regulation. In: *Metabolic Regulation*. Elsevier, pp. 349–387.

CANO, D.A. et al. (1998) Cell division inhibition in *Salmonella typhimurium* histidine-constitutive strains: An ftsI-like defect in the presence of wild-type penicillin-binding protein 3 levels. *Journal of Bacteriology*, 180(19), pp. 5231–5234.

CAPDEVILA, D.A., EDMONDS, K.A. and GIEDROC, D.P. (2017) Metallochaperones and metalloregulation in bacteria. *Essays in Biochemistry*, 61(2), pp. 177–200.

CARRINGTON, P.E. et al. (2003) Nickel coordination is regulated by the DNA-bound state of NikR. *Nature Structural Biology*, 10(2), pp. 126–130.

CELNIKER, G. et al. (2013) ConSurf: Using evolutionary data to raise testable hypotheses about protein function. *Israel Journal of Chemistry*, 53(3–4), pp. 199–206.

CHANDRANGSU, P., RENSING, C. and HELMANN, J.D. (2017) Metal homeostasis and resistance in bacteria. *Nature Reviews Microbiology*, 15(6), pp. 338–350.

CHEN, H. et al. (2010) Nickel Ions Inhibit Histone Demethylase JMJD1A and DNA Repair Enzyme ABH2 by Replacing the Ferrous Iron in the Catalytic Centers. *Journal of Biological Chemistry*, 285(10), pp. 7374–7383.

CHIVERS, P.T. et al. (2012) Identification of Ni-$(L\text{-}His)_2$ as a substrate for NikABCD-dependent nickel uptake in *Escherichia coli*. *Metallomics*, 4(10), pp. 1043–1050.

CHIVERS, P.T. (2017) Nickel Regulation. In: *RSC Metallobiology*. Royal Society of Chemistry, pp. 259–283.

CHIVERS, P.T. and SAUER, R.T. (1999) NikR is a ribbon-helix-helix DNA-binding protein. *Protein Science*, 8(11), pp. 2494–2500.

CHIVERS, P.T. and SAUER, R.T. (2002) NikR repressor: High-affinity nickel binding to the C-terminal domain regulates binding to operator DNA. *Chemistry & Biology*, 9(10), pp. 1141–1148.

CHIVERS, P.T. and SAUER, R.T. (2000) Regulation of high affinity nickel uptake in bacteria - Ni^{2+}-dependent interaction of NikR with wild-type and mutant operator sites. *Journal of Biological Chemistry*, 275(26), pp. 19735–19741.

CHUNG, K. and ZAMBLE, D. (2011) The *Escherichia coli* metal-binding chaperone SlyD interacts with the large subunit of [NiFe]-hydrogenase 3. *FEBS Lett*, 585(2), pp. 291–294.

DATSENKO, K.A. and WANNER, B.L. (2000) One-step inactivation of chromosomal genes in *Escherichia coli* K-12 using PCR products. *Proceedings of the National Academy of Sciences of the United States of America*, 97(12), pp. 6640–6645.

DELCOUR, A.H. (2003) Solute uptake through general porins. *Frontiers in Bioscience*, 8(1), pp. 1055–1071.

DJOKO, K.Y. et al. (2017) Interplay between tolerance mechanisms to copper and acid stress in *Escherichia coli*. *Proceedings of the National Academy of Sciences of the United States of America*, 114(26), pp. 6818–6823.

DJOKO, K.Y. et al. (2015) The role of copper and zinc toxicity in innate immune defense against bacterial pathogens. *Journal of Biological Chemistry*, 290(31), pp. 1854–1861.

DUDEV, T. and LIM, C. (2008) Metal binding affinity and selectivity in metalloproteins: Insights from computational studies. *Annual Review of Biophysics*, 37, pp. 97–116.

FINK, G.R., KŁOPOTOWSKI, T. and AMES, B.N. (1967) Histidine regulatory mutants in *Salmonella typhimurium*. IV. A positive selection for polar histidine-requiring mutants from histidine operator constitutive mutants. *Journal of Molecular Biology*, 30(1), pp. 81–95.

FLORES, A. and CASADESUS, J. (1995) Suppression of the pleiotropic effects of HisH and HisF overproduction identifies four novel loci on the *Salmonella typhimurium* chromosome: *osmH*, *sfiW*, *sfiX*, and *sfiY*. *Journal of Bacteriology*, 177(17), pp. 4841–4850.

FONTECILLA-CAMPS, J.C. et al. (2009) Structure-function relationships of anaerobic gas-processing metalloenzymes. *Nature*, 460(7257), pp. 814–822.

FORZI, L. and SAWERS, R.G. (2007) Maturation of [NiFe]-hydrogenases in *Escherichia coli*. *BioMetals*, 20(3–4), pp. 565–578.

FOSTER, A.W. et al. (2017) A tight tunable range for Ni(II) sensing and buffering in cells. *Nature Chemical Biology*, 13(4), pp. 409–414.

FOSTER, A.W. et al. (2014) Metal specificity of cyanobacterial nickel-responsive repressor InrS: Cells maintain zinc and copper below the detection threshold for InrS. *Molecular Microbiology*, 92(4), pp. 797–812.

FRANDSCEN, N. and D'ARI, R. (1993) Excess histidine enzymes cause AICAR-independent filamentation in *Escherichia coli*. *Molecular Genetics and Genomics*, 240, pp. 348–354.

FRASER, K.A. and HARDING, M.M. (1967) The crystal and molecular structure of bis(histidino)nickel(II) monohydrate. *Journal of the Chemical Society A: Inorganic, Physical, and Theoretical Chemistry*, pp. 415–420.

FRAUSTO DA SILVA, J.J.R. and WILLIAMS, R.J.P. (2001) *The Biological Chemistry of the Elements*. 2nd ed. Oxford University Press.

GEISSMANN, Q. (2013) OpenCFU, a New Free and Open-Source Software to Count Cell Colonies and Other Circular Objects. *PLoS ONE*, 8(2), p. e54072.

GEVORGYAN, H., TRCHOUNIAN, A. and TRCHOUNIAN, K. (2018) Understanding the Role of *Escherichia coli* Hydrogenases and Formate Dehydrogenases in the F_OF_1 - ATPase Activity during the Mixed Acid Fermentation of Mixture of Carbon Sources. *IUBMB Life*, 70(10), pp. 1040–1047.

GUERRA, A.J. and GIEDROC, D.P. (2012) Metal site occupancy and allosteric switching in bacterial metal sensor proteins. *Archives of Biochemistry and Biophysics*, 519(2, SI), pp. 210–222.

GUILHEN, C., TAHA, M.K. and VEYRIER, F.J. (2013) Role of transition metal exporters in virulence: The example of *Neisseria meningitidis*. *Frontiers in Cellular and Infection Microbiology*, 3(DEC), pp. 1–7.

HARTMAN, P.E. et al. (1971) Classification and mapping of spontaneous and induced mutations in the histidine operon of *Salmonella*. *Advances in Genetics*, 16, pp. 1–34.

HELBIG, K. et al. (2008) Glutathione and transition-metal homeostasis in *Escherichia coli*. *Journal of Bacteriology*, 190(15), pp. 5431–5438.

HIGGINS, K. (2019) Nickel metalloregulators and chaperones. *Inorganics*, 7(8), pp. 14–17.

HIGGINS, K.A. et al. (2013) Effects of Select Histidine to Cysteine Mutations on Transcriptional Regulation by *Escherichia coli* RcnR. *Biochemistry*, 52(1), pp. 84–97.

HIGGINS, K.A., CHIVERS, P.T. and MARONEY, M.J. (2012) Role of the N-terminus in Determining Metal-Specific Responses in the *E. coli* Ni- and Co-Responsive Metalloregulator, RcnR. *Journal of The American Chemical Society*, 134(16), pp. 7081–7093.

HOOD, M.I. and SKAAR, E.P. (2012) Nutritional immunity: transition metals at the pathogen-host interface. *Nature Reviews Microbiology*, 10(8), pp. 525–537.

HOPPE, I. et al. (1979) A refined map of the *hisG* gene of Salmonella typhimurium. *Genetics*, 92(1), pp. 17–26.

HUANG, X. and MILLER, W. (1991) A Time-Efficient, Linear-Space Local Similarity Algorithm. *Advances in Applied Mathematics*, 12, pp. 337–357.

HUBE, M., BLOKESCH, M. and BÖCK, A. (2002) Network of hydrogenase maturation in *Escherichia coli*: Role of accessory proteins HypA and HybF. *Journal of Bacteriology*, 184(14), pp. 3879–3885.

IRVING, H. and WILLIAMS, R.J.P. (1953) The stability of transition-metal complexes. *Journal of the Chemical Society*, pp. 3192–3210.

IWIG, J.S. et al. (2008) Ni(II) and Co(II) sensing by *Escherichia coli* RcnR. *Journal of The American Chemical Society*, 130(24), pp. 7592–7606.

IWIG, J.S., ROWE, J.L. and CHIVERS, P.T. (2006) Nickel homeostasis in *Escherichia coli* - The *rcnR-rcnA* efflux pathway and its linkage to NikR function. *Molecular*

Microbiology, 62(1), pp. 252–262.

JOHNSTON, H.M. et al. (1980) Model for regulation of the histidine operon of *Salmonella*. *Proceedings of the National Academy of Sciences of the United States of America*, 77(1), pp. 508–512.

JOHNSTON, H.M. and ROTH, J.R. (1981) DNA sequence changes of mutations altering attenuation control of the histidine operon of *Salmonella typhimurium*. *Journal of Molecular Biology*, 145(4), pp. 735–756.

JOHNSTON, H.M. and ROTH, J.R. (1979) Histidine mutants requiring adenine: selection of mutants with reduced *hisG* expression in Salmonella typhimurium. *Genetics*, 92(1), pp. 1–15.

KACZMAREK, P., SZCZEPANIK, W. and JEZOWSKA-BOJCZUK, M. (2005) Acid-base, coordination and oxidative properties of systems containing ATP, L-histidine and Ni(II) ions. *Dalton Transactions*, (22), pp. 3653–3657.

KEREN, N. et al. (2002) A light-dependent mechanism for massive accumulation of manganese in the photosynthetic bacterium *Synechocystis* sp. PCC 6803. *Biochemistry*, 41(50), pp. 15085–15092.

KULIS-HORN, R.K., PERSICKE, M. and KALINOWSKI, J. (2015) *Corynebacterium glutamicum* ATP-phosphoribosyl transferases suitable for L-histidine production - Strategies for the elimination of feedback inhibition. *Journal of Biotechnology*, 206, pp. 26–37.

KULIS-HORN, R.K., PERSICKE, M. and KALINOWSKI, J. (2014) Histidine biosynthesis, its regulation and biotechnological application in *Corynebacterium glutamicum*. *Microbial Biotechnology*, 7(1), pp. 5–25.

KUZMIČ, P. (1996) Program DYNAFIT for the analysis of enzyme kinetic data: Application to HIV proteinase. *Analytical Biochemistry*, 237(2), pp. 260–273.

LEACH, M.R. and ZAMBLE, D.B. (2007) Metallocenter assembly of the hydrogenase enzymes. *Current Opinion in Chemical Biology*, 11(2), pp. 159–165.

LEITCH, S. et al. (2007) Nickel-specific response in the transcriptional regulator, *Escherichia coli* NikR. *Journal of the American Chemical Society*, 129(16), pp.

5085–5095.

LEWIS, J.A. and AMES, B.N. (1972) Histidine regulation in *Salmonella typhimurium*. XI. The percentage of transfer RNA^{His} charged in vivo and its relation to the repression of the histidine operon. *Journal of Molecular Biology*, 66(1), pp. 131–142.

LI, Y. and ZAMBLE, D.B. (2009) Nickel homeostasis and nickel regulation: An overview. *Chemical Reviews*, 109(10), pp. 4617–4643.

LIU, T. et al. (2007) CsoR is a novel *Mycobacterium tuberculosis* copper-sensing transcriptional regulator. *Nature Chemical Biology*, 3(1), pp. 60–68.

LOHKAMP, B. et al. (2004) The Structure of *Escherichia coli* ATP-phosphoribosyltransferase: Identification of Substrate Binding Sites and Mode of AMP Inhibition. *Journal of Molecular Biology*, 336(1), pp. 131–144.

MA, Z. et al. (2014) Bacillithiol is a major buffer of the labile zinc pool in *Bacillus subtilis*. *Molecular Microbiology*, 94(4), pp. 756–770.

MA, Z., JACOBSEN, F.E. and GIEDROC, D.P. (2009) Coordination chemistry of bacterial metal transport and sensing. *Chemical Reviews*, 109(10), pp. 4644–4681.

MACOMBER, L., ELSEY, S.P. and HAUSINGER, R.P. (2011) Fructose-1,6-bisphosphate aldolase (class II) is the primary site of nickel toxicity in *Escherichia coli*. *Molecular Microbiology*, 82(5), pp. 1291–1300.

MACOMBER, L. and IMLAY, J.A. (2009) The iron-sulfur clusters of dehydratases are primary intracellular targets of copper toxicity. *Proceedings of the National Academy of Sciences of the United States of America*, 106(20), pp. 8344–8349.

MAIER, R.J. and BENOIT, S.L. (2019) Role of nickel in microbial pathogenesis. *Inorganics*, 7(7), pp. 1–31.

MÉDIGUE, C. et al. (1993) Colibri: a functional data base for the *Escherichia coli* genome. *Microbiological Reviews*, 57(3), pp. 623–654.

MILLER, J.H. (1972) *Experiments in Molecular Genetics*. Cold Spring Harbor Laboratory Press.

MILLER, J.K. and BARNES, W.M. (1986) Colony probing as an alternative to standard sequencing as a means of direct analysis of chromosomal DNA to determine the

spectrum of single-base changes in regions of known sequence. *Proceedings of the National Academy of Sciences of the United States of America*, 83(4), pp. 1026–1030.

MITTELSTÄDT, G. et al. (2018) A dimeric catalytic core relates the short and long forms of ATP-phosphoribosyltransferase. *Biochemical Journal*, 475(1), pp. 247–260.

MITTELSTÄDT, G. et al. (2016) *Campylobacter jejuni* adenosine triphosphate phosphoribosyltransferase is an active hexamer that is allosterically controlled by the twisting of a regulatory tail. *Protein Science*, 25, pp. 1492–1506.

MORTELMANS, K. and ZEIGER, E. (2000) The Ames *Salmonella*/microsome mutagenicity assay. *Fundamental and Molecular Mechanisms of Mutagenesis*, 455, pp. 29–60.

MOYED, H.S. (1961) Interference with the feed-back control of histidine biosynthesis. *The Journal of Biological Chemistry*, 236(8), pp. 2261–2267.

MULROONEY, S.B. and HAUSINGER, R.P. (2003) Nickel uptake and utilization by microorganisms. *FEMS Microbiology Reviews*, 27(2–3), pp. 239–261.

MURRAY, M.L. and HARTMAN, P.E. (1972) Overproduction of *hisH* and *hisF* gene products leads to inhibition of cell cell division in *Salmonella*. *Canadian Journal of Microbiology*, 18(5), pp. 671–681.

MYERS, K.S. et al. (2013) Genome-scale Analysis of *Escherichia coli* FNR Reveals Complex Features of Transcription Factor Binding. *PLoS Genetics*, 9(6), pp. 11–13.

NAIRN, B.L. et al. (2016) The Response of *Acinetobacter baumannii* to Zinc Starvation. *Cell Host and Microbe*, 19(6), pp. 826–836.

NATARO, J.P. and KAPER, J.B. (1998) Diarrheagenic *Escherichia coli*. *Clinical Microbiology Reviews*, 11(1), pp. 142–201.

NAVARRO, C., WU, L. and MANDRAND-BERTHELOT, M. (1993) The *nik* operon of Escherichia coli encodes a periplasmic binding-protein-dependent transport system for nickel. *Molecular Microbiology*, 9(6), pp. 1181–1191.

NG, H., INGRAHAM, J.L. and MARR, A.G. (1962) Damage and Derepression In

Escherichia coli Resulting From Growth At Low Temperatures. *Journal of Bacteriology*, 84(2), pp. 331–339.

NICHOLS, R.J. et al. (2011) Phenotypic landscape of a bacterial cell. *Cell*, 144(1), pp. 143–156.

NIES, D.H. (2003) Efflux-mediated heavy metal resistance in prokaryotes. *FEMS Microbiology Reviews*, 27(2–3), pp. 313–339.

NOINAJ, N. et al. (2010) TonB-dependent transporters: Regulation, structure, and function. *Annual Review of Microbiology*, 64, pp. 43–60.

O'DONOVAN, G.A. and INGRAHAM, J.L. (1965) Cold-sensitive mutants of *Escherichia coli* resulting from increased feedback inhibition. *Proceedings of the National Academy of Sciences of the United States of America*, 54(2), pp. 451–457.

O'DONOVAN, G.A., KEARNEY, C.L. and INGRAHAM, J.L. (1965) Mutants of *Escherichia coli* with High Minimal Temperatures of Growth. *Journal of Bacteriology*, 90(3), pp. 611–616.

OSMAN, D. et al. (2019) Bacterial sensors define intracellular free energies for correct enzyme metalation. *Nature Chemical Biology*, 15(3), pp. 241–249.

OUTTEN, C.E. and O'HALLORAN, T. V. (2001) Femtomolar sensitivity of metalloregulatory proteins controlling zinc homeostasis. *Science*, 292(5526), pp. 2488–2492.

PACHOLARZ, K.J. et al. (2017) Hybrid Mass Spectrometry Approaches to Determine How L-Histidine Feedback Regulates the Enzyzme MtATP-Phosphoribosyltransferase. *Structure*, 25(5), pp. 730-738.e4.

PATZER, S.I. and HANTKE, K. (1998) The ZnuABC high-affinity zinc uptake system and its regulator Zur in *Escherichia coli*. *Molecular Microbiology*, 28(6), pp. 1199–1210.

DE PINA, K. et al. (1999) Isolation and characterization of the nikR gene encoding a nickel-responsive regulator in *Escherichia coli*. *Journal of Bacteriology*, 181(2), pp. 670–674.

PINSKE, C. and SAWERS, R.G. (2016) Anaerobic Formate and Hydrogen Metabolism.

EcoSal Plus, 7(1), [Online] Available from: doi.org/10.1128/ecosalplus.esp-0011-2016 [Accessed 29/11/2020].

RANQUET, C. et al. (2007) Cobalt stress in *Escherichia coli*: The effect on the iron-sulfur proteins. *Journal of Biological Chemistry*, 282(42), pp. 30442–30451.

REISSMANN, S. et al. (2003) Taming of a poison: biosynthesis of the NiFe-hydrogenase cyanide ligands. *Science (New York, N.Y.)*, 299(5609), pp. 1067–1070.

RIGGS, D.L. et al. (1986) Promoter domain mediates guanosine tetraphosphate activation of the histidine operon. *Proceedings of the National Academy of Sciences*, 83(24), pp. 9333–9337.

ROBINSON, N.J. and GLASFELD, A. (2020) Metalation: nature's challenge in bioinorganic chemistry. *Journal of Biological Inorganic Chemistry*, 25(4), pp. 543–545.

RODIONOV, D.A. et al. (2006) Comparative and functional genomic analysis of prokaryotic nickel and cobalt uptake transporters: Evidence for a novel group of ATP-binding cassette transporters. *Journal of Bacteriology*, 188(1), pp. 317–327.

RODRIGUE, A., EFFANTIN, G. and MANDRAND-BERTHELOT, M.A. (2005) Identification of *rcnA* (*yohM*), a nickel and cobalt resistance gene in Escherichia coli. *Journal of Bacteriology*, 187(8), pp. 2912–2916.

RODRIGUEZ, G.M. and SMITH, I. (2006) Identification of an ABC transporter required for iron acquisition and virulence in *Mycobacterium tuberculosis*. *Journal of Bacteriology*, 188(2), pp. 424–430.

ROTH, J.R., ANTÓN, D.N. and HARTMAN, P.E. (1966) Histidine regulatory mutants in *Salmonella typhimurium*. I: Isolation and general properties. *Journal of Molecular Biology*, 22(2), pp. 305–323.

ROWE, J.L., STARNES, G.L. and CHIVERS, P.T. (2005) Complex transcriptional control links NikABCDE-dependent nickel transport with hydrogenase expression in *Escherichia coli*. *Journal of Bacteriology*, 187(18), pp. 6317–6323.

SCHNEIDER, C.A., RASBAND, W.S. and ELICEIRI, K.W. (2012) NIH Image to ImageJ: 25 years of image analysis. *Nature Methods*, 9(7), pp. 671–675.

SCHREITER, E.R. et al. (2003) Crystal structure of the nickel-responsive transcription factor NikR. *Nature Structural Biology*, 10(10), pp. 794–799.

SCHREITER, E.R. et al. (2006) NikR-operator complex structure and the mechanism of repressor activation by metal ions. *Proceedings of the National Academy of Sciences of the United States of America*, 103(37), pp. 13676–13681.

SCHRÖDINGER, L. and DELANO, W. (2020) *PyMOL*.

SCOTT, A.J.P. (2018) *Determinants of metal-specific transcriptional responses in bacteria*. Durham University.

SHAND, R.F. et al. (1989) Correlation between histidine operon expression and guanosine 5'-diphosphate-3'-diphosphate levels during amino acid downshift in stringent and relaxed strains of Salmonella typhimurium. *Journal of Bacteriology*, 171(2), pp. 737–743.

SHEPPARDZ, D.E. (1964) Mutants of *Salmonella typhimurium* Resistant To Feedback Inhibition By L-Histidine. *Genetics*, 50, pp. 611–623.

SPROUFFSKE, K. and WAGNER, A. (2016) Growthcurver: an R package for obtaining interpretable metrics from microbial growth curves. *BMC Bioinformatics 2016 17:1*, 17(1), pp. 1–4.

STEPHENS, J.C., ARTZ, S.W. and AMES, B.N. (1975) Guanosine 5' diphosphate 3' diphosphate (ppGpp): positive effector for histidine operon transcription and general signal for amino acid deficiency. *Proceedings of the National Academy of Sciences of the United States of America*, 72(11), pp. 4389–4393.

STERBOUL, C.C., KLEEMAN, J.E. and PARSONS, S.M. (1977) Purification and Characterization of a Mutant ATP Phosphoribosyltransferase Hypersensitive to Histidine Feedback Inhibition. *Archives of Biochemistry and Biophysics*, 181(2), pp. 632–642.

STEVENSON, K. et al. (2016) General calibration of microbial growth in microplate readers. *Scientific Reports*, 6(December), pp. 4–10.

STEWART, L.J. et al. (2020) Role of Glutathione in Buffering Excess Intracellular Copper in *Streptococcus pyogenes*. *mBio*, 11(6), pp. 1–19.

SYDOR, A.M. and ZAMBLE, D.B. (2013) Nickel Metallomics: General Themes Guiding Nickel Homeostasis. In: BANCI, L. (ed.) *Metal Ions in Life Sciences*. Dordrecht: Springer Netherlands, pp. 375–416.

THE UNIPROT CONSORTIUM et al. (2021) UniProt: the universal protein knowledgebase in 2021. *Nucleic Acids Research*, 49(D1), pp. D480–D489.

VALKO, M., MORRIS, H. and CRONIN, M.T.D. (2005) Metals, Toxicity and Oxidative Stress. *Current Medicinal Chemistry*, 12, pp. 1161–1208.

WALDRON, K.J. et al. (2009) Metalloproteins and metal sensing. *Nature*, 460(7257), pp. 823–830.

WALDRON, K.J. and ROBINSON, N.J. (2009) How do bacterial cells ensure that metalloproteins get the correct metal? *Nature Reviews Microbiology*, 7(1), pp. 25–35.

WINKLER, M.E. and RAMOS-MONTAÑEZ, S. (2009) Biosynthesis of Histidine. *EcoSal Plus*, 3(2), pp. 1–34.

WINKLER, M.E., ROTH, D.J. and HARTMAN, P.E. (1978) Promoter- and attenuator-related metabolic regulation of the *Salmonella typhimurium* histidine operon. *Journal of Bacteriology*, 133(2).

WINKLER, M.E., ZAWODNY, R. V. and HARTMAN, P.E. (1979) Mutation *spoT* of *Escherichia coli* increases expression of the histidine operon deleted for the attenuator. *Journal of Bacteriology*, 139(3), pp. 993–1000.

WU, H. et al. (2020) Highly Efficient Production of L-Histidine from Glucose by Metabolically Engineered *Escherichia coli*. *ACS Synthetic Biology*, 9(7), pp. 1813–1822.

WU, L.F. et al. (1994) Antagonistic Effect of Nickel on the Fermentative Growth of *Escherichia coli* K-12 and Comparison of Nickel and Cobalt Toxicity on the Aerobic and Anaerobic Growth. *Environmental Health Perspectives*, 102, p. 297.

WU, L.F. et al. (1989) Nickel deficiency gives rise to the defective hydrogenase phenotype of *hydc* and *fnr* mutants in *Escherichia coli*. *Molecular Microbiology*, 3(12), pp. 1709–1718.

WU, L.F. and MANDRAND-BERTHELOT, M.A. (1986) Genetic and physiological characterization of new *Escherichia coli* mutants impaired in hydrogenase activity. *Biochimie*, 68(1), pp. 167–179.

XU, F.F. and IMLAY, J.A. (2012) Silver(I), mercury(II), cadmium(II), and zinc(II) target exposed enzymic iron-sulfur clusters when they toxify *Escherichia coli*. *Applied and Environmental Microbiology*, 78(10), pp. 3614–3621.

YOUNG, T.R. et al. (2021) Calculating metalation in cells reveals CobW acquires Co^{II} for vitamin B12 biosynthesis while related proteins prefer Zn^{II}. *Nature Communications*, 12(1), [Online] Available from: doi.org/10.1038/s41467-021-21479-8.

ZEER-WANKLYN, C.J. and ZAMBLE, D.B. (2017) Microbial nickel: cellular uptake and delivery to enzyme centers. *Current Opinion in Chemical Biology*, 37, pp. 80–88.

ZHANG, J.W. et al. (2005) A role for SlyD in the *Escherichia coli* hydrogenase biosynthetic pathway. *Journal of Biological Chemistry*, 280(6), pp. 4360–4366.

ZHANG, Y. et al. (2012) Genetic and biochemical characterization of *Corynebacterium glutamicum* ATP phosphoribosyltransferase and its three mutants resistant to feedback inhibition by histidine. *Biochimie*, 94(3), pp. 829–838.

ZHANG, Y., AKILESH, S. and WILCOX, D.E. (2000) Isothermal titration calorimetry measurements of Ni(II) and Cu(II) binding to His, GlyGlyHis, HisGlyHis, and bovine serum albumin: a critical evaluation. *Inorganic Chemistry*, 39(14), pp. 3057–3064.